

PUBLISHER

On Behalf of Textile and Apparel Research
Application Center

Arif Taner ÖZGÜNEY

EDITOR IN CHIEF

Arif Taner ÖZGÜNEY
arif.taner.ozguney@ege.edu.tr

ASSOCIATE EDITORS

Mehmet KÜÇÜK
mehmet.kucuk@ege.edu.tr

Pelin SEÇİM KARAKAYA
pelinsecim@mail.ege.edu.tr

EDITORIAL BOARD

Aslı DEMİR

Gözde ERTEKİN

Hale KARAKAŞ

Hüseyin Aksel EREN

Pınar ÇELİK

ENGLISH EDITING SERVICE

Mengü Noyan ÇENGEL

SCIENTIFIC ADVISORY BOARD

Ahmet ÇAY

Andrej DEMŠAR

Arzu MARMARALI

Bojana VONČINA

Bülent ÖZİPEK

E. Perrin AKÇAKOCA KUMBASAR

Ender BULGUN

Esen ÖZDOĞAN

Hüseyin KADOĞLU

Mirela BLAGA

Nilgün ÖZDİL

Oktay PAMUK

Ozan AVİNÇ

Peter J. HAUSER

Recep EREN

Rıza ATAV

Savvas G. VASSILIADIS

Turan ATILGAN

ABSTRACTING / INDEXING

Science Citation Index Expanded (SCIE)

Scopus

WOS

TYPESETTING AND PRINTING

AK-MAT Matbaacılık Yayıncılık Kır. Malz. San. Tic. Ltd. Şti
Barbaros Mah. Refik Tulga Cd. No: 13, Bornova – İzmir
akmatlimited@gmail.com Tel: 0 232 444 28 23

Printed Date: 29 October, 2023

Annual subscription rate: 40 TL (VAT included)

Annual subscription rate for textile students: 15 TL

For subscription: T. C. Ziraat Bankası Ege Tıp Şubesi, Tekstil ve
Konfeksiyon Araştırma ve Uygulama Merkezi İBAN No: TR32 0001 0014
4607 2168 9350 32

Price: 10 TL (VAT included)

A Machine Vision Solution for Industrial Application of Abrage Inspection and Diameter Measurement on Yarn Bobbins

Elif Gültekin, Halil İbrahim Çelik, Lale Canan Dülger,

Halil İbrahim Sünbül..... 1

Effects of different types of surfactant treatments on the electromechanical properties of multiwalled carbon nanotubes decorated electrospun nanofibers

Abdulkadir Şanlı, Şule Pınar Cinfer, Afife Binnaz Hazar Yoruç 11

Exploratory Study on the Properties of Compact Three-Roving Yarn: Comparison the Properties of Compact Spun, Compact Siro- Spun and Compact Three-Roving Yarns

Murat Demir, Musa Kılıç, Serdar Sayın, Zeki Kırıl, Kıymet Kübra Denge

..... 19

Strength and Elasticity Properties of Denim Fabrics Produced from Core Spun Yarns

Gonca Balcı Kılıç..... 32

Simultaneous Coloring and Antibacterial Finishing to Cotton Through Environmentally-Friendly Way

Burcu Sancar Beşen, Pınar Parlakyiğit, Erkan Yılmaz 44

Effect of UV Exposure on the Mechanical Properties of Polyurethane-Coated Fabrics

Memik Bünyamin Üzümcü, Burak Sarı, Emrah Temel 51

The Effects of Sustainability and Fast Fashion Factors on Apparel Buying Behavior

Derya Bilen, Turan Atılğan, Seher Kanat 69

Application of Neural Network for the Prediction of Loss in Mechanical Properties of Aramid Fabrics After Thermal Aging

Banu Özgen Keleş..... 77

CONTACT

Ege Üniversitesi Tekstil ve Konfeksiyon Araştırma-Uygulama Merkezi
35100 Bornova – İzmir, TÜRKİYE
Tel: +90 232 311 38 89-83

www.dergipark.gov.tr/tekstilvekonfeksiyon
E-mail: tekstilkonfeksiyon@mail.ege.edu.tr

A Machine Vision Solution for Industrial Application of Abrage Inspection and Diameter Measurement on Yarn Bobbins

Elif Gültekin¹  0000-0003-4910-4081

Halil İbrahim Çelik^{1*}  0000-0002-1145-6471

Lale Canan Dülger²  0000-0002-1167-1737

Halil İbrahim Sünbül³  0009-0000-6587-8373*

¹Gaziantep University / Faculty of Engineering / Textile Engineering Department / Gaziantep / Türkiye

²İzmir University of Economics / Faculty of Engineering / Department of Mechanical Engineering / İzmir / Türkiye

³KİPAŞ Mensucat R&D Center / Kahramanmaraş / Türkiye

Corresponding Author: Halil İbrahim Çelik, hcelik@gantep.edu.tr

ABSTRACT

The abrage fault inspection and bobbin diameter measurement are very important processes in yarn manufacturing industry. These processes are performed manually, and so they are difficult, low efficient, time-consuming processes. The abrage faults are seen as colour or shade difference on the dyed fabric. This happens when the bobbins including abrage are converted to the fabric form, mistakes in colour differences are seen after dyeing process. An automatic machine vision system was developed for detecting abrage fault, and bobbin diameter from yarn bobbin cross-section view. Image processing software was developed and applied on different sizes of bobbin samples including different types of abrage fault. The success of vision system was statistically evaluated by detecting the bobbin abrage faults with 95.83% accuracy. In addition, the bobbin diameters obtained from the developed image processing algorithm were statistically analysed and the correlation coefficient ($R^2=0.99$) was calculated.

1. INTRODUCTION

In recent years, Industry 4.0, image processing applications, machine vision systems and artificial intelligence applications are extended as Textile 4.0 as in other sectors. Machine vision systems are becoming more common to perform objective evaluations automatically with less errors and in shorter time. Machine vision is used in textile sector while manufacturing high quality products with minimum defects. The machine vision systems and different image processing approaches can be used for determination of fiber, yarn, and fabric characteristics. New developments of industry 4.0 in terms of machine vision systems are also noticed in textile manufacturing sectors covering spinning, weaving, finishing, and clothing. These new technology systems are adapted to manufacturing line instead of manually controlled or human evaluated processes.

The fibers have different dyeability properties and different light reflectance characteristics. Accidental mixing of raw materials used in different stages of yarn production (blending or winding) results in a fault called "Abrage".

To cite this article: Gültekin E, Çelik H İ, Dülger L C, Sünbül H İ. 2024. A machine vision solution for industrial application of abrage inspection and diameter measurement on yarn bobbins. *Tekstil ve Konfeksiyon*, 34(1), 1-10.

ARTICLE HISTORY

Received: 16.09.2022

Accepted: 01.11.2022

KEYWORDS

Bilinear interpolation, local thresholding, machine vision system, yarn faults, bobbin diameter

This fault is detected on the bobbin after the yarn production and on the fabric before the ready-made process. Currently, its control is performed manually with the human eye both on the yarn package and the fabric under the UV light (Figure 1). The yarn bobbins are placed in a creel prior to packing. They are then transported to a special room illuminated by UV light, where the bobbins are individually controlled. According to the research and analyses on yarn bobbin abrage control process in different firms, it is revealed that in an enterprise with an average daily production capacity of 15 tons of yarn, approximately 7500 bobbins are controlled in a day requiring 4 workers at least. Thus, the workers can inspect only 40% of the abrage faults and so this type of manual quality control process results higher labor costs with lower efficiency. This process is undoubtedly time consuming and tiring. When the number of bobbins to be checked daily is considered, the risk of overlooked bobbin gets higher. When the bobbins are overlooked, the production efficiency can decrease by at least 60%.



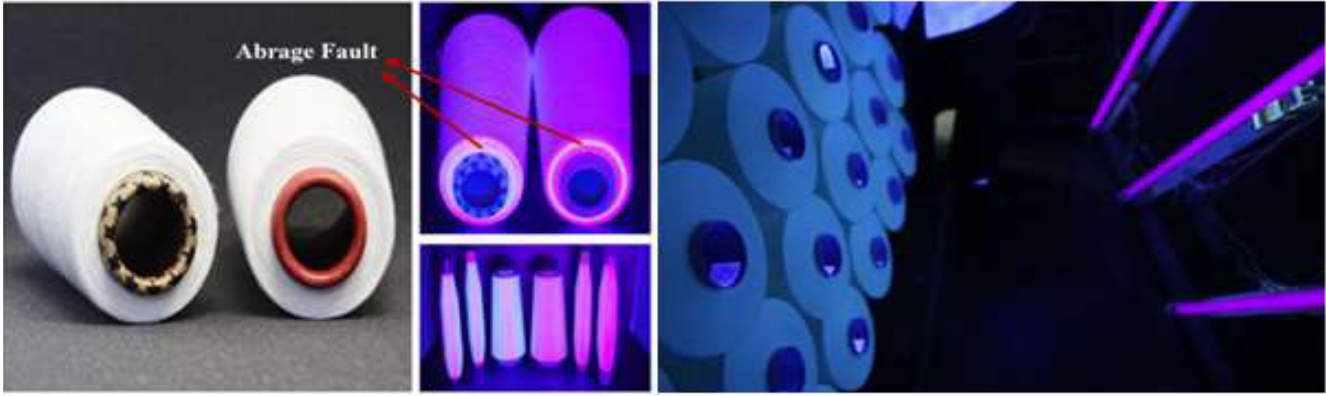


Figure 1. Abrage view under UV light [1, 2]

The yarn bobbin diameter measurement is also an important parameter for yarn packaging process. Normally, the diameter of the bobbins produced in the spinning mills is measured manually at certain intervals. This process is a significant value to perform packaging plan and to evaluate the efficiency of the winding process. It provides reliable inference about the yarn weight on bobbin, packaging tension and winding quality. If there is a problem in the winding stage, which is the last stage of the yarn production line, the diameter of the winding bobbins will be different or vice versa.

According to the literature research, it was seen that the most used method for determining circular objects in image processing is Hough transformation [3-5]. Circular objects in an image frame were distinguished from the complex background and highlighted. On the other hand, it was stated that the diameter values of the objects determined by Hough Transform can also be found. Since the yarn bobbin has a rounded appearance, Hough transformer was the most convenient way to determine the bobbin diameter. According to the literature research to segment the defective region in the image, the thresholding method plays a major role in binarization stage. Looking at the published scientific research about thresholding, histogram shape, measurement space clustering, entropy, object attributes, spatial correlation, and local gray-level surface methods are categorized according to the information they are exploiting by thresholding. Thresholding is an efficient way to distinguish objects from their surroundings thus this process produces a binary image with one state representing the foreground objects, such as written text, a defective part of a substance, and so on [6, 7].

Many studies are conducted on the detection of foreign matter in the fibers using image processing techniques [8-16]. Studies on image processing applications to yarn characteristics are mostly about the determination of yarn hairiness, yarn unevenness and yarn defects (thick place, thin place and neps) [17-26]. Apart from these, very few studies have dealt with the subject of abrage fault on the yarn package. Silvestre et al. conducted a study to

determine the abrage faults caused by the mixing the different types of fibers on the yarn spool (cops). Yarn samples were raw yarn and dyed yarn. The detection of fault in HSV color space has given better results in the study. The proposed system ultimately showed 100% detection of faulty yarn packages in the product with an error margin of 0.5%. The defective parts of the bobbin are detected by using the different reflectance properties of the fibers the under the UV light [27]. In Çelik's study [28], a prototype of vision inspection system was designed for abrage fault detection. The vision system components were lightening unit, High Density (HD) web camera, a cabin and PC. A user interface was prepared for applying the fault detection algorithm on the yarn bobbin samples by using MATLAB®. The abrage faults of different bobbin samples were detected and labeled successfully. This study was performed to set up a prototype system for a start study. As a result of study performed by Çelik [28], it was decided that the system hardware components should be revised, and system should be rearranged with more professional hardware parts for industrial applications. After the necessary hardware component changes were achieved and system revision were completed, Gültekin et al. [29] presented a machine vision system for automatic inspection of yarn bobbin and fabric abrage defect. The prototype system is introduced, and properties of its components are investigated. The optimum image acquisition parameters that are useful for abrage inspection were also determined. In another study performed by Gültekin et al. [30], an image processing algorithm based on pixel intensity transform and morphological operations were developed, and it was applied on different bobbin and fabric samples including abrage fault. The success of the given machine vision system was discussed. However, this study is conducted to develop a more effective and sensitive image processing algorithm in terms of abrage defect segmentation and bobbin diameter measurement by using same machine vision hardware. The method and algorithm used in this study has been improved. With developed algorithm in this study, it is attempted that more robust and proper to industrial application system will be developed.

The most important contribution of this study is the establishment of a machine vision system and the proposal of a user-interfaced image processing algorithm to automatically control abrage faults and measure the bobbin diameter. Both two important inspections are achieved with a single system and single user-interface. The outputs of the machine vision system can be adapted to yarn packaging unit. So, the yarn bobbins can be automatically sorted according to their size and the yarn bobbins including abrage fault can be automatically removed. In the current yarn packaging system, the bobbins moving on the conveyor belt are taken one by one by the robot arm and placed on the pallets. With the developed machine vision system, which can be adapted to the robot arm, the diameter of the bobbins and the abrage fault will be detected automatically. In the packaging unit, which is the last stage of the yarn production line, the surface images of the yarn bobbins will be taken with the machine vision system that will be mounted on a robot arm. Then the bobbin diameter calculation and surface scanning process will be performed on the images taken, and if defect is detected, the faulty bobbins will be transported to another department by means of a robot arm. To highlight the originality of this work to show the difference of algorithm steps between current design and previous study, which was published earlier, Gültekin et al. [29] introduced the system components by discussing the design of the developed machine vision system and the materials used in detail. Later, in another study [30], the same authors explained the camera settings and lighting unit of the machine vision system. They developed and carried out preliminary studies with a simple algorithm. The biggest difference of this submitted article from the other two previous studies is the applied image processing algorithm. In contrary to the previous studies [29, 30], the circular image of the yarn bobbin cross-section is cropped and converted to linear formation by using “Polar to Cartesian Transform” technique in proposed method. So, the proposed algorithm detects the abrage fault in a more detailed and more sensitive way. Thanks to the machine vision system developed, the faults in the yarn bobbin and bobbin diameter can be performed precisely and reliably. Thus, it will be possible to increase the production efficiency of yarn manufacturers by 60%. In the meantime, the profit margin of the manufacturers will increase due to the decrease in worker incentives and the decrease in the rate of advertising caused by faulty bobbins.

2. MATERIAL AND METHOD

2.1 Material

The abrage bobbin samples are collected as three groups: blend abrage, cops abrage and abrage free ones. The blend abrage was produced by deliberately blending different fibers during fiber opening. Cops abrage samples were produced by feeding different cops to the same bobbin winding machine in a controlled manner. On the other

hand, the abrage fault can occur at different location of the bobbin cross-section. In the content of this study, all possible abrage fault occurrence types were considered, and 36 different yarn bobbin samples were produced. Different fiber materials: USA cotton, domestic cotton, Tencel and polyester were used in the production of abrage bobbins. The bobbin abrages were produced at three different places of bobbin cross-section: at the beginning of the bobbin, in the middle of the bobbin and at the end of the bobbin with different sizes. Totally, 36 different yarn bobbin samples were produced by KİPAŞ Mensucat R&D Center, Kahramanmaraş, Turkey.

2.2 Method

To create an efficient and fully automatic system for the abrage fault detection and bobbin diameter measurement under industrial application condition, the inspection should be achieved while the bobbins are also automatically transferred through the process zone. However, such a system must be built on an industrial yarn production mill and the real-time trials must be made under the manufacturing condition. Since this type of application is difficult and, requires long time, high effort, and high construction cost, it was seen easier and effective to develop a robust inspection algorithm with prototype system consists of industrial hardware components. After the required success is obtained, the machine vision system can be adapted to industrial application and necessary modifications for real-time inspection can be carried out quickly.

In this study, MATLAB® software program was used for preparing user interface and image processing algorithm. Since such a vision inspection system consists of image acquisition and processing parts, first the components of the image acquisition system were introduced and then the image processing algorithms were explained.

2.2.1 Description of vision inspection system

A prototype vision inspection system was developed to acquire and analyze the image frame of the yarn bobbin samples. According to the experience-based knowledge received from the yarn industry, 95% of the abrage fault in the yarn bobbin was encountered on the bobbin surface, and so it was stated that it will be sufficient to inspect only the upper cross-section of the yarn bobbin. The prototype machine vision system was designed in accordance with these criteria. The system consists of a lightening unit, a camera system, a cabin, and a computer (Figure 2). The BASLER acA1920-40uc area scan camera with the Sony IMX249 CMOS sensor delivers 41 frames per second at 2.3 MP resolution, and the sensor size of camera is 11.3 mm x 7.1 mm was used. A top-lightening unit consisting of 12 LED UV fluorescent lamps and positioned around the camera system. The dimensions of the cabin are given as 80

cm x 80 cm x 85 cm to provide easy location of bobbin samples. The cabin was painted in matt black color to provide a homogeneous illumination and eliminating reflection inside the cabin. The camera was placed to the top of the cabin by using a properly designed attachment frame. A suitable apparatus was designed for positioning the bobbin samples at the bottom of the system. The distance of the bobbin sample to camera lens is to be arranged. This is necessary so that the camera field of view can be adjusted according to the bobbin size. A screw system was used to adjust the camera distance. The other adjustments related to camera and algorithm performance were achieved via computer. High image quality is essential for the system response, the parameters in the camera software interface (Pylon5) were analyzed. The related camera parameters: Light Source Pre-set, Gain, Gamma and Exposure time etc. have been adjusted until the required image frame was obtained. Determined camera parameters were set during inspection tests. In this study, the gain was set to 30, gamma was set to 2, and exposure time was set to 5000. These values can vary according to different light intensity. Therefore, these parameters must be changed in different application areas. The optimum values of these parameters were determined by trial-and-error method in different applications.

Before adapting the proposed system to yarn production line for real-time inspection, the hardware of the system;

industrial camera properties, lighting conditions and cabin design, which are the most important equipment of the system, were completed. As it will be difficult to test such a smart quality control system directly on the production line, firstly, experiments were carried out on a prototype structure.

2.2.2 Abridge detection algorithm

When an operation is performed for an object in any image, it is desired that the applied filter or operation should affect only the target object in the image size. This process can only be possible when the image frame completely consists of the target object. Considering the visual evaluation of the yarn bobbin in the image frame, a circular area is occupied within a rectangular image frame with a size of $M \times N$. When the image frame of yarn bobbin cross-section view is seen in the machine vision system, the yarn bobbin has shades of gray, while the areas outside the circular bobbin area are seen as completely black. During processing of image frame with any filter, a neighborhood operation is performed. The value of any given pixel in the output image is determined by applying an algorithm to the values of the pixels about the corresponding input pixel. Filtering is valid for whole image matrix. Because of the filtering restrictions, the area covered by yarn bobbin cross-section surface should be extracted from the image frame.

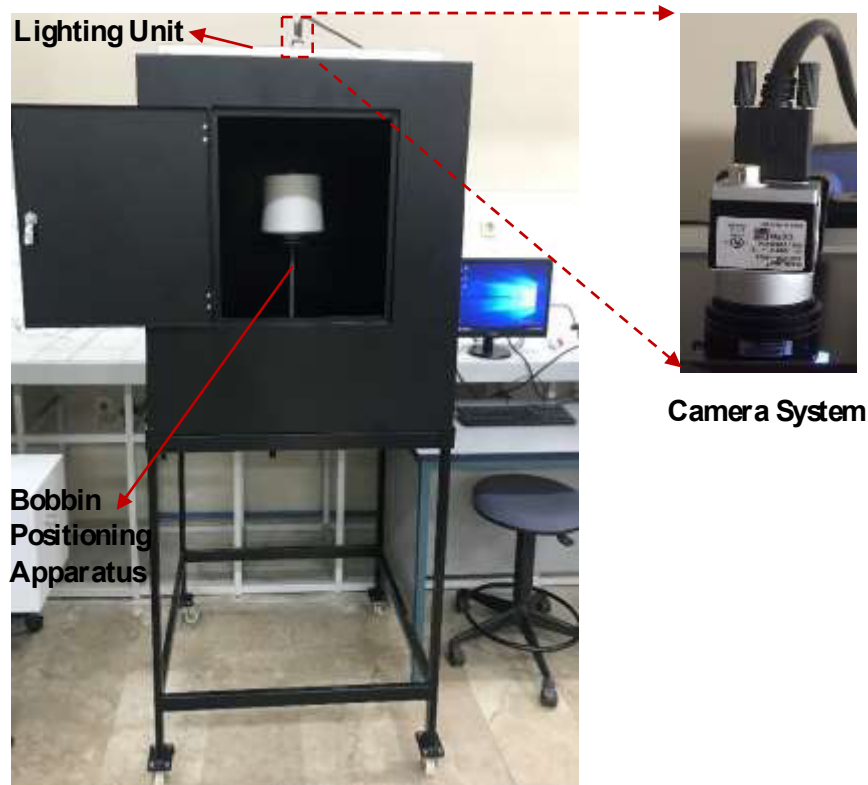


Figure 2. A prototype bobbin inspection cabin design

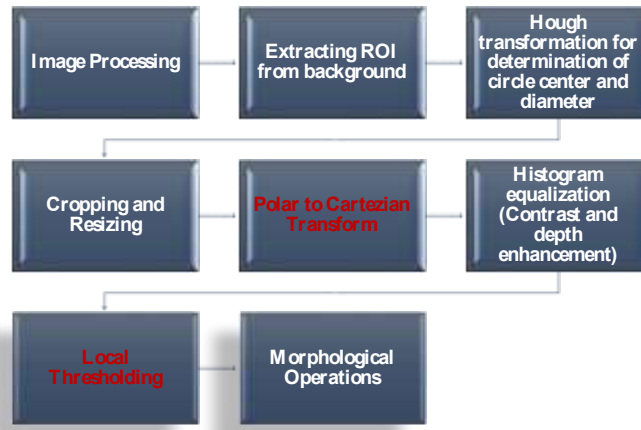


Figure 3. Steps of the algorithm

The flow chart of the algorithm developed for diameter measurement and abrage detection is given in the Figure 3. Before this object extraction operation, some preprocessing phases were achieved. All color images were taken from the machine vision system were converted to gray format. The images in gray format were converted to binary form, where the bobbin was completely white, and the rest was black. The Hough transformation approach was used to calculate the center of the bobbin where the boundaries were defined by drawing its contour (Figure 4). The inner (r_{in}) and outer (r_{out}) radiuses of the bobbin was determined via Hough transform (Figure 4).

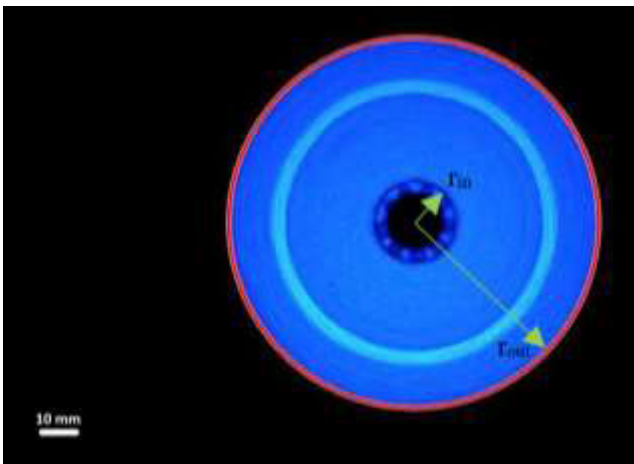


Figure 4. Bobbin diameter boundary image with Hough transformation

2.2.3 Polar to Cartesian transform

The method for this problem is based on the transformation of object polar coordinate into a cartesian coordinate system by bilinear interpolation. The Cartesian coordinates (x, y) in two dimensions describe the direction of a point P in the plane. Polar coordinates are another two-dimensional coordinate scheme. Polar coordinates specify the direction

of a point P in the plane by its distance r from the origin and the angle (θ) formed by the line segment from the origin to P instead of signed distances along the two coordinate axes. Calculation of a point's cartesian coordinates using polar coordinates (r, θ) by constructing the right triangle shown in (Figure 5). The hypotenuse is a line section that runs from the origin to the point and is r in length. The side of the triangle adjacent to the angle, $x = r \cos \theta$ is the projection of this line section on the x -axis (Figure 5(a)). The other side determines the y -component, $y = r \sin \theta$ (Figure 5(a)).

The polar coordinates can be transformed to area map (Figure 5(b)). The transformation from polar (r, θ) plane (left in Figure 5(a)) to cartesian coordinates (x, y) plane (right in Figure 5(b)) with $(x,y) = T(r, \theta) = (r \cos \theta, r \sin \theta)$ maps a rectangular. As seen in Figure 5(b), the yellow dot on the right panel corresponds to the rectangular area on the left panel. Each small curvy rectangular cell of the polar plane is also mapped to small rectangular cells of the cartesian plane. As seen from this simulation (Figure 5), it can be proved that area between the inner and outer diameters of the yarn bobbin can be transformed to rectangular area [31].

The boundaries of the bobbin with the inner and outer diameters were determined by Hough transformation (Figure 6(a)). The image was segmented according to the boundaries of an object whose diameter was already known (Figure 6(b)). Thus, the region occupied by yarn bobbin was cut out from the image frame. Then interpolation was performed on the segmented image. In this conversion, M is the number of pixels from the minimum r to the maximum r along the radius. Eventually, the output image was an $M \times N$ image with M points along the r -axis, and N points along θ -axis. An object in the form of a circle was extracted and then it is transformed into a rectangular image frame (Figure 6(c)).

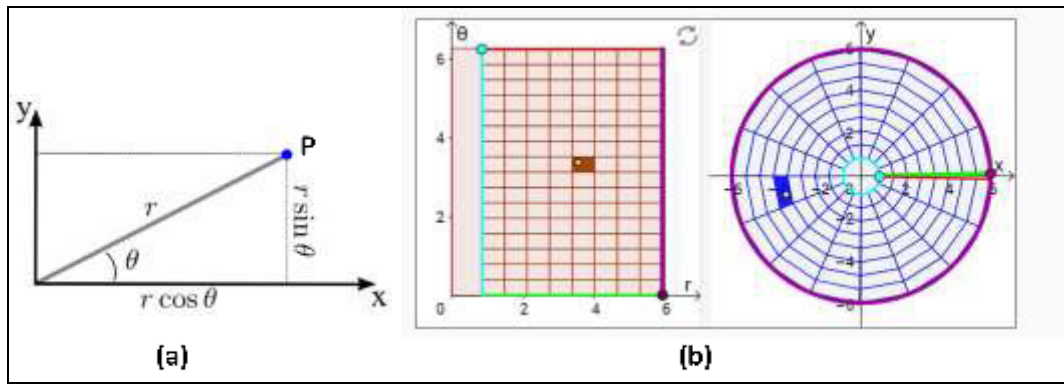


Figure 5. Schematic representation of area transformation of polar coordinates map [31]

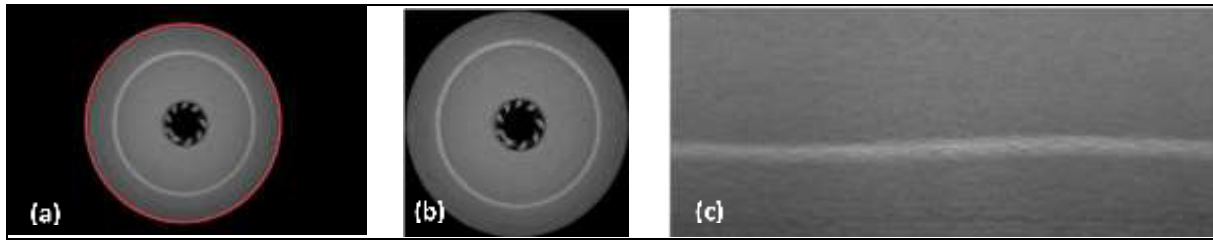


Figure 6. (a) Plotted bobbin boundary, (b) Image cropped according to bobbin outer boundary, (c) Bobbin cross-section extracted and transformed into rectangular image frame

2.2.4 Adaptive thresholding based on local statistics

Adaptive thresholding should be preferred in cases where the ghosting in the image caused by the lighting source is high. The adaptive thresholding approach based on computing threshold pixel intensity value of each local pixel (x, y) from the pixel values of (x, y) neighbors in $m \times n$ size (Figure 7).

Let $S_{x,y}$ demonstrate the set of coordinates of a neighborhood centered on a gray image. Neighborhood processing generates a corresponding pixel at the same coordinates in an output (processed) binary image. This specified operation comprises the pixels in the input image with coordinates in $S_{x,y}$. The defined procedure is to calculate the average value of pixels in a rectangular neighborhood of size $M \times N$ based on the specified point (x, y) . Binary image is obtained sliding the $N \times M$ thresholding window along the gray image frame and so the specific threshold value of each pixel is obtained according to the center (x, y) coordinate pixel and corresponding neighbor pixels [32].

As the basic approach for local thresholding, the standard deviations and means of the pixels adjacent to each point in an image are used. Since these two values define the local contrast and the average intensity, they are very useful in calculating local threshold. Although this process appears to be a laborious task, the modern algorithms and the hardware allow fast neighbor processing with common functions, logical and arithmetic operations.

Let σ_{xy} and m_{xy} indicate the standard deviation and mean value of the set of pixels contained in a neighborhood

centered at the coordinate (x, y) in an image. The format of local thresholds (T_{xy}) is given as follows Equation (1):

$$T_{xy} = a\sigma_{xy} + bm_G \quad (1)$$

where m_G is the global image mean, a and b represent nonnegative constants. The segmented image $g(x, y)$ is computed as Equation (2):

$$g(x, y) = \begin{cases} 1 & \text{if } f(x, y) > T_{xy} \\ 0 & \text{if } f(x, y) \leq T_{xy} \end{cases} \quad (2)$$

where $f(x, y)$ represents the input image. This equation is evaluated and applied at all pixel locations.

Thresholding can be categorized into global and local thresholding. In images with uniform contrast distribution of background and foreground like yarn bobbin images, global thresholding is more appropriate. Therefore, in this study, global thresholding was used with the standard deviation and average pixel values obtained from the entire image frame according to Equation 1. The optimum values of a and b constants in Equation 1 have been obtained because of different trying, as made in many image processing studies.

3. RESULTS AND DISCUSSION

3.1 Results of Local Thresholding Algorithm

Abrage fault detection application was achieved by using Local Thresholding Algorithm. The results of the local thresholding method are given in Figure 8.

Since the pixel intensity values of faultless region was different from abrage region, the defective region was distinguished from the average and standard deviation calculated from the neighbor relations of each pixel give high accurate results.

The success rate was determined by applying the algorithm to all bobbin samples. Once the model is developed, the next phase is to calculate the performance of the developed model using confusion matrix criteria.

Confusion Matrix is a tool to determine the performance of classifier. It contains information about actual and predicted classifications. The below table shows confusion matrix of two-class, positive and negative classifier [33]. The terms in Table 1 are.

True Positive (TP) is the number of correct predictions that an example is positive which means positive class correctly identified as positive.

False Negative (FN) is the number of incorrect predictions that an example is negative which means positive class incorrectly identified as negative.

False Positive (FP) is the number of incorrect predictions that an example is positive which means negative class incorrectly identified as positive.

True Negative (TN) is the number of correct predictions that an example is negative which means negative class correctly identified as negative.

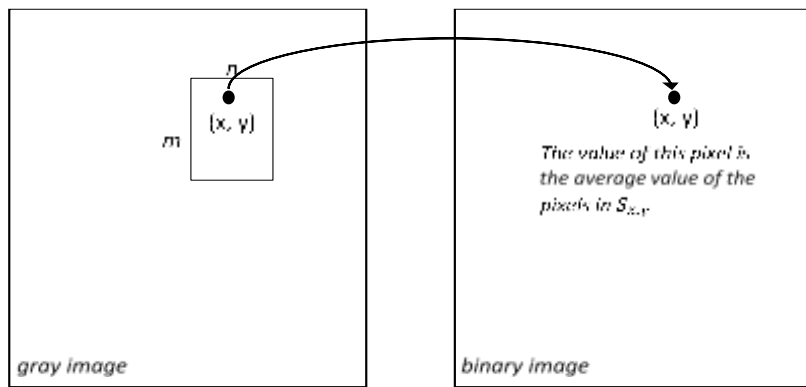


Figure 7. Local averaging using neighborhood processing

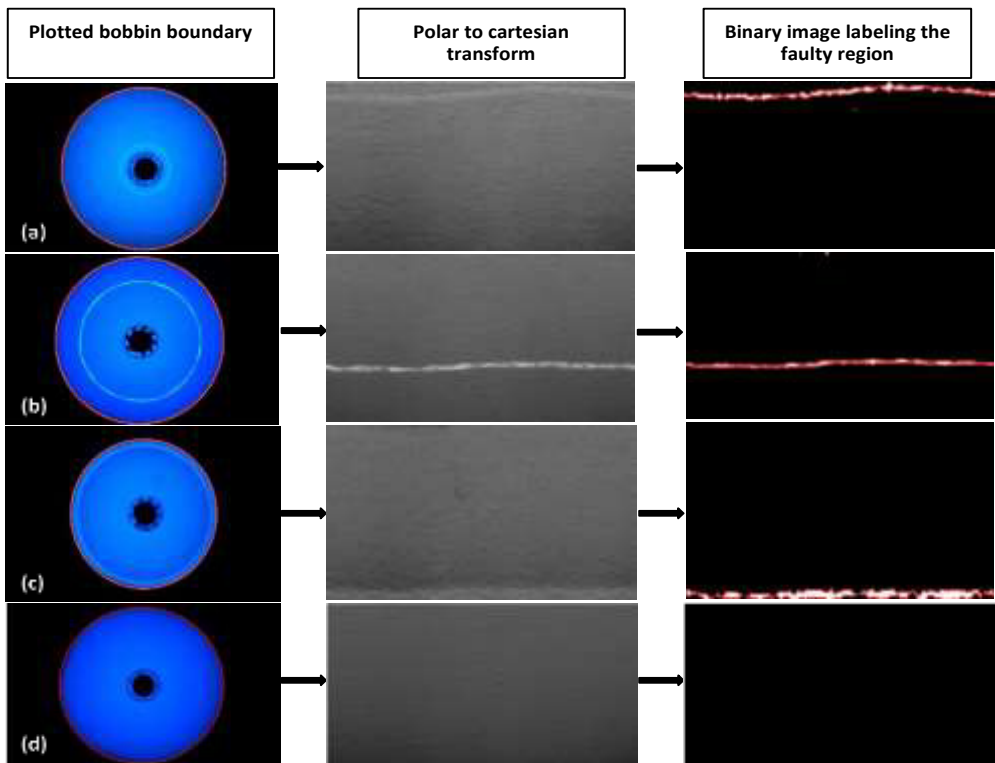


Figure 8. Algorithm results prepared by Local Thresholding method (a) abrage at the beginning of the bobbin, (b) abrage in the middle of the bobbin, (c) abrage at the end of the bobbin, (d) faultless bobbin

Table 1. Confusion matrix with advanced classification metrics

		Predicted Class		
		Positive	Negative	
Actual Class	Positive	True Positive (TP)	False Negative (FN)	Sensitivity $\frac{TP}{(TP + FN)}$
	Negative	False Positive (FP)	True Negative (TN)	Specificity $\frac{TN}{(TN + FP)}$
		Precision $\frac{TP}{(TP + FP)}$	Negative Predictive Value $\frac{TN}{(TN + FN)}$	Accuracy $\frac{TP + TN}{(TP + TN + FP + FN)}$

Sensitivity is also referred as “True Positive Rate” or “Recall”. It is a measure of positive examples labeled as positive by classifier required to be higher. Specificity is also known as “True Negative Rate”. There should be high specificity. Precision is ratio of total number of correctly classified positive examples and the total number of predicted positive examples. It shows correctness achieved in positive prediction. Accuracy is the proportion of the total true predictions to all predictions. Figure 9 shows confusion matrix of yarn bobbins. The bobbin samples were evaluated manually under UV light via human eye and compared with the results of the image processing algorithm. The comparison results were categorized according to confusion matrix. The image processing algorithm results were evaluated in four classes as: (1) at the beginning of the bobbin, (2) in the middle of the bobbin, (3) at the end of the bobbin, and (4) faultless bobbins, respectively.

After creating a confusion matrix chart from the true labels and the predicted labels, the true positive rates and false positive rates in the row summary were displayed as sensitivity and specificity. Also, column summary displayed the positive predictive rates and false predictive rates as precision and negative predictive value.

Finally, the success rates, which called sensitivity, were obtained as; 100% at the beginning of the bobbin abrage (1), 91.7% at the middle of the bobbin abrage (2), 91.7% at the end of the bobbin abrage (3), in 100% abrage-free bobbins (4). An average accuracy of 95.83% were achieved. This ratio is a very good result for determining the abrage error in the yarn package. When the abrage fault, which are evaluated manually in the UV light room by the experienced employees, the success rate obtained from the machine vision system is evaluated as acceptable level.

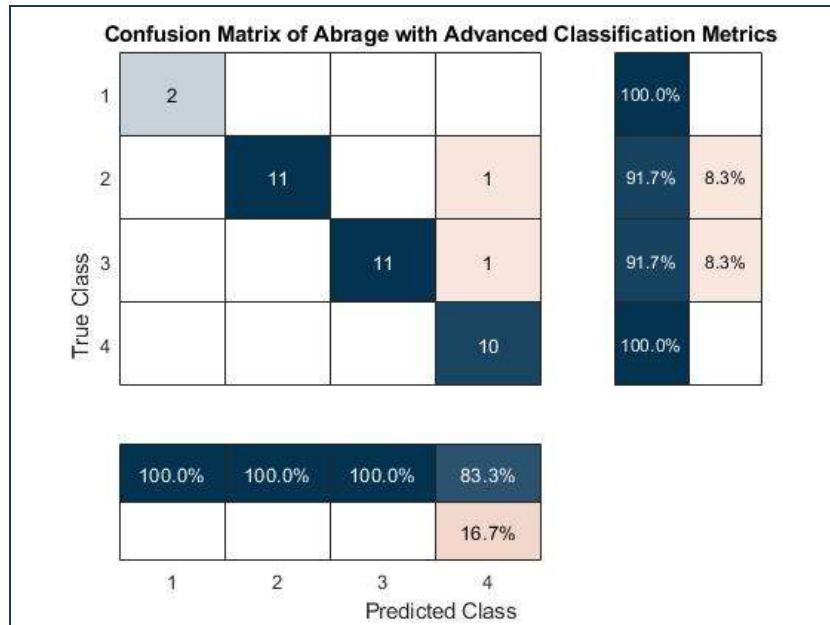


Figure 9. Confusion matrix of yarn abrage classification according to fault class

3.2 Bobbin Diameter Measurement Results

The bobbin measurement verification was performed using 25 bobbin samples. Bobbin diameter was measured manually with calipers as the actual results. The same bobbins were placed in the machine vision system and the diameter values were then determined. Since the diameter measurement made with image processing algorithm is in pixel unit, it must be transformed to mm unit. A calibration process is performed to determine the size of each pixel in mm. Thus, the diameter of each bobbin was obtained by multiplying the pixel size with the measured number of pixels in diameter. The accuracy of the bobbin diameter measurement via machine vision system was determined by using the mean absolute percentage error (MAPE) statistical model (Equation (3)) that is calculated from Hough transformation results of developed image processing algorithm (Figure 4) and the actual diameter measurement results. The bobbin diameter results of both methods and corresponding MAPE values are presented in Table 2.

$$MAPE = \frac{\sum_{i=1}^n \left| \frac{y_i - \hat{y}_i}{y_i} \right| \times 100}{n} \quad (3)$$

Table 2. Actual and predicted bobbin diameter results

Number of Samples	Actual Measurements (mm)	MATLAB IP Measurements (mm)	MAPE
1	188	189.46	0.78
2	191	190.00	0.52
3	189	190.14	0.60
4	208	209.54	0.74
5	199	200.12	0.56
6	211	210.67	0.16
7	211	212.90	0.90
8	210	209.91	0.04
9	211	212.18	0.56
10	211	212.72	0.82
11	212	212.69	0.33
12	209	210.53	0.73
13	207	208.09	0.53
14	190	190.37	0.20
15	206	205.96	0.02
16	195	196.91	0.98
17	213	213.20	0.10
18	211	212.50	0.71
19	186	187.00	0.54
20	208	207.67	0.16
21	205	205.09	0.04
22	202	202.82	0.41
23	199	200.55	0.78
24	196	197.44	0.74
25	216	217.88	0.87
Average	203.36	204.34	0.51

According to Table 2, the lowest and highest error percentage values were obtained as 0.04% and 0.98%, respectively. The mean absolute percentage error of the results was calculated as 0.51%. The linear regression analysis is made between the actual and image processing measurement results and displayed in Figure 10. It can be clearly seen that there is high correlation between two value sets and so the actual and the image processing results are progressing on the same trend (Figure 10(a)). The regression coefficient between actual and image processing values was calculated as $R^2 = 0.9921$ (Figure 10(a)). In the residual graph (Figure 10(b)), each point indicates the yarn bobbin diameter measurement, where the measurements made by the image processing algorithm are on the x-axis and the accuracy of the measurements is on the y-axis. The distance from the line at 0 is how bad the image processing measurement was performed for that value. So, the residual is the bit that subtracting the image processing value from the actual value.

3.3 Abrage Fault Inspection System User Interface

The Image Processing and Image Acquisition Toolboxes in MATLAB program were used in the user interface preparation stage. The prepared GUI (Figure 11) has buttons such as “Start Camera”, “Capture Image”, “Exposure Time”, “Image Processing” and “Exit” with its functions separately. The relevant codes are inserted to the working extension of the interface. The camera is started via the interface. An option is then provided where you can set the Exposure Time manually. The “Exposure Time” option provides the adjustment of the lightening duration according to the yellowness of the fibers on the yarn bobbin. Therefore, the pixel intensity values can be adjusted for different products. Otherwise, it is not appropriate to use a fixed Exposure Time value for all fiber types. The Capture Image button is used to get a yarn bobbin cross-section image frame. After all these adjustments, the abrage detection process is started with the Image Processing button. When image processing is performed, the image of inspected bobbin, the histogram graph of the image, binary transform of the image was represented on related axes of user interface. Besides to all these fault detections, the bobbin diameter is also given to the user in mm. If abrage fault exist in the inspected image, the percentage of the abrage fault to the total bobbin cross-section area is calculated and presented to the user. If any abrage fault is detected, the bobbin sample is named as “Abrage Found” and saved. If the detected sample has not got abrage fault, it is displayed as “Faultless”.

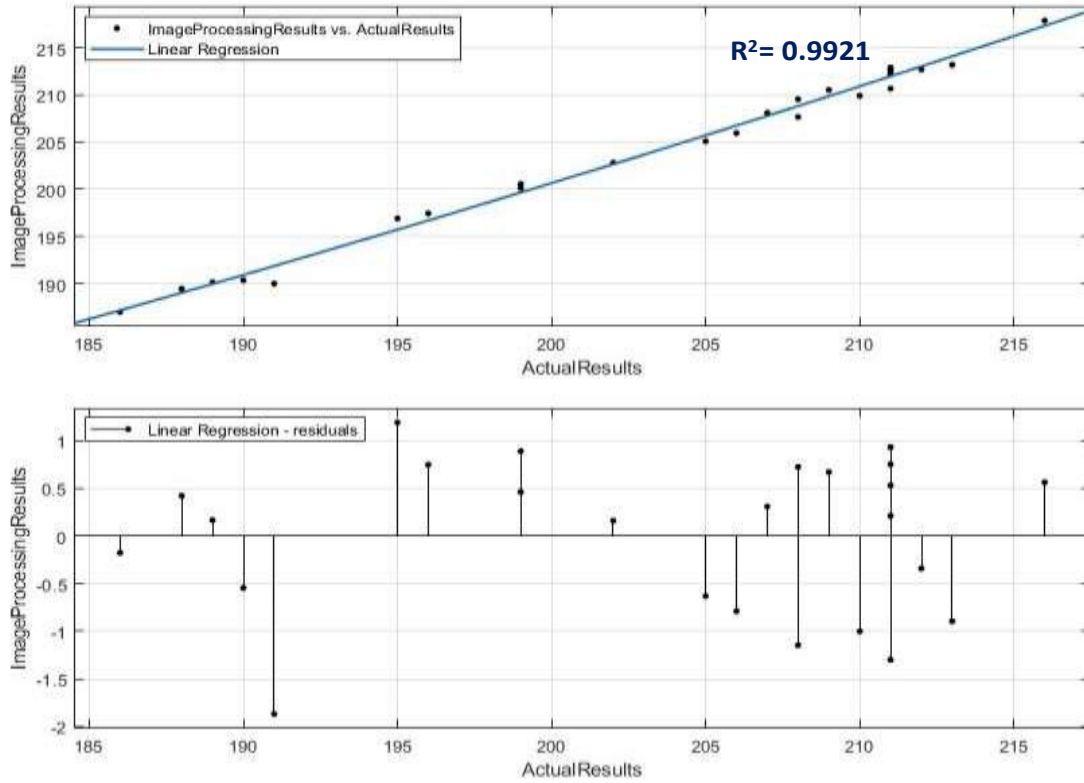


Figure 10. Q-Q plot of the actual and image processing measured bobbin diameter values (a) correlation graph, (b) residual graph of each measurement

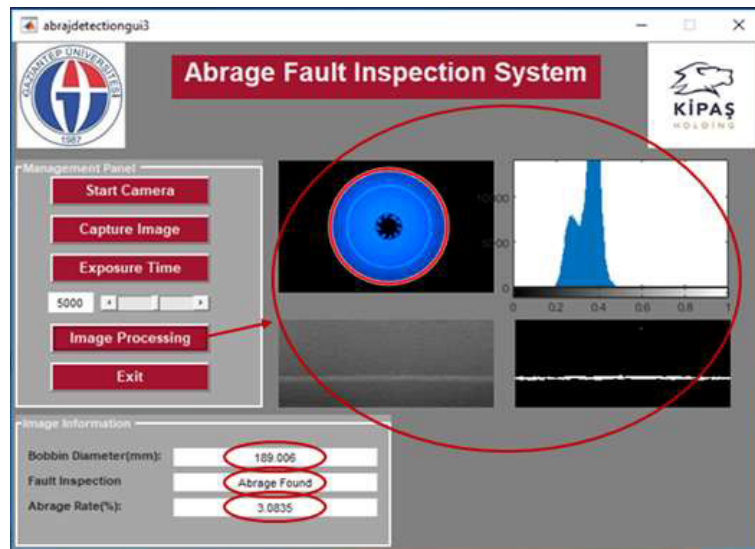


Figure 11. Abridge fault inspection system- User Interface

4. CONCLUSION

A machine vision system was proposed for bobbin abridge fault detection and bobbin diameter measurement. Thirty-six yarn bobbin samples were inspected with a success rate of 95.83%. This ratio is quite high for a spinning mill even it has full automation line. The system can easily be improved by building necessary hardware and software and so it will be possible to access the system remotely and acquire the number of abridge and fault free bobbins in real-time. In addition, since the automatic measurement of the

yarn bobbin diameter is very important in terms of determining the packaging tension and the winding quality of the winding machine, the automatic measurement of the bobbin diameter was achieved with a high success rate of $R^2 = 0.9921$.

The study is performed as a part of a research project involving an industrial application. The machine vision system was created by using the correct illumination system and high-resolution camera. The operation duration of the machine vision system that is the time required for abridge

inspection and bobbin diameter measurement was determined as 10 seconds. The conveyor band that is used for yarn bobbin transformation is driven with approximately 15 rev/min motor speed. The developed machine vision system and image processing algorithm can be adapted easily on the yarn bobbin conveyor band currently used in the spinning mill and run successfully.

The proposed system can be replaced with the manual inspection process. It can be estimated that production efficiency can be increased by at least 60% by saving labor

costs with the proposed machine vision system. The developed image processing approach technique can be used to achieve the current time-consuming quality control process automatically, sensitively and in shorter time.

Acknowledgement

This study is supported by the Scientific and Technological Research Council of Turkey (TUBİTAK) under grant Project Number: 5160116. The author(s) wish to thank for their financial support.

REFERENCES

1. The Textile Association (India). 2019, 06 17. Leopfe – Synthetic yarns don't need foreign matter detection, or do they? Retrieved from www.etextilemagazine.com/en/synthetic-yarns-dont-need-foreign-matter-detection-or-do-they.html.
2. Technocrat Industries India. 2019. 07 25. Cotton yarn Overview. Retrieved from <https://www.technocraftgroup.com/Cotton-Yarn.aspx>.
3. Okokpujie K, Noma-Osaghae E, John S, Ajulibe A. 2018. An improved iris segmentation technique using circular Hough transform. In IT Convergence and Security. Springer. Singapore, 203-211.
4. Bindu S, Prudhvi S, Hemalatha G, Sekhar MN, Nanchariahl MV. 2014. Object detection from complex background image using circular Hough transform. *International Journal of Engineering Research and Applications*, 4(4), 23-28.
5. Cherabit N, Chelali FZ, Djeradi A. 2012. Circular hough transform for iris localization. *Science and Technology*, 2(5), 114-121.
6. Singh TR, Roy S, Singh OI, Sinam T, Singh K. 2012. A new local adaptive thresholding technique in binarization. *arXiv preprint arXiv*, 1201.5227.
7. Sezgin M, Sankur B. 2004. Survey over image thresholding techniques and quantitative performance evaluation. *Journal of Electronic imaging*, 13(1), 146-165.
8. Kang TJ, Kim SC. 2002. Objective Evaluation of the Trash and Color of Raw Cotton by Image Processing and Neural Network. *Textile Research Journal*, 72, 776-782.
9. Lawrence CA. 2003. Fundamentals of spun yarn technology. CRC Press LLC. Boca Raton, London, New York, Washington, D.C.
10. Li D, Yang W, Wang S. 2010. Classification of Foreign Fibers in Cotton Lint Using Machine Vision and Multi-Class Support Vector Machine. *Computers and Electronics in Agriculture*, 74(2), 274-279.
11. Su Z, Tian YG, Gao C. 2006. A Machine Vision System for On-Line Removal Of Contaminants In Wool. *Mechatronics*, 16(5), 243-247.
12. Yuhong D, Yongheng L, Xiuming J. 2015. Research Of Foreign Fibers In Cotton Yarn Defect Model Based On Regression Analysis. *The Journal of The Textile Institute*, 107(9), 1089-1095.
13. Xinhua W, Shu W, Laiqi X, Baoguo S. 2014. Identification of Foreign Fibers of Seed Cotton Using Hyper-Spectral Images Based on Minimum Noise Fraction. *Transactions of the Chinese Society of Agricultural Engineering*, 30(9), 243-248.
14. Pai A, Sari-Sarraf H, Hequet EF. 2004. Recognition of Cotton Contaminants Via X-Ray Microtomographic Image Analysis. *IEEE Transactions on Industry Applications*, 40(1), 77-85.
15. Mehta P, Kumar N. 2010. Detection of foreign fibers and cotton contaminants by using intensity and hue properties. *International Journal of Advances in Electronics Engineering*, 1(1), 230-240.
16. Wang XH, Wang JY, Zhang JL. 2010. Study on The Detection of Yarn Hairiness Morphology Based on Image Processing Technique. *Proceedings of the Ninth International Conference on Machine Learning and Cybernetics*, 2332-2336.
17. Kuzanski M. 2008. The Algorithms of The Yarn Shape Detection and Calculation of The Protruding Fibres Length. *Memstech*, 98-100.
18. Fabijanska A, Strumillo LJ. 2012. Image Processing and Analysis Algorithms for Yarn Hairiness Determination. *Machine Vision and Applications*, 23, 527-540.
19. Xu BG, Murrells CM, Tao XM. 2008. Automatic Measurement and Recognition of Yarn Snarls by Digital Image and Signal Processing Methods. *Textile Research Journal*, 78(5), 439-456.
20. Guha A, Amarnath C, Pateria S. 2010. Measurement of yarn hairiness by digital image processing. *The Journal of The Textile Institute*, 101(3), 214-222.
21. Carvalho V, Cardoso P, Belsley M. 2006. Development of a Yarn Evenness Measurement and Hairiness Analysis System. *IECON - 32nd Annual Conference on IEEE Industrial Electronics*, 3621-3626.
22. Asgari H, Mokhtari F, Latifi M. 2014. Characterizing cotton yarn appearance due to yarn-to-yarn abrasion by image processing. *The Journal of The Textile Institute*, 105(5), 477-482.
23. Ozkaya YA, Acar M, Jackson MR. 2010. Yarn twist measurement using digital imaging. *Journal of the Textile Industry*, 101(2), 91 – 100.
24. Yang Li D, Zhu L, Kang Y. 2009. A New Approach for Image Processing in Foreign Fiber Detection. *Computers and Electronics in Agriculture*, 68(1), 68-77.
25. Roy S, Sengupta A, Sengupta S. 2013. Determination of the Diameter Spectrogram and Neps for Yarn Parameterization using Image Processing. *International Journal of Electrical, Electronics and Computer Engineering*, 2(2), 72-76.
26. Shams NA, Ebrahimi F, Sadeghzade N. 2014. Evaluation of yarn defects by image processing technique. *Optik*, 125, 5998-6002.
27. Silvestre J, Perez R, Mufnoz J. 2005. System Integration of a Mixed Fibre Detection Process in Raw Yarn Packages by Computer Vision. *IEEE*.
28. Çelik HI, 2016. Development of a machine vision system for yarn bobbin inspection. *Industria Textila*, 67(5), 292-296.
29. Çelik Hİ, Gültekin E, Dülger LC. 2019. An Innovative Solution for Abrage Fault Detection On Yarn Bobbin And Fabric Surface. *ICENS*. Praha.
30. Gültekin E, Çelik Hİ, Dülger LC, Sünbül Hİ, Harun K. 2019. Image Processing Applications on Yarn Characteristics and Fault Inspection. *Tekstil ve Mühendis*, 26(116), 340-345.
31. Math Insight, Polar coordinates mapping. 2020, 01 04. Retrieved from [https://mathinsight.org/polar_coordinates_mapping#:~:text=The%20transformation%20from%20polar%20coordinates,%20plane%20\(right%20panel\)](https://mathinsight.org/polar_coordinates_mapping#:~:text=The%20transformation%20from%20polar%20coordinates,%20plane%20(right%20panel)).
32. Gonzalez RC. 2004. Digital Image Processing Using Matlab-*Gonzalez Woods & Eddins 2nd edition*, Saddle River, New Jersey.
33. Confusion Matrix. 2020, 10 25. Retrieved from https://en.wikipedia.org/wiki/Confusion_matrix.

Effects of Different Types of Surfactant Treatments on the Electromechanical Properties of Multiwalled Carbon Nanotubes Decorated Electrospun Nanofibers

Abdulkadir Şanlı*¹  0000-0002-9768-9005

Şule Pınar Cinfer²  0000-0003-1075-0609

Afife Binnaz Hazar Yoruç³  0000-0001-7281-2305

¹ Faculty of Engineering, Department of Bioengineering, Royal School of Mines, Imperial College London, London, UK

² Yıldız Technical University / Faculty of Chemical and Metallurgical Engineering, Department of Metallurgical and Materials Engineering / Davutpaşa Mah. Davutpaşa Caddesi, 34210 Esenler, İstanbul, Türkiye

³ Yıldız Technical University / Faculty of Chemical and Metallurgical Engineering, Department of Metallurgical and Materials Engineering / Davutpaşa Mah. Davutpaşa Caddesi, 34210 Esenler, İstanbul, Türkiye

Corresponding Author: Abdulkadir Şanlı, sanli@tau.edu.tr

ABSTRACT

Carbon nanotubes (CNTs) have a strong tendency to form agglomeration due to van der Waals interactions, which hinders their practical utilization. Therefore, an effective and stable dispersion of CNTs in a surfactant based solvent is very important for the realization of CNTs based nanocomposites in various applications. In this paper, influence of different types of surfactant on the electromechanical properties of multiwalled carbon nanotubes (MWCNTs) decorated electrospun thermoplastic polyurethane (TPU) nanofibers were investigated by UV-VIS spectroscopy, zeta potential, FT-IR analysis, scanning electron microscopy (SEM) and uniaxial tensile strain sensing. Obtained results suggest that type of surfactant has not only effecting the dispersion level of CNTs but also has a significant influence on the electromechanical properties of CNTs decorated electrospun CNTs/TPU nanofibers. The results of the present study provide new insights into the design and tailoring the electromechanical properties of CNTs decorated electrospun nanofibers.

1. INTRODUCTION

Among various carbonaceous nanofillers, carbon nanotubes (CNTs) has inspired many scientist owing to their unique physical properties which make them ideal as reinforcing material for high performance nanocomposites. High performance nanocomposites can be synthesized by combining them with CNTs that enables their usage in numerous industrial applications including flexible electronics [1], mechanical sensors [2-7] electromagnetic interference shielding [8] etc. Fabrication of high performance CNTs based nanocomposites still challenging since CNTs have a great tendency of forming bundles due to strong van der Waals interactions [9, 10]. These bundles and agglomerations cause a deterioration in the mechanical and electrical properties of CNTs based composites [11, 12]. Realization of aforementioned applications of CNTs based nanocomposites can be achieved by ensuring a reliable and

effective dispersion of CNTs. To break down the CNTs bundles or agglomerates and disperse them in surfactant containing solution, several approaches including mechanical methods and physical (non-covalent) or chemical (covalent) processes have been adopted to their surface energies [13, 14]. It has been reported that surface modification of CNTs by introducing functional groups, which interacts with surfactant through polar- polar interaction resulting prevention of CNTs to form bundles that helps to better and more stable dispersion [15]. Chemical methods are surface functionalization methods used to improve properties such as wettability, agglomeration, chemical compatibility. With the functionalization process, the dispersibility, reactivity, processability and biocompatibility of CNTs can be increased [16]. Non-covalent surface treatments are a preferred method because of the ability to adsorb various functional groups to the surface without disturbing the structures of π -bonds in

ARTICLE HISTORY

Received: 16.05.2022

Accepted: 08.11.2022

KEYWORDS

Multiwalled carbon nanotubes, thermoplastic polyurethane, electrospinning, nanofibers

To cite this article: Şanlı A, Cinfer Ş P, Hazar Yoruç A B. 2024. Effects of different types of surfactant treatments on the electromechanical properties of multiwalled carbon nanotubes decorated electrospun nanofibers. *Tekstil ve Konfeksiyon*, 34(1), 11-18

graphene sheets [17]. However, surfactants and polymers that can be used in this functionalization process are limited and their dispersions are not stable. Functionalized CNTs are difficult to re-modify. Covalent functionalization can greatly improve the solubility, dispersibility and chemical compatibility of CNTs. Covalent functionalization occurs when the π -bonds in the basic structures of CNTs are broken, and the functional group is bonded by forming a covalent bond that shares at least one electron with the functional group. It is this deterioration and restructuring in the structure that changes and improves the properties of the CNTs [18-20]. Mechanical methods such as ultrasonication and high shear mixing on the other hand can indeed separate the CNTs from each other. However, with increasing time and power aspect ratio of CNTs can shorten the by breaking the tubes.

For the modification of CNTs in the preparation of CNTs based polymer nanocomposites various surfactants are employed [21-24]. Depending on the polarity of the surfactant head group, surfactants can be categorized into four types, which are non-ionic, anionic, cationic, and amphoteric [25]. Among various surfactants, sodium dodecyl sulfate (SDS) and cetyltrimethylammonium bromide (CTAB) have drawn attention. SDS is an organic compound and it is the most widely studied anionic (negatively charged) surface agent. It consists of a head and tail with amphiphilic properties, consisting of a 12-carbon chain attached to a sulfate group [26]. At low concentrations of SDS, which allows the CNTs to be suspended, CNTs agglomeration can be observed even after ultrasonication. By increasing and optimizing the SDS concentration, a homogeneous carbon nanotube solution appearance can be achieved [27, 28]. CTAB on the other hand is an important cationic (positively charged) surfactant consisting of a head with three methyl and an ammonium group and a tail with 16 carbons [29]. It is used as coating, stabilization and passivation agent. Through CTAB modification sensitivity and detection limits of materials can be improved by increasing their detection performance. To date, there are various studies dealing with the role of the surfactants on the dispersion of CNTs and their mechanisms [30-35]. Zou et al. [35] conducted the absorbance of CNTs: polycarboxylate-based cement superplasticizer at different concentrations at different sonication energies. It was seen that absorbance rate increases gradually with the increase of the sonication power that is proportional to the CNTs concentration. Recently, Rajendran et al. [33] has studied a comparative analysis of the dispersion of CNTs in polar solvents. It was suggested that the degree of affinity CNTs with -COOH group depends on the polarity of the solvent type. Chatterjee et al. [36] investigated the effect of the different surfactants i.e. DOC, SDBS, CTAB, BnzlkCl, and TX405 on the selectivity and sensitivity of CNTs based volatile organic compounds (VOC) biomarkers of lung cancer. For the assessment of the influence of surfactant type on the properties of MWCNTs decorated electrospun nanofibers, there are still various aspects to be investigated. In this work, the effect of dispersion type on the properties of -COOH functionalized MWCNTs-TPU based nanofibrous structures fabricated by

electrospinning technology was investigated. Samples were fabricated by dip coating electrospun TPU nanofibers into MWCNTs based dispersed solution. Dispersion quality of MWCNTs were assessed by UV-Vis and Zeta potential analysis. Results are finally further discussed by assessing FTIR, SEM, 2P-4P probe electrical resistance and uniaxial tensile strain measurements.

2. MATERIAL AND METHOD

2.1 Materials and Chemicals

From Molchem Technologies (London, United Kingdom) purchased industrial -COOH functionalized MWCNTs has 92% purity and 8– 15 nm outer diameter. Thermoplastic polyurethane (TPU) (Elastollan 1185A10) was obtained from Biesterfeld in granule form with 1.12 kg/dm³ density, N, N-Dimethylformamide (DMF), Sodium Dodecyl Sulfate (SDS) and Cetyltrimethylammonium bromide (CTAB) were bought from Labor Teknik (Istanbul, Turkey), Akbel Kimya (Bursa, Turkey) and Alfa Aesar (Thermo Fisher GmbH, Germany), respectively. All chemicals used in this study were used and received without any further treatment.

2.2 Characterization of electrospun MWCNTs/TPU Nanofibers

To understand the morphology as well as complex piezoresistive behavior of MWCNTs/TPU nanofibers, various characterization methods including SEM, U-Vis, FTIR, Zeta potential, 2-point and 4-point probe resistance measurements and uniaxial loading measurements were conducted. For the electrospinning process, samples were electrospun by an electrospinning unit (Inovenso NS24XP). SEM analysis (Zeiss Supra 55 VP) was used to see the microstructure and dispersion quality of the fibers decorated with MWCNTs. To do this, all samples were coated with gold and all analysis was performed at 10 kV and 13 mm WD (work distance). In order to determine the stability of the mixed solutions containing MWCNTs/surfactant agents, samples were analyzed by UV-Vis Spectroscopy (NanoPlus). For the precipitation of the MWCNTs contained solutions for UV-Vis analysis, the solutions were first centrifuged by a centrifugation device (Hermle Z206A) at 6000 rpm for 30 minutes and then passed through a 0.2 μ m Polytetrafluoroethylene (PTFE) filter syringe. FTIR analysis was performed with Bruker brand Tensor 27 model device in order to see interface interaction between TPU fibers and dispersed MWCNTs structures. To perform electrical measurements (2-point probe resistance measurement), copper tapes were applied on the both side of films with a distance of 3 cm. A digital multimeter (Fluke 179) with a resolution of 0.1 Ω was then used to measure the electrical resistance of the electrospun TPU films coated with MWCNTs. Moreover, a high precision instrument (Keithley 2400) was used to evaluate surface resistivity measurements (4-point probe resistance measurement). The average of the measurements taken from 10 different locations in the area between the copper wires was calculated. Subsequently, to see the relative

resistance change of the electrospun MWCNTs decorated TPU samples under uniaxial strain, a custom-made uniaxial strain device was used. Here, samples were fixed from one side and pulled from the other side with a strain rate of 1 mm/hour through a system controlled by a microprocessor (Arduino Nano) and a stepper motor (17HS4401 Nema 17 Step Motor). During the uniaxial strain measurements, corresponding resistance values was measured by a Fluke 179 multimeter.

2.3 Synthesis of electrospun MWCNTs/TPU Nanofibers

For the synthesis of MWCNTs decorated electrospun TPU nanofibers shown in Figure 1, TPU granules were first dried in a vacuum oven at 100 °C for 3 h to remove any absorbed moisture on them. After that, 1.5 g of TPU granules were dissolved in 10 ml of DMF solvent. Here, TPU solution was prepared without any additives by mixing it with DMF mixture by magnetic stirrer for 2 h at 60 °C to ensure complete dissolution and a homogeneous solution for electrospinning. After that, as a first part of synthesis of MWCNTs decorated electrospun TPU fibrous film, TPU:DMF mixture was taken to a 10 ml syringe and placed in the syringe pump. Subsequently, dissolved TPU solution was electrospun by electrospinning unit (Inovenso NS24XP) with following parameters: applied voltage (15 kV), collector speed (700 rpm), feed rate (3 ml/h), tip to collector distance (20 cm) and spinning time (2 h). Here, the tip of the syringe was set to move 40 mm from left to right at the speed of 20 mm/h. The ambient temperature and humidity were set $25 \pm 2^\circ\text{C}$ and $60 \pm 5\text{ RH}\%$, respectively. Electrospun thin layer of TPU was then removed carefully from the thin aluminum layer wrapped around the rotating collector with an average diameter of 10 cm to 10 cm. Then in total 3 samples were cut in the dimensions of 3 cm x 6

cm for further characterizations. As a next step shown in Figure 2, MWCNTs were dispersed in two different surfactants, which are SDS and CTAB. To do this, MWCNTs/surfactant solutions for a pre-determined concentration of 1 wt.%/v were prepared. Prepared solutions were sonicated in ultrasonic bath for 1 h. Finally, electrospun samples were immersed in MWCNTs based dispersions and this mixture further sonicated in ultrasonic bath for 60 min to ensure the electrical conductivity. Then, samples were washed several times by distilled water and finally dried in oven at 60 °C for 1h. The appearance of the electrospun TPU sample is white color while it turned to the black after dipping into the MWCNTs dispersion.

3 RESULTS AND DISCUSSION

Obtained results with respect to microscopic tests, UV-Vis, FTIR, Zeta potential as well as electrical properties of MWCNTs decorated electrospun MWCNTs/ TPU for different MWCNTs dispersions are given in detailed below. From the SEM images taken for electrospun TPU nanofibers (Figure 3), it is seen that electrospun TPU fibers exhibit relatively smooth and homogenous distribution. From the fiber thickness distribution measurements taken by ImageJ software [37] (Figure 4), the mean value of TPU fibers thickness are around $1.28 \pm 0.788\ \mu\text{m}$. Further, the morphology of dispersed MWCNTs decorated electrospun TPU nanofibers shown in Figure 5. Compared to the MWCNTs: CTAB/TPU samples MWCNTs are dispersed more homogeneously and therefore attached more on the TPU fibers for MWCNTs: SDS/TPU samples. Hence, it was expected that this will led to better electrical properties due to the contribution of more MWCNTs to the network.

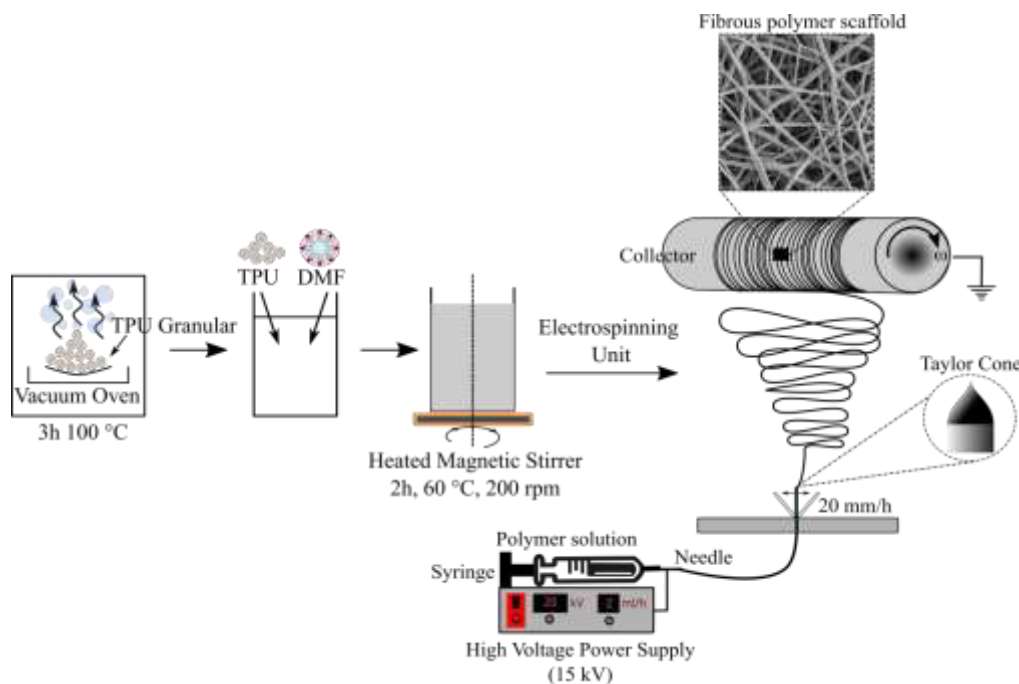


Figure 1. A detailed schematic illustration of the fabrication process of electrospun TPU and corresponding electrospinning unit

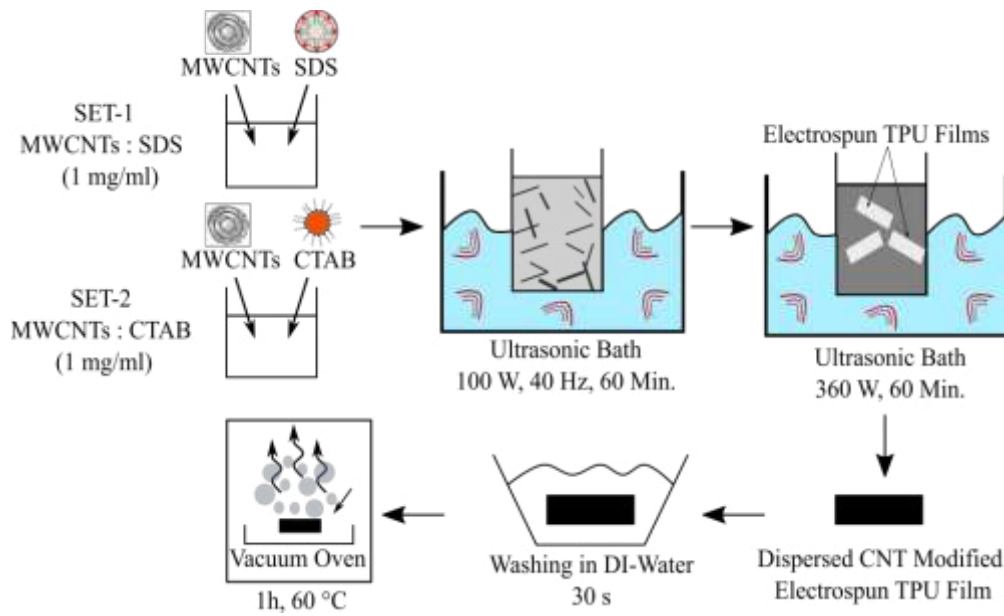


Figure 2. Schematic representation of dispersion of MWCNTs at different surfactants and decoration of electrospun TPU nanofibers by dipping them in dispersed MWCNTs-surfactant solutions

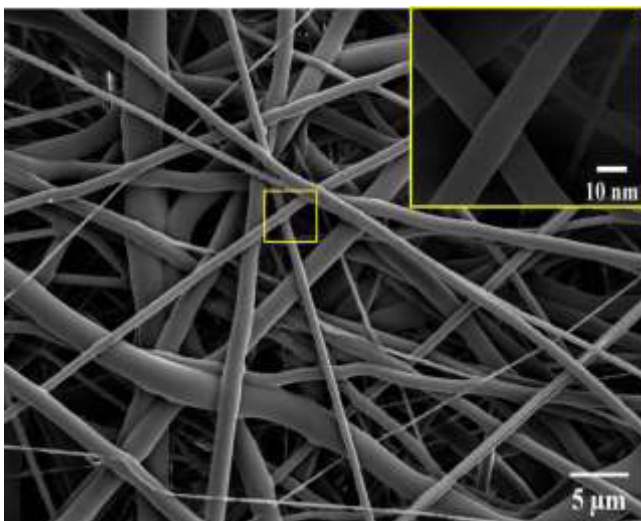


Figure 3. Morphology and structure of electrospun TPU fibers. Inset shows closer image of morphology of TPU fibers

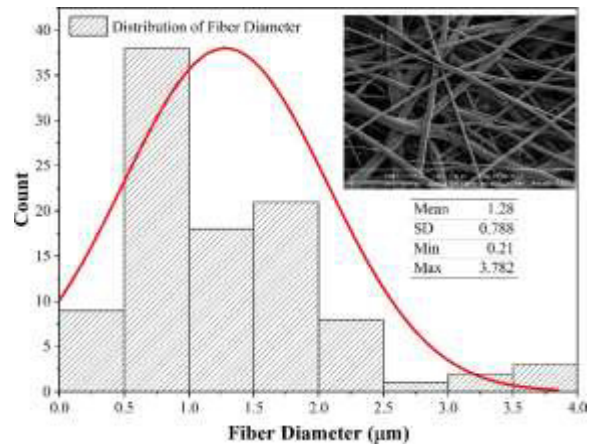


Figure 4. Distribution of fiber diameter of electrospun TPU fibers calculated by ImageJ software

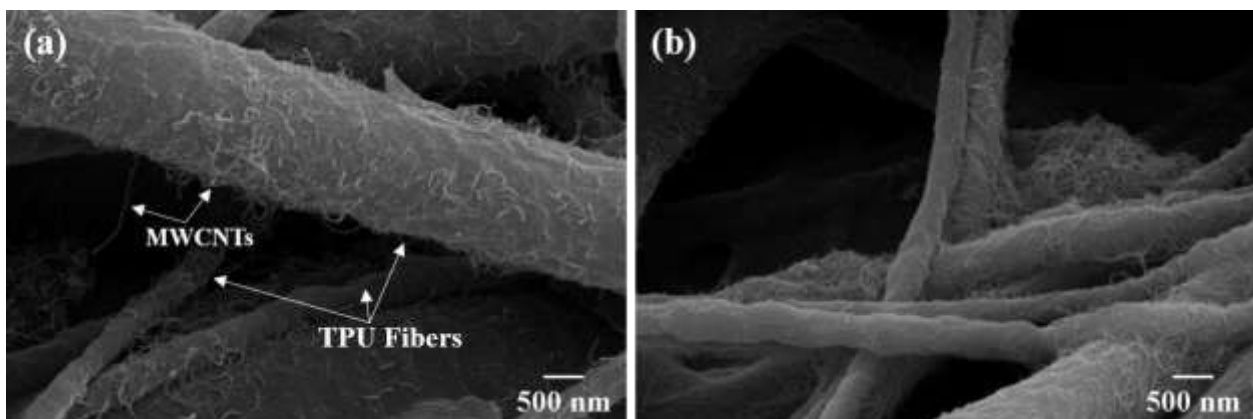


Figure 5. SEM image of electrospun (a) MWCNTs-SDS/TPU and (b) MWCNTs-CTAB/TPU sample. Here, MWCNTs concentration is set for both sample as 1 wt.%/v

UV-Vis analysis was performed to determine the dispersion efficiency of MWCNTs in MWCNTs-surfactant solutions. Owing to 1D van Hove singularities, individual CNTs exhibit characteristic bands and they are active in the UV-vis region. Whereas, agglomerated carbon nanotubes do not exhibit active behavior at wavelengths between 200-1200 nm [38-40]. Therefore, it is possible to relate the amount of individual CNTs dispersed in solution to the absorption intensity [41]. Figure 6 shows the UV-Vis spectra of bundled MWCNTs, MWCNTs-SDS and MWCNTs-CTAB solutions. It is clear to see that non-sonicated MWCNTs show almost no absorption in the UV-spectrum (see inset Figure 6a) due to existence of big agglomerates due to strong van der Waals attractions between the CNTs [42]. Introduction of SDS and CTAB surfactants with provided mechanical energy with sonication overcame the strong van der Waals interactions that lead to disentanglement of MWCNTs. Through UV-Vis spectra, it is seen that absorbance for both MWCNTs-SDS and MWCNTs-CTAB solutions give maximum peak between 200 nm and 250 nm and this absorbance gradually decreases [43]. It is important to note that, compared to the CTAB, dispersions with SDS surfactant give higher absorbance indicating better dispersion which lead to higher electrical conductivity.

Moreover, in order to determine the stability of the dispersions, zeta potential measurements for MWCNTs-SDS and MWCNTs-CTAB were conducted shown in Figure 7b. Basically, as shown in inset Figure 7b, zeta potential is an electrical potential at slipping plane or at boundary of the double layer which is a technique for the evaluation of the surface charge of nanoparticles including CNTs in a colloidal solution. Here, nanotubes have a charge on the surface that attracts a thin layer of ions to the nanotube surface which is called stern layer [44]. To evaluate this, the surface of MWCNTs was modified by cationic (CTAB) and anionic (SDS) surfactant at a fixed MWCNTs concentration (1 wt.%/v) using sonication technique. From the conducted studies, it is indicated that the magnitude of zeta potential is predictive for the colloidal stability of the dispersion and a zeta potential value greater than ± 60 mV indicates that the dispersions have excellent stability [45]. Obtained results show that MWCNTs-CTAB dispersions have peaks at around 71 mV and 72 mV, whereas MWCNTs-SDS dispersions have -101 mV and -96 mV zeta potential values, indicating that the MWCNT have better and more stable dispersion with SDS rather than CTAB due to higher level of zeta potential at same concentration and dispersion parameters. Positive values of MWCNTs-CTAB and negative values for MWCNTs-SDS based dispersions are attributed to the absorption of cationic and anionic charge on the MWCNTs surface [46]. Depending on the nature of the surfactants, cation and anion are forming. Here, surfactants are absorbed in the MWCNTs surface where either positive or

negative change result in electrostatic repulsion between the molecules that leads to stabilization of the nanotubes colloids [47].

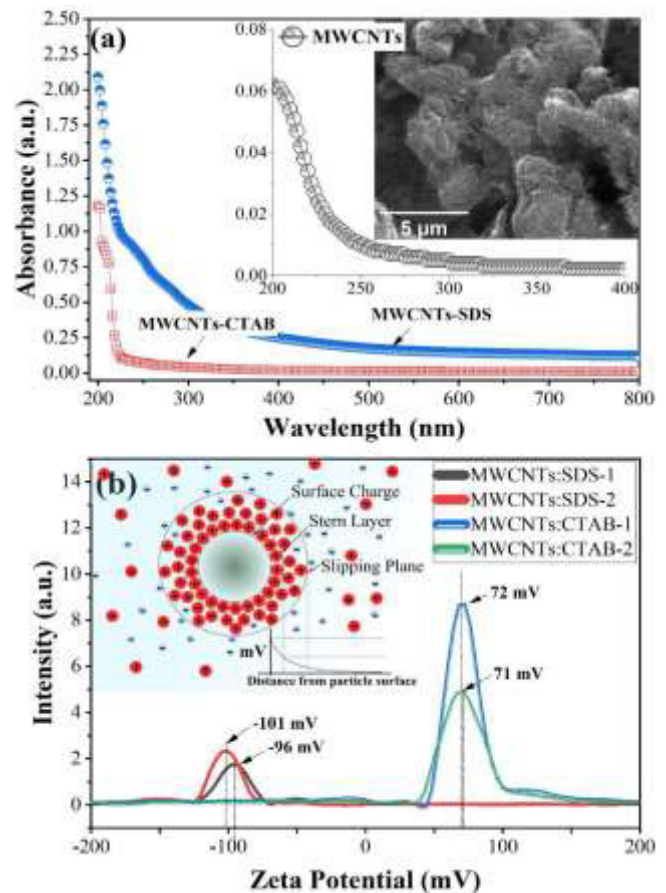


Figure 6. (a) UV-Vis spectra and (b) Zeta potential of MWCNTs-SDS and MWCNTs-CTAB dispersions. Inset figure in (a) shows UV-Vis and SEM image of non-dispersed MWCNTs and (b) shows the basic working principle of zeta potential

Furthermore, MWCNTs-surfactant/TPU nanofibrous structures were examined by FT-IR device to analyze the interface interaction between TPU fibers and dispersed MWCNTs structures. The FT-IR spectrum of the electrospun TPU film, MWCNTs-SDS/TPU and MWCNTs-CTAB/TPU are given in Figure 7a. Here, it is seen that for the electrospun neat TPU fibers, the peak at 3302 cm^{-1} is the characteristic N-H stretching band of the urethane structure, and the peak at 1728 cm^{-1} and at 1699 cm^{-1} are indicative of the free carbonyl group in the urethane bonds ($-\text{H}-\text{N}-\text{COO}$) and free H bonded C-O bonds respectively. The peaks at 2920 cm^{-1} and 2820 cm^{-1} are characteristics of medium alkenes-CH stretching vibrations. Also, the peak at the wavelength of 1525 cm^{-1} correlates with C-H. In addition, the C-O and C-O-C bands are available at wavelengths of 1219 cm^{-1} and 1074 cm^{-1} , respectively. Peaks at similar wavelengths were also observed in the FT-IR spectrum in the literature [48, 49]. Moreover, the FT-IR spectra of the MWCNTs decorated films match the spectra of the TPU film. It is seen that bathochromic shift (red shift) occurs as the TPU peaks shift

to the right in the coated films. Related studies indicating that the red shift can be attributed to the effects of increasing electron conjugation of conductive and semiconductor materials and the effect of increasing electron conjugation of CNTs [50-52]. Namely, abovementioned shifts indicate strong interactions between TPU chains and MWCNTs that is critical for the enhancement of electromechanical properties of electrospun MWCNTs decorated TPU fibrous structures. Subsequently, to study the effect of different type of surfactants on the electrical properties of electrospun MWCNTs-surfactant/TPU nanofibrous structures were measured by 2-point and 4-point probe resistance measurements given in Figure 7b. From the 2-points probe resistance measurements, it is calculated that electrospun samples based on MWCNTs-SDS/TPU and MWCNTs-CTAB/TPU have a resistance value around 25 k Ω and 31.3 k Ω , respectively. From the 4-point surface resistance measurements these resistance values decreased to 19 k Ω \pm 3.52% and 27 k Ω \pm 4.79% for MWCNTs-SDS/TPU and MWCNTs-CTAB/TPU samples, respectively. These findings suggest that MWCNTs are better dispersed in SDS surfactant that leads lower resistance values.

Finally, to see the effect of surfactant on the strain sensing characteristics of electrospun nanofibers, samples were undergone to uniaxial loading with the tensile speed of 1 mm/h and relative resistance changes at each strain value were recorded. It is seen that both samples show strain sensitivity with two linear regions. As previously reported [6], the piezoresistive working mechanism of MWCNTs decorated electrospun nanofibers can be explained as follows (see inset Figure 7c). At low strain range (region I) up to 36%, randomly oriented TPU fibers starts to move away from each other that lead to increase in resistance value. With the further increase of uniaxial strain (Region II), the distance between dispersed MWCNTs on the TPU fibers increase that results in a rapid increase in resistance [53]. Up to 50% of tensile strain, the relative resistance change for the MWCNTs-CTAB sample is nearly 264%, this value gets to 292% for the MWCNTs-SDS/TPU sample, which is attributed again a better dispersion of MWCNTs that contributes the piezoresistivity of nanofibrous structure with enhanced sensitivity. Namely, formation of more homogeneously dispersed MWCNTs networks enhance the overall relative resistance change under uniaxial applied strain.

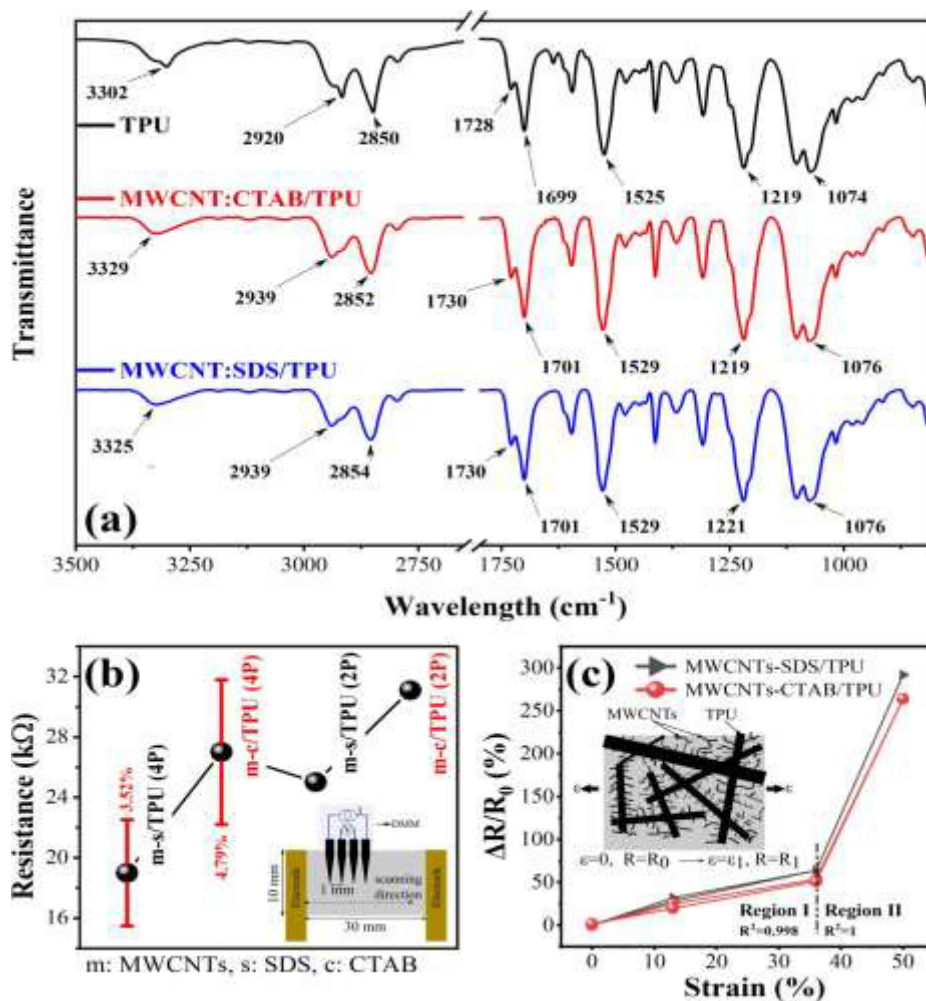


Figure 7. (a) FT-IR Spectra, (b) 2-point and 4-point probe resistance measurements and (c) uniaxial tensile strain measurement of electrospun MWCNTs-SDS/TPU and MWCNTs-CTAB/TPU samples. Inset figure in (b) and (c) shows the measurement setup for 4-point probe resistance measurement and piezoresistive working mechanism of electrospun sample under uniaxial tensile strain

4 CONCLUSION

This study investigates the effect of surfactant type (SDS and CTAB) on the electromechanical properties of MWCNTs decorated flexible electrospun TPU nanofibers. From the morphological investigations of electrospun nanofibers, it is seen that TPU fibers are homogeneously distributed and for both surfactant type and slightly better dispersion for MWCNTs-SDS solution based nanofibers were formed. Dispersion characterizations based on UV-Vis and zeta potential analysis also suggest that MWCNTs-SDS solutions have higher absorbance. Zeta potential results showing that MWCNTs dispersion with SDS have higher level of zeta potential than CTAB solutions which leads again better and more stable dispersion. FTIR analysis of the MWCNTs decorated TPU nanofibers shows a shift at peaks that is attributed to increasing electron conjugation of carbon nanotubes. From both 2P and 4P electrical

resistance measurement MWCNTs-SDS/TPU samples has lower resistance owing to better dispersion of MWCNTs. Subsequently, from the uniaxial tensile strain measurement, MWCNTs-SDS dispersions decorated electrospun TPU nanofibers give higher sensitivity which is as a consequence of better dispersion of MWCNTs that are responsible for piezoresistivity of nanofibers. Obtained results of this study provide new insights into the tailoring the electromechanical properties of MWCNTs decorated electrospun nanofibers by adjusting the type of the surfactant.

Acknowledgement

This study was funded by The Scientific and Technological Research Council of Turkey (Turkiye Bilimsel ve Teknolojik Arastirma Kurumu- TÜBİTAK) (Grant number 121M137).

REFERENCES

1. Park S, Vosguerichian M, Bao Z. 2013. A review of fabrication and applications of carbon nanotube film-based flexible electronics. *Nanoscale* 5(5), 1727-1752.
2. Sanli A. 2020. Investigation of temperature effect on the electrical properties of MWCNTs/epoxy nanocomposites by electrochemical impedance spectroscopy. *Advanced Composite Materials* 29(1), 31-41.
3. Sanli A, Kanoun O. 2020. Electrical impedance analysis of carbon nanotube/epoxy nanocomposite-based piezoresistive strain sensors under uniaxial cyclic static tensile loading. *Journal of Composite Materials* 54(6), 845-855.
4. Sanli A, Benchirouf A, Müller C, Kanoun O. 2017. Piezoresistive performance characterization of strain sensitive multi-walled carbon nanotube-epoxy nanocomposites. *Sensors and Actuators A: Physical* 254, 61-68.
5. Sanli A, Müller C, Kanoun O, Elibol C, Wagner MFX. 2016. Piezoresistive characterization of multi-walled carbon nanotube-epoxy based flexible strain sensitive films by impedance spectroscopy. *Composites Science and Technology* 122, 18-26.
6. Sanli A, Yıldız K, Uzun M. 2021. Experimental study of the impact of electrospinning parameters on the electromechanical properties of strain sensitive electrospun multiwalled carbon nanotubes/thermoplastic polyurethane nanofibers. *Advanced Composite Materials* 1-16.
7. Kanoun O, Müller C, Benchirouf A, Sanli A, Dinh TN, Al-Hamry A, Bu L, Gerlach C, Bouhamed A. 2014. Flexible carbon nanotube films for high performance strain sensors. *Sensors* 14(6), 10042-10071.
8. Al-Saleh MH, Sundararaj U. 2009. Electromagnetic interference shielding mechanisms of CNT/polymer composites. *Carbon* 47(7), 1738-1746.
9. Sandler JKW, Pegel S, Cadek M, Gojny F, Van Es M, Lohmar J, Blau WJ, Schulte K, Windle AH, Shaffer, MSP. 2004. A comparative study of melt spun polyamide-12 fibres reinforced with carbon nanotubes and nanofibres. *Polymer* 45(6), 2001-2015.
10. Narh KA, Jallo L, Rhee KY. 2008. The effect of carbon nanotube agglomeration on the thermal and mechanical properties of polyethylene oxide. *Polymer Composites* 29(7), 809-817.
11. Ma PC, Siddiqui NA, Marom G, Kim JK. 2010. Dispersion and functionalization of carbon nanotubes for polymer-based nanocomposites: A review. *Composites Part A: Applied Science and Manufacturing* 41(10), 1345-1367.
12. Vaisman L, Wagner HD, Marom G. 2006. The role of surfactants in dispersion of carbon nanotubes. *Advances in Colloid and Interface Science* 128, 37-46.
13. Duan WH, Wang Q, Collins F. 2011. Dispersion of carbon nanotubes with SDS surfactants: A study from a binding energy perspective. *Chemical Science* 2(7), 1407-1413.
14. Yook JY, Jun J, Kwak S. 2010. Amino functionalization of carbon nanotube surfaces with NH₃ plasma treatment. *Applied Surface Science* 256(23), 6941-6944.
15. Rahman MJ, Mieno T. 2016. Safer production of water dispersible carbon nanotubes and nanotube/cotton composite materials. In *Carbon Nanotubes-Current Progress of their Polymer Composites*. IntechOpen.
16. Labille J, Pelinovskaya N, Botta C, Bottero JY, Masion A. 2016. Fabrication of Graphene or Graphene Fabrication.
17. Georgakilas V, Otyepka M, Bourlino AB, Chandra V, Kim N, Kemp KC, Hobza P, Zboril R, Kim KS. 2012. Functionalization of graphene: covalent and non-covalent approaches, derivatives and applications. *Chemical Reviews* 112(11), 6156-6214.
18. Ngo CL, Le QT, Ngo TT, Nguyen DN, Vu MT. 2013. Surface modification and functionalization of carbon nanotube with some organic compounds. *Advances in Natural Sciences: Nanoscience and Nanotechnology* 4(3), 035017.
19. Rausch J, Zhuang RC, Mäder E. 2010. Surfactant assisted dispersion of functionalized multi-walled carbon nanotubes in aqueous media. *Composites Part A: Applied Science and Manufacturing* 41(9), 1038-1046.
20. Syrgiannis Z, Hauke F, Röhr J, Hundhausen M, Graupner R, Elemes Y, Hirsch A. 2008. Covalent sidewall functionalization of SWNTs by nucleophilic addition of lithium amides. *European Journal of Organic Chemistry* 2008(15), 2544-2550.
21. Lin Y, Ng KM, Chan CM, Sun G, Wu J. 2011. High-impact polystyrene/halloysite nanocomposites prepared by emulsion polymerization using sodium dodecyl sulfate as surfactant. *Journal of Colloid and Interface Science* 358(2), 423-429.
22. Zhang G, Wang F, Dai J, Huang Z. 2016. Effect of functionalization of graphene nanoplatelets on the mechanical and thermal properties of silicone rubber composites. *Materials* 9(2), 92.



23. Emami Z, Meng Q, Pircheraghi G, Manas-Zloczower I. 2015. Use of surfactants in cellulose nanowhisker/epoxy nanocomposites: effect on filler dispersion and system properties. *Cellulose* 22(5), 3161-3176.
24. Zang J, Wan YJ, Zhao L, Tang LC. 2015. Fracture behaviors of TRGO-Filled epoxy nanocomposites with different dispersion/interface levels. *Macromolecular Materials and Engineering* 300(7), 737-749.
25. Shamsuri AA, Md. Jamil SNA. 2020. A short review on the effect of surfactants on the mechanico-thermal properties of polymer nanocomposites. *Applied Sciences* 10(14), 4867.
26. Choudhary M, Kamil SM. 2020. Phase diagram study of sodium dodecyl sulfate using dissipative particle dynamics. *ACS Omega* 5(36), 22891- 22900.
27. Miraç A, Toçuoğlu U, Kayış F, Akbulut H. 2016. Karbon Nano Tüplerin Dispersiyonuna SDS Yüzey Aktif Maddesinin Etkisi. *Bilecik Şeyh Edebali Üniversitesi Fen Bilimleri Dergisi* 3(1), 16-19.
28. Niraula TP, Bhattarai A, Chatterjee SK, Biratnagar N. 2014. Sodium dodecylsulphate: A very useful surfactant for scientific investigations. *Journal of Knowledge and Innovation* 2(1), 111-113.
29. Nnyigide OS, Lee SG, Hyun K. 2019. In silico characterization of the binding modes of surfactants with bovine serum albumin. *Scientific Reports* 9(1), 1-16.
30. Cui H, Yan X, Monasterio M, Xing F. 2017. Effects of various surfactants on the dispersion of MWCNTs-OH in aqueous solution. *Nanomaterials* 7(9), 262.
31. Wang H. 2009. Dispersing carbon nanotubes using surfactants. *Current Opinion in Colloid & Interface Science* 14(5), 364-371.
32. Madni I, Hwang CY, Park SD, Choa YH, Kim HT. 2010. Mixed surfactant system for stable suspension of multiwalled carbon nanotubes. *Colloids and Surfaces A: Physicochemical and Engineering Aspects* 358(1-3), 101-107.
33. Rajendran D, Ramalingame R, Adiraju A, Nouri H, Kanoun O. 2022. Role of solvent polarity on dispersion quality and stability of functionalized carbon nanotubes. *Journal of Composites Science* 6(1), 26.
34. Ndiaye AL, Varenne C, Bonnet P, Petit E, Spinelle L, Brunet J, Pauly A, Lauron B. 2012. Elaboration of SWNTs-based gas sensors using dispersion techniques: Evaluating the role of the surfactant and its influence on the sensor response. *Sensors and Actuators B: Chemical* 162(1), 95- 101.
35. Zou B, Chen SJ, Korayem AH, Collins F, Wang CM, Duan WH. 2015. Effect of ultrasonication energy on engineering properties of carbon nanotube reinforced cement pastes. *Carbon* 85, 212-220.
36. Chatterjee S, Castro M, Feller JF. 2015. Tailoring selectivity of sprayed carbon nanotube sensors (CNT) towards volatile organic compounds (VOC) with surfactants. *Sensors and Actuators B: Chemical* 220, 840-849.
37. Schneider CA, Rasband WS, Eliceiri KW. 2012. NIH Image to ImageJ: 25 years of image analysis. *Nature methods* 9(7), 671-675.
38. Kataura H, Kumazawa Y, Maniwa Y, Umezū I, Suzuki S, Ohtsuka Y, Achiba Y. 1999. Optical properties of single-wall carbon nanotubes. *Synthetic Metals* 103(1-3), 2555-2558.
39. Hamada N, Sawada SI, Oshiyama A. 1992. New one-dimensional conductors: Graphitic microtubules. *Physical Review Letters* 68(10), 1579.
40. Saito R, Fujita M, Dresselhaus G, Dresselhaus UM. 1992. Electronic structure of chiral graphene tubules. *Applied Physics Letters* 60(18), 2204-2206.
41. Jiang L, Gao L, Sun J. 2003. Production of aqueous colloidal dispersions of carbon nanotubes. *Journal of Colloid and Interface Science* 260(1), 89-94.
42. Hertel T, Walkup RE, Avouris P. 1998. Deformation of carbon nanotubes by surface van der Waals forces. *Physical Review B* 58(20), 13870.
43. Yu J, Grossiord N, Koning CE, Loos J. 2007. Controlling the dispersion of multi-wall carbon nanotubes in aqueous surfactant solution. *Carbon* 45(3), 618-623.
44. Lee SH, Woo SP, Kakati N, Kim DJ, Yoon YS. 2018. A comprehensive review of nanomaterials developed using electrophoresis process for high-efficiency energy conversion and storage systems. *Energies* 11(11), 3122.
45. Kumar A, Dixit CK. 2017. Methods for characterization of nanoparticles. In *Advances in nanomedicine for the delivery of therapeutic nucleic acids* (pp. 43-58). Woodhead Publishing.
46. Bai Y, Gao J, Wang C, Zhang R, Ma W. 2016. Mixed surfactant solutions for the dispersion of multiwalled carbon nanotubes and the study of their antibacterial activity. *Journal of Nanoscience and Nanotechnology* 16(3), 2239-2245.
47. de la Cruz EF, Zheng Y, Torres E, Li W, Song W, Burugapalli K. 2012. Zeta potential of modified multi-walled carbon nanotubes in presence of poly (vinyl alcohol) hydrogel. *International Journal of Electrochemical Science* 7(4), 3577-3590.
48. Ren M, Zhou Y, Wang Y, Zheng G, Dai K, Liu C, Shen C. 2019. Highly stretchable and durable strain sensor based on carbon nanotubes decorated thermoplastic polyurethane fibrous network with aligned wave-like structure. *Chemical Engineering Journal* 360, 762-777.
49. Li Y, Zhou B, Zheng G, Liu X, Li T, Yan C, Cheng C, Dai K, Liu C, Shen C, Guo Z. 2018. Continuously prepared highly conductive and stretchable SWNT/MWNT synergistically composited electrospun thermoplastic polyurethane yarns for wearable sensing. *Journal of Materials Chemistry C* 6(9), 2258-2269.
50. Ugraskan V, Karaman F. 2021. Polyaniline/Graphitic carbon nitride nanocomposites with improved thermoelectric properties. *Journal of Electronic Materials* 50(6), 3455-3461.
51. Ugraskan V, Tari E, Yazici O. 2021. Poly (3, 4-Ethylenedioxythiophene): Poly (Styrene Sulfonate)/Boron carbide hybrid composites with improved thermoelectric performance. *Journal of Electronic Materials* 50(10), 5618-5624.
52. Rohlřing M. 2012. Redshift of excitons in carbon nanotubes caused by the environment polarizability. *Physical Review Letters* 108(8), 087402.
53. Wang Y, Hao J, Huang Z, Zheng G, Dai K, Liu C, Shen C. 2018. Flexible electrically resistive-type strain sensors based on reduced graphene oxide-decorated electrospun polymer fibrous mats for human motion monitoring. *Carbon* 126, 360-371.

Exploratory Study on the Properties of Compact Three-Roving Yarn: Comparison The Properties of Compact Spun, Compact Siro-Spun and Compact Three-Roving Yarns

Murat Demir¹  0000-0001-8670-5412
Musa Kılıç¹  0000-0003-1171-356X
Serdar Sayın²  0000-0001-9029-0387
Zeki Kırıl³  0000-0002-9154-0509
Furkan Balduk⁴  0000-0002-5501-8430
Kıymet Kübra Denge⁴  0000-0003-0579-2046

¹Dokuz Eylül University / Department of Textile Engineering / Tınaztepe Campus, Buca, İzmir, Türkiye

²The Graduate School of Natural and Applied Sciences, Department of Mechatronics Engineering, Dokuz Eylül University, Turkey

³Department of Mechanical Engineering, Dokuz Eylül University, Turkey

⁴KİPAŞ Mensucat R&D Center, Turkey

Corresponding Author: Murat Demir, murat.demir@deu.edu.tr

ABSTRACT

This study presents the novel compact three-rovings technology which developed on the working principle of siro-spun and compact spinning technologies. In the study, auxiliary parts of siro-spun and pneumatic compact spinning are newly designed for the production of compact three-rovings yarns. The properties of new compact three-rovings yarns were compared with compact spun and compact siro-spun yarns that produced at the same yarn count and at the same twist level from natural, synthetic and regenerated fibers. Besides, three-types of yarns were also used in the weft direction for the production of the woven fabric. Comparing yarn and fabric properties showed that, compact three-rovings yarns have similar results to commercially used yarns such as compact and siro-spun yarns in general. In addition, it should also be noted that three-rovings yarn can be also used for specific purposes owing to its composite structure.

1. INTRODUCTION

Recently, the continuous development of market demand, needs of yarn in different structures, and demand for producing yarn in a more economic way lead to the emergence of alternative spinning technologies [1]. During this period, developing technologies from ring spinning, which is the most widely used and also produces the optimum quality of yarn, provides the rapid spread of alternative technologies and better-quality yarn production. Compact spinning and siro-spun can be the example of the most widely used alternative spinning technologies that developed from ring spinning by adding some auxiliary parts.

The basis of the compact spinning technology is to reduce the spinning triangle that occurs after the front cylinder by negative air pressure and provides more fibers to join the

yarn structure. Currently, there are number of available methods that the condensing zones are created with different auxiliary parts, such as perforated drum compacting, lattice apron compacting, and mechanical compacting. In the literature, many researchers underline the fact that taking advantage of compacting technology results in better yarn qualities than conventional systems. Compared the conventional yarns, compact yarns have better hairiness, packing densities, and unevenness [3-7]. In addition to the investigation of yarn properties, studies that compared fabric properties also showed that fabrics produced from compact yarns have better properties. Raja *et al.*[8] compared the fabric properties produced from ring, compact and ring-compact folded yarns and claimed that fabrics produced from compact folded yarns have higher water and air permeability values. Akhtar *et al.*[9]

To cite this article: Demir M, Kılıç M, Sayın S, Kırıl Z, Balduk F, Denge K K. 2024. Exploratory Study on the Properties of Compact Three-Roving Yarn: Comparison The Properties of Compact Spun, Compact Siro-Spun and Compact Three-Roving Yarns *Tekstil ve Konfeksiyon*, 34(1), 19-31.

compared the woven fabric properties that produced from ring, compact, rotor, and vortex yarns, and results showed that compact yarns and its fabrics have the highest tensile strength. Kim [10] investigated the properties of ring, compact, and vortex yarns and their knitted fabrics. Results showed that compact yarns have better irregularity and imperfection values than ring and vortex yarns and fabrics produced from compact yarns have the higher thermal conductivity than others. Kaynak and Celik [11] compared the ring, compact, siro spun yarns and thermophysiological comfort properties of the fabrics produced from those yarns. Results showed that compact yarns have better unevenness, imperfections and hairiness values than ring and siro-spun yarns. Comparing fabric properties showed that fabrics produced from compact and ring yarns have better abrasion resistance than siro-spun yarns.

Siro-spun is the other derivative spinning technology that developed from the conventional system and produces two-ply yarn structure in a single process. The basis of siro-spun technology is to feed two separate rovings into the drafting zone with the help of the roving funnel and delivery cylinder [12]. In siro-spun spinning, the structure of the spinning triangle, which occurs between the front cylinder and yarn formation point, is an important production parameter and directly related to roving space. Effects of the spinning triangle on siro-spun yarns have been investigated and researches pointed out that until the optimum level increasing roving space has a positive influence on yarn properties and after a certain level, greater roving space negatively affect yarn quality [13-18]. In the studies that compare the properties of siro-spun yarns with other spun technologies also showed that siro-spun yarns have better hairiness and unevenness values than conventional yarns [3,17,19,20]. In addition, compact siro-spun is the combination of the compact and siro-spun technologies and researches showed that compact siro-spun yarns are in more compact structure than compact yarns, have better hairiness values than siro-spun yarns and have better strength and evenness properties than ring yarns [21-22].

Three roving spinning has been the subject of many researches in recent years, due to its composite structure that allows more than one raw material in a single yarn structure, and also less production process than three-ply yarns that have a similar structure. In the literature, some researchers investigated the effects of fiber length, fiber fineness, distribution of the fibers in the yarn cross-section [23-25]. In the studies that compared three-roving and three-ply yarns showed that three-roving yarns have better hairiness, similar mechanical properties, but, imperfections and unevenness properties need to be improved [26-27]. In some studies, researchers also investigated the production parameters and the effects of roving space on the spinning triangle. In three-roving yarns, the structure of the spinning triangle is directly related to roving space and different spaces can cause more than one yarn formation point, eventually uneven yarn structure [28]. However, studies on

three-roving spinings are mostly focused on developing from conventional ring spinning [26-27 and 30]. There are also available studies about producing three roving yarns but these studies are mainly about producing core spun yarn structures [28-29].

It is seen from related literature that three-roving yarn technology is a promising spinning method that could provide superior yarn properties and economically competitive advantages. This study mainly presents the benefits of compacting effect and its application in three-roving yarn production to produce three roving yarns with better qualities. In the experimental part of the study, novel compact three-roving yarns were produced and compared with compact and compact siro-spun yarns in order to see the differences between compact three-roving and commercially used derivative yarns. For the production of compact three-roving yarns, auxiliary parts of pneumatic compact spinning with perforated drum and siro-spun technologies such as roving funnel, delivery cylinder, suction insert, and air-suction guides were redesigned. Newly designed auxiliary parts were assembled on pneumatic compact spun technology. Ne 50/1 compact spun, Ne 100/2 compact siro-spun, and Ne 150/3 compact three-roving yarns were produced at the twist level $\alpha_e=4.12$. Later, these yarns were used for woven fabric production. Properties of the yarns and fabrics were measured and statistically analysed at the confidence level of 95%.

2. MATERIAL AND METHOD

2.1 Material

In this study, compact, compact siro-spun and compact three-roving yarns were produced from all main material groups and physical, mechanical, and structural properties were measured. Cotton, Modal (1.3 dtex and 38 mm), PES (1.3 mm dtex and 38 mm) were used from natural, regenerated and synthetic fiber groups, respectively. HVI results of cotton fibers are given in Table 1.

Table 1. Properties of cotton fibers (HVI results)

Fiber Properties	Averaged Value
Fineness (microner index)	4.0
Length (mm)	37.4
Tenacity (cN/tex)	45.5
Elongation (%)	5.7
SCI	214
Uniformity (%)	86.7
Maturity	4.6
SFI (%)	8.6

Ne 50/1 compact yarns, Ne 100/2 compact siro-spun yarns, Ne 150/3 compact three-roving yarns with $\alpha_e=4.12$ twist multiplier were produced from 100% cotton, 100% Modal, 100% PES fibers. Experimental design of the yarn production is given in Table 2. In addition, these yarns were used in weft direction in plain weave structure of fabric production and structural details of fabrics are given in Table 3. Ne 50/1 compact combed cotton yarns were used in warp direction. All slivers used in the study were

produced with Rieter B34 Bale opener, Rieter A81 UniBlend, Rieter A79 UniStore and Rieter C70. Rieter SBD-24 draw frame was used for drawing process. All yarns were produced with Rieter K 45 compact spinning machine simultaneously, therefore in order to obtain same count for all yarn types, Ne 1.2 rovings for compact spun yarns, Ne 2.4 rovings for compact siro-spun yarns and Ne 3.6 rovings for compact three-roving yarns were produced with Marzoli FTSDN roving frame. For compact three-roving yarn production, newly designed auxiliary parts were assembled on Rieter K 45 machine.

2.2 Method

2.2.1 Compact Three-Roving Yarn Production System

Compact three-roving yarn technology can be counted as the combination of compact spun and siro-spun technologies. From this point of view auxiliary parts of the both technologies were redesigned for compact three-roving yarn production. With the same principle of siro-spun, three individuals rovings were fed into the drafting zone simultaneously. In order to control roving space and roving movements into the drafting zone, three-roving funnel and three-grooved delivery cylinders were designed (Figure 1-2).

In order to create condensing zone for individual fiber strands, suction insert and air-suction guide, which are the essential parts of pneumatic compact technologies with perforated drum, were designed and assembled on the inner and outer surface of the perforated drum. In pneumatic compact spinning technology with perforated drum, the width of the condensing zone is restricted by the width of air-holes on the perforated drum. In Rieter K 45 compact technology, the width of the air-holes on the perforated drum is 12 mm, therefore, this restriction is taken into consideration for the design of new parts. For compact three-roving technology, roving space is set as 3 mm with using the three-grooved delivery cylinder. In addition, the new air suction guides and suction inserts are also designed to create a condensation zone for individual rovings within the width of the air hole zone, which is 12 mm on the perforated drum of the Rieter K 45 (Fig. 3-4). All auxiliary parts were produced with 3D printer and were assembled on Rieter K 45 pneumatic compact spinning machine (Figure 5). Figure 6 shows the successful condensing effect for three-rovings with redesigned auxiliary parts. All detailed parameters of designed parts were given in Demir and Demir *et al.* [31-32].

Table 2. Experimental design of the yarn production

Yarn Production Technology	Raw Material	Roving Count (Ne)	Yarn Count (Ne)	Twist of produced yarn (T/m)
Compact Spun	Cotton, Modal, PES	1.2	50/1	1150
Compact Siro-spun	Cotton, Modal, PES	2.4	100/2	1150
Compact Three-roving	Cotton, Modal, PES	3.6	150/3	1150

Table 3. Structural details of fabrics

Yarn	Raw Material	Yarn Count (Ne)	Weft density (cm ⁻¹)	Warp density (cm ⁻¹)
Compact Spun	Cotton, Modal, PES	50/1	32	54
Compact Siro-spun	Cotton, Modal, PES	100/2	32	54
Compact Three-roving	Cotton, Modal, PES	150/3	32	54



Figure 1. 3D printed three roving funnel a) front view b) back view

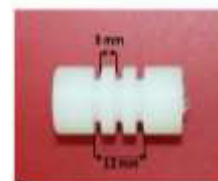


Figure 2. Three-grooved delivery cylinder

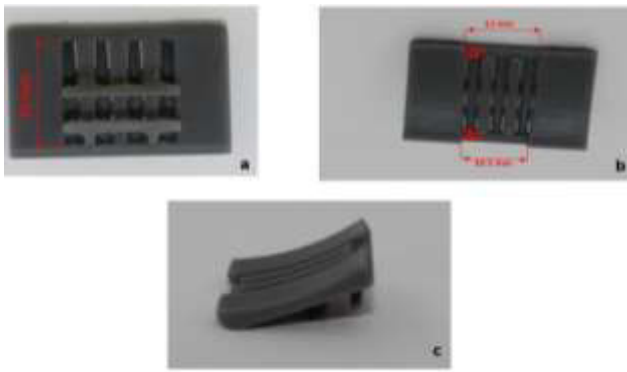


Figure 3. 3D printed air-suction guide for compact three-roving yarn a) front view b) back view c) side view



Figure 4. 3D printed suction-insert for compact three-roving yarn a) front view b) side view

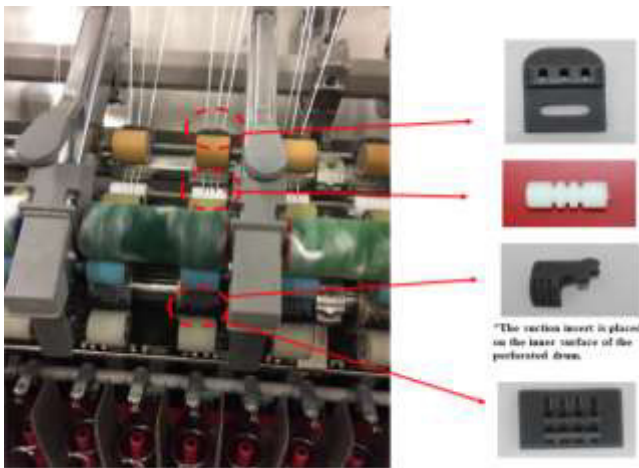


Figure 5. Compact three-roving spinning technology

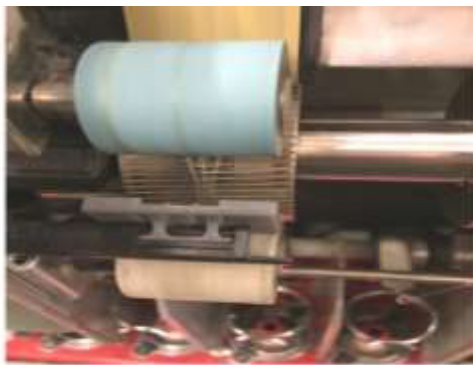


Figure 6. Compacting three individual rovings

2.2.2 Experimental

To measure yarn properties, 5 packages of each yarn types were produced and tested. Hairiness, unevenness, imperfections, diameter, density, roughness and roundness values of yarns were measured with USTER Tester 6 S800 at 400 m/min production speed and each test were performed during 2.5 minutes. Breaking force and breaking elongation values of yarns were measured with Uster Tensorapid 4. Every test was performed at 400 m/min and 500 mm gauge length. Friction properties of yarns were measured with Lawson Hemphill CTT and input tensions were set for 12 cN for both friction types. Yarn-to-yarn friction tests were performed at 20 m/min test speed and 5 minutes test duration and yarn-to-metal frictions tests were performed at 100 m/min test speed. In addition, tensile strength according to the EN ISO 13934-1, tear strength according to the EN ISO 13937-2, seam slippage resistance according to the EN ISO 13936-1, abrasion resistance EN-ISO 12947-2 and pilling according to the EN ISO 12945-2 were performed for produced fabrics. All yarn samples were prepared for hard sectioning with Leica Historsin Kit and cross-section samples of the yarns were obtained with Leica Rotary microtome (RM2125RT) as described in Demir [29]. Olympus BX43 microscope was used for cross-section image acquisition at 100X zoom.

3. RESULTS AND DISCUSSION

In this section, physical, mechanical, and structural properties of novel compact three roving yarns were compared with compact spun and compact siro-spun yarns. Besides, the properties of fabrics produced from these yarns were also compared. All statistical analyses performed for $\alpha=0.05$ significance level and confidence interval graphs were also given.

3.1 Yarn Properties

3.1.1. Physical and structural properties

Cross-section images of the compact spun, compact siro-spun and compact three roving Modal yarns are illustrated in Figure 7. It is seen from the figure that, novel compact three-roving yarn is in circular cross-sectional shape and all fibers are located in an assumed circular packing row. It is seen from Figure 7 that, compact three-roving yarns show similarities to compact spun yarns as each roving is placed in the yarn structure, while two different components of siro-spun yarns are more visible.

Hairiness parameters H (total length of protruding fibers of 1 cm of yarn length), sh (standrt deviation of H), S3 (number of protruding fibers greater than 3 mm along 100 m of yarn length) and S 1+2 (number of protruding fibers smaller than 3 mm along 100 m of yarn length) were measured. Mean values of the hairiness (H, sh, S1+2, S3) of produced yarns were given in Table 4 and the 95% confidence interval graphs of those values were given in Figure 8. Results showed that compact spun yarns have higher hairiness values for all hairiness types (H, sh, S1+2, S3) and compact siro-spun and compact three-roving yarns have similar values. Similar results are shown in some

studies where siro-spun yarns have better hairiness values than single spun yarn [17, 20]. It can be explained by yarn formation trapping model that occurs while playing single rovings to folded structure in multi-strand spinning. In addition, rovings in the spinning triangle that occurs for compact siro-spun and compact three-rovings, are exposed greater tension than single plied yarn and it results in better fiber orientation in the yarn structure. However, the positive relationship between the geometry of the spinning triangle and hairiness is restricted until a certain point. After that point, greater spinning triangle can cause fiber loss and uneven yarn structure [15, 18].

Unevenness (CVm%) and optical unevenness (CV2D8mm%) values of compact spun, compact siro-spun and compact three-rovings yarns are given in Table 5 and 95% confidence interval of those values are given in Figure 9. Comparing results showed that compact siro-spun yarns have the better unevenness values, compact spun and

compact three-rovings yarns have similar unevenness values in general. The possible explanation of this situation could be related to the number of rovings that used for yarn production and fiber orientation in the yarn structure. The number of rovings in the yarn production may display similar effects with Poisson distribution like in the draw frame process. In the draw frame, the even number of slivers is doubled and drawn and the aim behind this process is to eliminate thin and thick places in the sliver with the possibility of covering each other. Similarly, in compact siro-spun where two rovings are used for yarn production, uneven structures of each roving can eliminate each other in the final yarn structure. However, the same effects can not be seen in the yarns that consist of an odd number of components like compact spun and compact three-rovings.

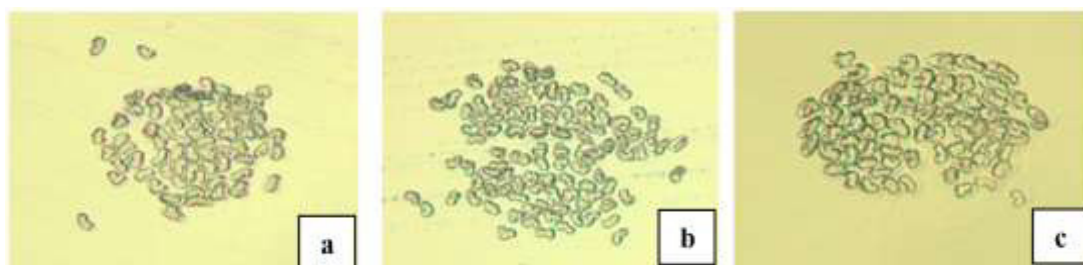
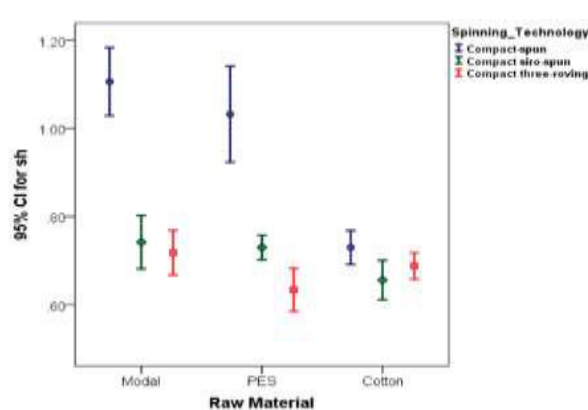
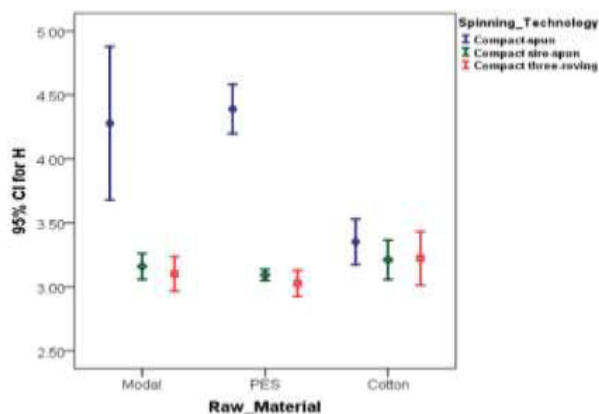


Figure 7. Cross section images of Modal yarns a) compact spun b) compact siro-spun c) compact three-rovings

Table 4. Hairiness values (H, sh, S1+2, S3) of compact spun, compact siro-spun, and compact three-rovings yarns

Spinning Technology	Raw Material	H	sh	S3	S 1+2
Compact spun	Modal	4.28	1.11	5167.40	14817.00
	PES	4.39	1.03	3986.60	13895.80
	Cotton	3.35	0.73	2544.20	12899.20
Compact siro-spun	Modal	3.16	0.74	2217.40	7464.80
	PES	3.09	0.73	2224.20	7696.20
	Cotton	3.21	0.66	1774.00	10773.60
Compact three-rovings	Modal	3.10	0.72	1858.40	7339.20
	PES	3.03	0.63	1280.00	5942.60
	Cotton	3.22	0.69	2270.80	11781.00



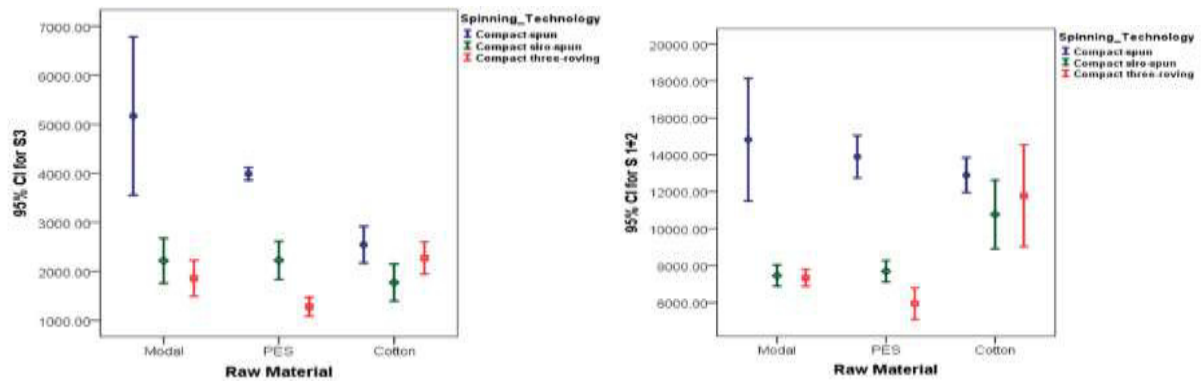


Figure 8. 95% confidence interval graphs for hairiness values of compact spun, compact siro-spun and compact three-roving yarns

On the other hand, although the yarn unevenness is defined and related to the number of the fibers in the yarn cross-section [33-34], there are also studies that pointed out the relation between unevenness and fiber position in the yarn structure [35-36]. For a better understanding of fiber orientation in the yarn structure for compact siro-spun and compact three-roving, the spinning triangle and its effects of yarn structure should be analyzed. When the fiber bundle leaves the front cylinder's nip point and starts to twist into the yarn form, a triangle occurs between the front cylinder and yarn formation point. For the same yarn production conditions, the structure of the triangles is related to the width of the fiber bundle for single spun yarn, and roving space for the multi-strand spun yarn [15,37]. The tension of the fiber is related to its path in the spinning triangle and effects the fiber position in the yarn structure. Fibers at the edge of the triangle follow a longer path hence exposed to greater tension, while fibers at the middle of the bundle follow a shorter path and hence exposed lower tension [3]. For the compact spun yarn, the triangle is reduced by the negative air-pressure and it can be assumed to be eliminated. In siro-spun, the spinning triangle consists of two components and a greater geometry of triangle occurs. A greater spinning triangle means greater tension on the fibers and better fiber orientation in the yarn structure until a certain point. The significant point for the spinning triangle that should be kept on the eye is that fluctuation on the nip point of the spinning triangle changes the length of each roving hence the tension. However, for the two

components of the spinning triangle like the one in siro-spun, changes in the length of each roving could be assumed to be similar, and owing to plied structure, uneven structures of the single roving can be tolerated ($|R1-R1'| \approx |R2-R2'|$) (Figure 10a). For the three-roving spinning, changes on both edge of the spinning triangle are not equal due to the third component in the middle. In any time of fluctuation during the yarn production, two of the rovings are closer than the other one, and displacements of the location of each roving are not been equal. Therefore, uneven structures of single roving can not be tolerated with the plying structure ($|R1-R1'| \neq |R2-R2'| \neq |R3-R3'|$) (Figure 10b).

Imperfection values of produced yarns are given in Table 6 and 95% confidence interval graphs of those values are illustrated in Figure 11. Results of imperfection values are mostly related with yarn preparation process and compact three-roving yarns show similar results with commercially used yarns in general.

Diameter ($2D\emptyset$ mm), density (D g/cm³), roughness (%CV FS) and roundness (shape) values of compact spun, compact siro-spun and compact three-roving yarns are given in Table 7 and 95% confidence interval graphs are given in Figure 12. Results showed that, there is no statistically significant difference between three types of yarns in general ($p > 0.05$). In the other words, similar structures of compact three-roving yarns with compact spun and compact siro-spun were successfully produced.

Table 5. Unevenness (CVm%) and optical unevenness (CV2D8mm%) values of compact spun, compact siro-spun, and compact three-roving yarns

Spinning Technology	Raw Material	CVm (%)	CV2D 8mm (%)
Compact spun	Modal	12.26	9.13
	PES	14.47	10.34
	Cotton	11.03	8.17
Compact siro-spun	Modal	11.15	7.65
	PES	11.10	7.52
	Cotton	10.68	7.83
Compact three-roving	Modal	12.02	8.44
	PES	13.62	9.21
	Cotton	11.38	8.37

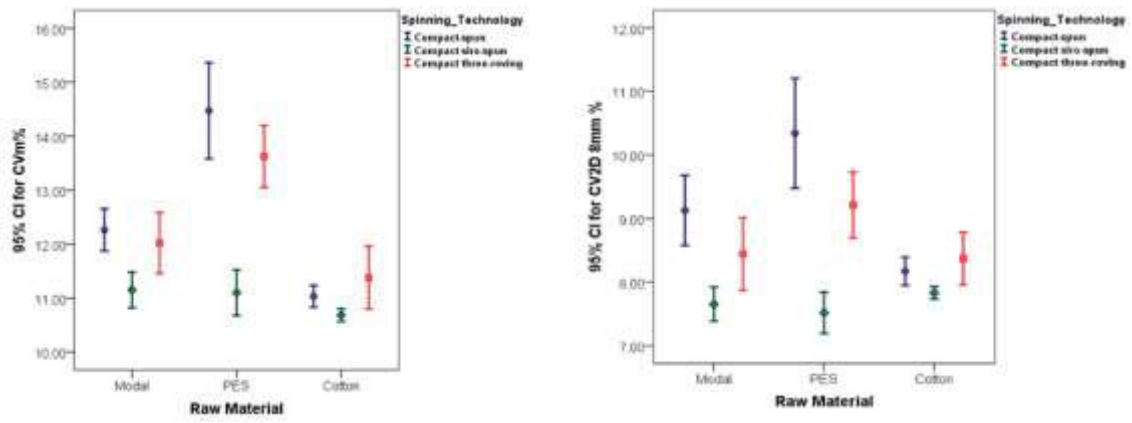


Figure 9. 95% confidence interval graphs for unevenness (CVm%) and optical unevenness (CV2D8mm%) values of compact spun, compact siro-spun and compact three-roving yarns

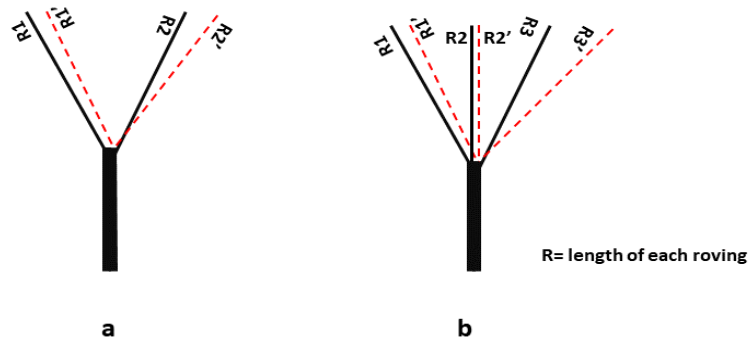
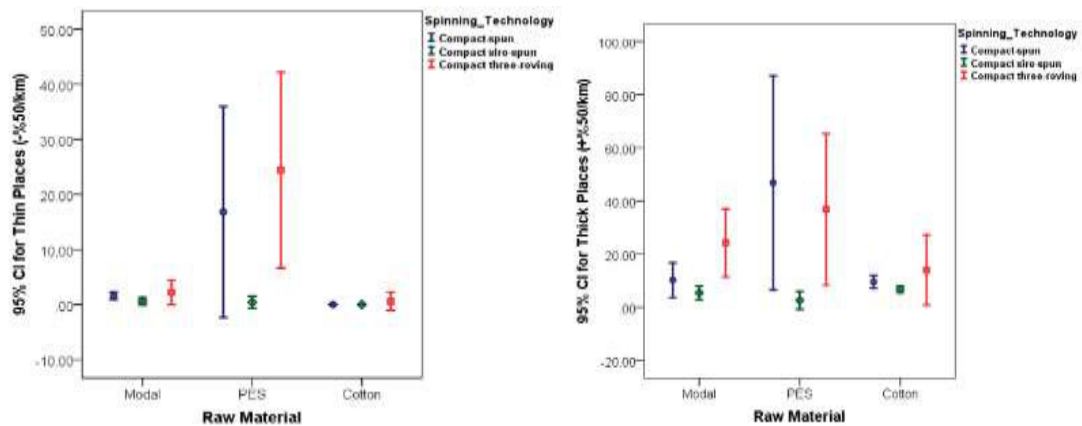


Figure 10. Geometrical changes of spinning triangles in siro-spun and three-roving yarns

Table 6. Imperfections values of compact spun, compact siro-spun, and compact three-roving yarns

Spinning Technology	Raw Material	Thin Places (-50%/km)	Thick Places (+50%/km)	Neps (+200 %/km)
Compact spun	Modal	1.60	10.20	59.60
	PES	16.80	46.80	15.20
	Cotton	0.00	9.60	41.40
Compact siro-spun	Modal	0.60	5.40	16.40
	PES	0.40	2.60	12.40
	Cotton	0.00	6.80	46.40
Compact three-roving	Modal	2.20	24.20	37.80
	PES	24.40	36.80	21.60
	Cotton	0.60	14.00	62.20



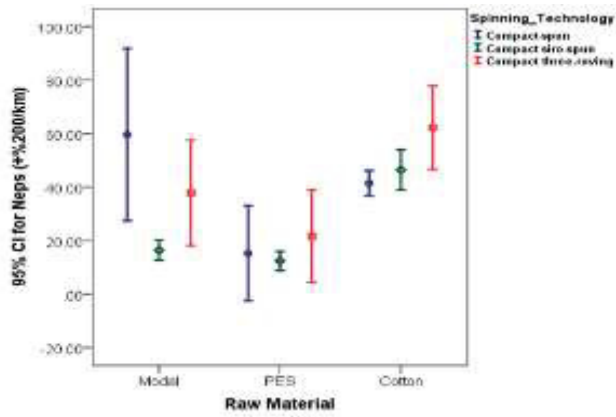


Figure 11. 95% confidence interval graphs for imperfections values of compact spun, compact siro-spun, and compact three-rovng yarns

Table 8 shows the yarn-to-yarn and yarn-to-metal friction coefficients of three types of yarns and Figure 13 illustrates the 95% confidence interval of those values. Both of the friction coefficients are related to the yarn surface structures [38-39]. Since all three-types of yarns show similar surface characteristics, there are no statistically significant differences for friction properties in general.

Table 7. Diameter (2DØ mm), density (D g/cm³), roughness (%CV FS) and roundness (shape) values of compact spun, compact siro-spun and compact three-rovng yarns

Spinning Technology	Raw Material	Diameter (mm)	Density (g/cm ³)	Roughness (CV FS %)	Roundness
Compact spun	Modal	0.140	0.760	9.21	0.844
	PES	0.141	0.752	8.79	0.866
	Cotton	0.147	0.698	7.84	0.854
Compact siro-spun	Modal	0.140	0.766	6.93	0.848
	PES	0.141	0.760	6.74	0.846
	Cotton	0.149	0.682	7.97	0.840
Compact three-rovng	Modal	0.139	0.776	6.89	0.850
	PES	0.140	0.750	6.55	0.874
	Cotton	0.147	0.696	7.92	0.844

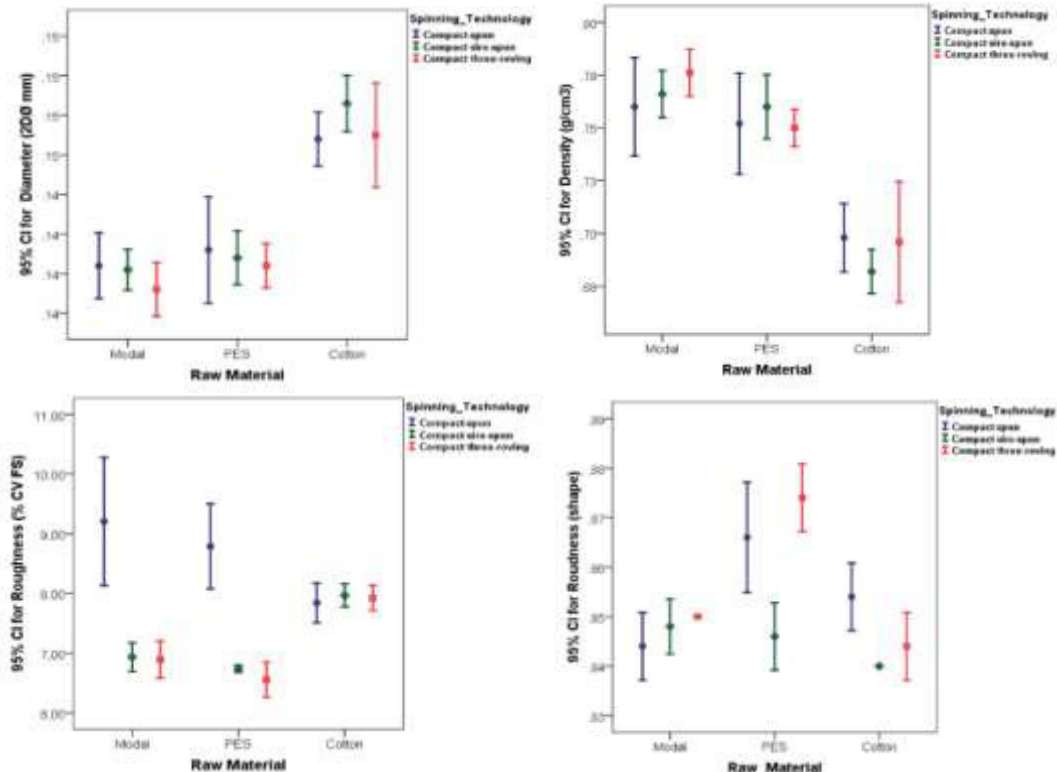


Figure 12. 95% confidence interval graphs for diameter (2DØ mm), density (D g/cm³), roughness (%CV FS) and roundness (shape) values of compact spun, compact siro-spun and compact three-rovng yarns

Table 8. Yarn-to-yarn and yarn-to-metal friction coefficients of compact spun, compact siro-spun and compact three-rovng yarns

Spinning Technology	Raw Material	yarn-to-yarn	yarn-to-metal
Compact spun	Modal	0.1480	0.2977
	PES	0.1718	0.2556
	Cotton	0.1640	0.2578
Compact siro-spun	Modal	0.1456	0.3072
	PES	0.1692	0.2642
	Cotton	0.1646	0.2588
Compact three-rovng	Modal	0.1429	0.3001
	PES	0.1698	0.2359
	Cotton	0.1602	0.2584

3.1.2 Mechanical Properties

Breaking force (cN/tex) and breaking elongation (%) values of compact spun, compact siro-spun, and compact three-rovng yarns are given in Table 9 and 95% confidence interval graphs are shown in Figure 14. Results showed that for all raw material, results of novel compact three-rovng yarns are similar with compact spun and compact siro-spun yarns. Comparing the breaking force and breaking elongation of the yarns that produced at the same twist level and same yarn count, the number of the fibers in the yarn cross-section is decisive for those properties. According to the results, it can be said that compact three-rovng yarns

are successfully produced with proposed new method in terms of mechanical properties.

3.2 Fabric Properties

In this section, tensile strength, tear strength, seam slippage resistance, pilling and abrasion resistance of the fabrics produced from compact spun, compact siro-spun and compact three-rovng yarns were compared. For fabric production, produced yarns were only used in the weft direction. Therefore, fabric properties in weft directions were investigated.

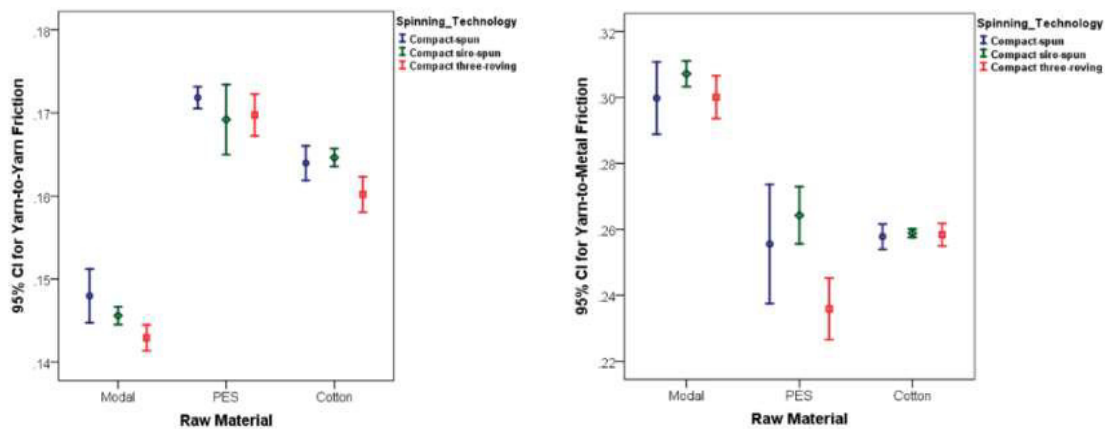


Figure 13. 95% confidence interval graphs for yarn-to-yarn and yarn-to-metal friction coefficients of compact spun, compact siro-spun and compact three-rovng yarns

Table 9. Breaking force and breaking elongation values of compact spun, compact siro-spun, and compact three-rovng yarns

Spinning Technology	Raw Material	Breaking Force (cN/tex)	Breaking Elongation (%)
Compact spun	Modal	19.89	8.13
	PES	22.81	9.42
	Cotton	21.89	9.23
Compact siro-spun	Modal	30.05	10.22
	PES	30.76	9.34
	Cotton	32.01	10.01
Compact three-rovng	Modal	29.13	5.49
	PES	28.29	5.22
	Cotton	27.75	4.98



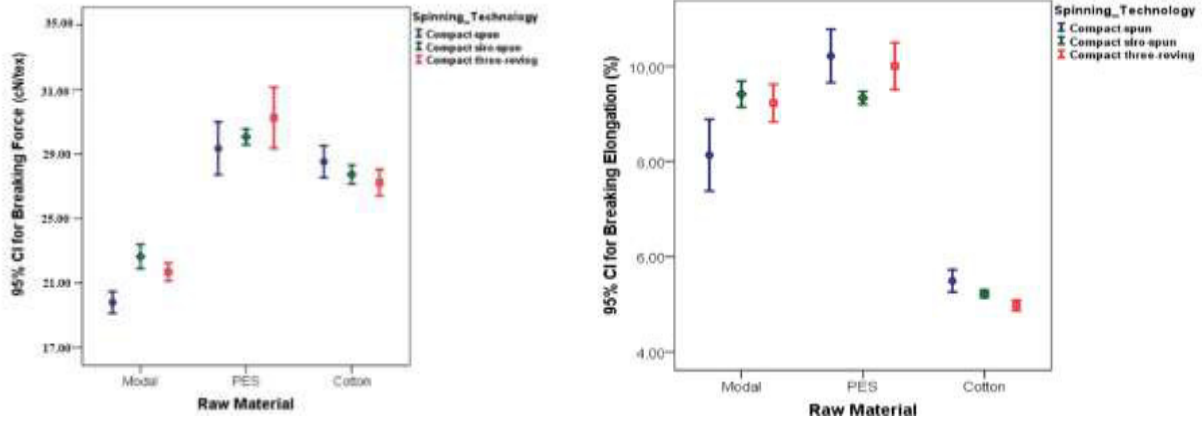


Figure 14. 95% confidence interval graphs for breaking force and breaking elongation values of compact spun, compact siro-spun and compact three-rovng yarns

3.2.1 Mechanical Properties

Tensile Strength

Tensile strength (N) of the fabrics produced from three types of yarns are given in Table 10 and 95% confidence interval graph of those values are given in Figure 15. Results showed that, there is no statistically significant difference between all fabrics for all material groups ($p>0.05$). This is an expected result for the produced fabrics, since the tensile strength of the fabrics with similar woven structure is mostly related to yarn tenacity [40].

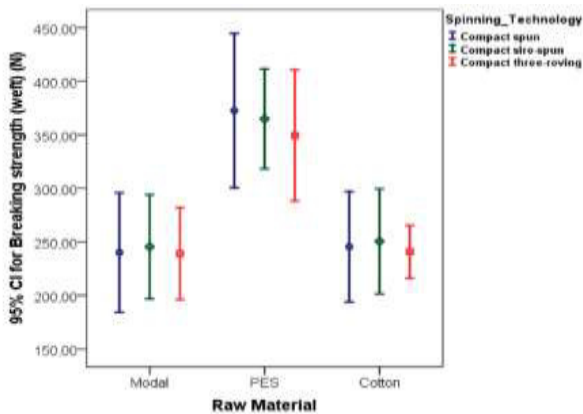


Figure 15. 95% confidence interval graphs for breaking strength values of fabrics produced from compact spun, compact siro-spun and compact three-rovng yarns

Tear Strength

Tear strength (N) values of the produced fabrics are given in Table 11 and Figure 16 illustrates the 95% confidence interval of those values. Results showed that there is no

statistically significant difference for tear strength values in weft direction in general. From the same reason of tensile strength, similar results were obtained for tear strength.

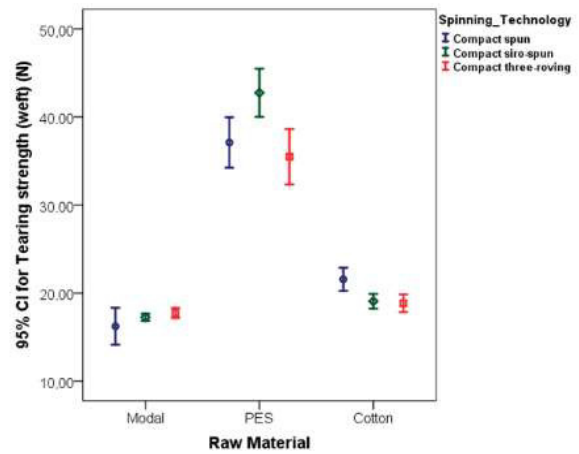


Figure 16. 95% confidence interval graphs for tear strength values of fabrics produced from compact spun, compact siro-spun and compact three-rovng yarns

Seam Slippage Resistance

Results of seam slippage resistance (N) of produced fabrics are given in Table 12 and 95% confidence interval graphs for those results are given in Figure 17. It can be seen from the results that there is no statistically significant difference between three types of fabrics in general. Seam slippage results of fabrics produced from PES yarns are relatively high, however, greater confidence intervals are observed, particularly for siro-spun yarns.

Table 10. Breaking strength (N) values of fabrics produced from compact spun, compact siro-spun and compact three-rovng yarns

Spinning Technology	Raw Material	Breaking Strength (N)
Compact spun	Modal	240.1
	PES	372.5
	Cotton	245.4
Compact siro-spun	Modal	245.4
	PES	364.8

Compact three-rovng	Cotton	250.5
	Modal	239.1
	PES	349.4
	Cotton	240.8

Table 11 Tear strength (N) values of fabrics produced from compact spun, compact siro-spun and compact three-rovng yarns

Spinning Technology	Raw Material	Tearing Strength (N)
Compact spun	Modal	16.2
	PES	37.1
	Cotton	21.6
Compact siro-spun	Modal	17.3
	PES	42.7
	Cotton	19.1
Compact three-rovng	Modal	17.7
	PES	35.5
	Cotton	18.9

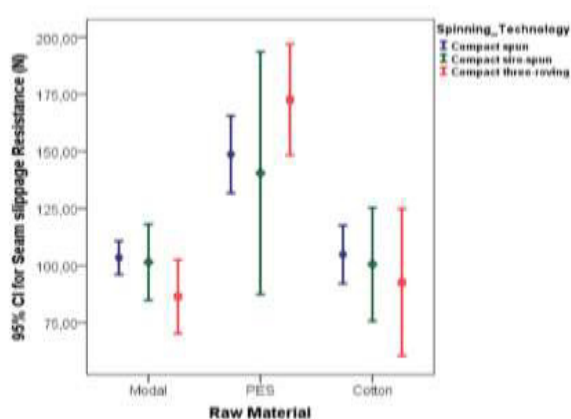


Figure 17. 95% confidence interval graphs for slippage resistance values of fabrics produced from compact spun, compact siro-spun and compact three-rovng yarns

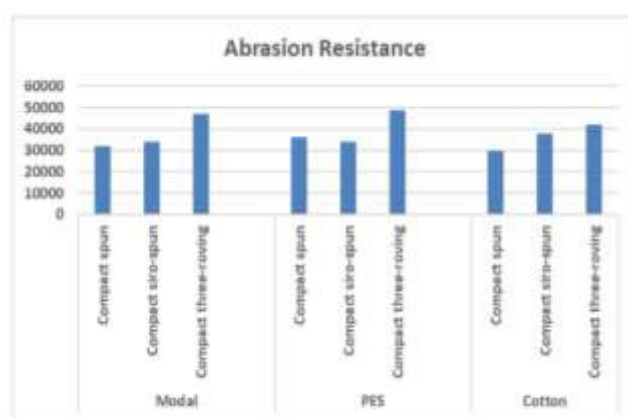


Figure 18. Abrasion resistance values of fabrics produced from compact spun, compact siro-spun and compact three-rovng yarns

3.2.2 Surface Properties

Pilling and Abrasion Resistance

The results of the pilling tests are given in Table 13 and the results of the abrasion resistance are given in Figure 18. It's seen from the table that pilling results of the fabrics that produced from compact siro-spun and compact three-rovng yarns are similar and better than compact-spun yarns. Pilling tests results are parallel to the hairiness values of three types of yarns. For the abrasion resistance according to the specimen breakdown, it is clearly seen that compact three-rovng yarns have better values for all raw materials owing to the three-component structures.

4. CONCLUSION

This study presents the novel compact three-rovng yarn production and investigates the physical, mechanical, and structural properties of the compact three-rovng yarn. For the production of three-rovng yarn, auxiliary parts of compact and siro-spun yarn production technologies were

redesigned and assembled on a pneumatic compact spinning machine. For a better assessment, commercially used yarn technologies compact spun and compact siro-spun yarns were also produced at the same yarn count and twist multiplier. Results showed that, compact three-rovng have better hairiness and similar unevenness values than compact-spun yarns. Mechanical and other structural parameters of the yarns also show similar values. Three-types of yarns were used for fabric production, and the mechanical and surface properties of the fabrics were also compared. Similar mechanical and better surface properties were obtained for fabrics produced from three-rovng yarns. In overall assessment, it can be concluded that novel compact three-rovng technology is successful method for yarn production. In addition, it should also be noted that beside being an alternative of commercially used yarns, three-rovng yarns can be also used for specific purposes owing to its composite structure that enables to feed different raw materials into the yarn structure.

Table 12. Seam slippage resistance (N) values of fabrics produced from compact spun, compact siro-spun and compact three-roving yarns

Spinning Technology	Raw Material	Seam slippage Resistance (N)
Compact spun	Modal	103.4
	PES	148.7
	Cotton	104.8
Compact siro-spun	Modal	101.5
	PES	140.5
	Cotton	100.6
Compact three-roving	Modal	86.4
	PES	172.6
	Cotton	92.6

Table 13. Pilling values of fabrics produced from compact spun, compact siro-spun and compact three-roving yarns

Spinning Technology	Raw Material	Pilling					
		125	500	1000	2000	5000	7000
Compact spun	Modal	4-5	2-3	2-3	2	1-2	1-2
	PES	4-5	2-3	2-3	2	2	1-2
	Cotton	4-5	2-3	2-3	2	2	1-2
Compact siro-spun	Modal	4-5	3-4	3-4	2-3	2	1-2
	PES	4-5	4	3-4	2-3	2	1-2
	Cotton	4-5	4	3-4	2-3	2	1-2
Compact three-roving	Modal	4-5	3-4	3	2-3	2	1-2
	PES	4-5	3	3	2-3	2	1-2
	Cotton	4-5	3-4	3	2-3	2-3	2

Acknowledgement

This study is supported by TÜBİTAK - TEYDEB 1505 University - Industry Collaboration Grant Programme with the project number 5160091 and accompanied with KİPAŞ

Mensucat R&D Center and Dokuz Eylül University Scientific Research Project with the grant number of 2020.KB.FEN.018.

REFERENCES

- Kilic M., Balci Kilic G., Okur A. 2011. Effects of Spinning System on Yarn Properties. *Journal of Textiles and Engineer* 18(81): 22-34.
- Song, Y. 2016. Comparison between Conventional Ring Spinning and Compact Spinning, Master Thesis, North Carolina State University.
- Soltani, P. & Johari, M.S. 2012. A study on siro-, solo-, compact-, and conventional ring-spun yarns. PartII: yarn strength with relation to physical and structural properties of yarns, *The Journal of The Textile Institute*, 103(9):921-930.
- Basal, G. & Oxenham, W. 2006. Comparison of Properties and Structures of Compact and Conventional Spun Yarns *Textile Research Journal* 76(7): 567-575.
- Cheng, K.P.S. & YU, C. 2003. A study of Compact Spun Yarns. *Textile Research Journal* 73 (4): 345-349.
- Ganesan S. & Ramakrishnan G. 2006. Fibre migration in compact spun yarns: Part I- Pneumatic compact Yarn. *Indian Journal of Fibre & Textile Research* 31: 381-386.
- Altas, S. & Kadoglu, H. 2012 Comparison of Conventional Ring, Mechanical Compact and Pneumatic Compact Yarn Spinning Systems. *Journal of Engineered Fibers and Fabrics* 7(1) page(s) .
- Raja, D., Prakash, C., Gunasekaran G. & Koushik, C.V. 2015. A study on thermal properties of single-jersey knitted fabrics produced from ring and compact folded yarns, *The Journal of The Textile Institute*, 106:4, 359-365.
- Akhtar, K.S., Ahmad, S., Afzal,A., Anam,W., Ali,Z. & Hussain, T. 2020. Influence and comparison of emerging techniques of yarn manufacturing on physical-mechanical properties of polyester-/cotton-blended yarns and their woven fabrics, *The Journal of The Textile Institute* 111(4): 555-564.
- Kim, H. A. 2017. Physical properties of ring, compact, and air vortex yarns made of PTT/wool/modal and wearing comfort of their knitted fabrics for high emotional garments, *The Journal of The Textile Institute* 108(9):1647-1656.
- Kaynak, H. K. & Celik, H.İ. 2018. Thermophysiological comfort and performance properties of knitted fabrics produced from different spinning technologies, *The Journal of The Textile Institute* 109(4):536-542.
- Stalder, H. 2014. *Rieter Manuel of Spinning, Issue 6: Alternative Spinning Technologies*, Winterthur: Rieter Machine Works.
- Emanuel A., Plate, D. 1982. Alternative Approach to Two-Fold Weaving Yarn, Part II. The Theoretical Model. *The Journal of The Textile Institute* 73 (3): 108-116.

13. Miao, M., Cai, Z., Zhang, Y. 1993. Influence of Machine Variables on Two-strand Yarn Spinning Geometry. *Textile Research Journal* 63 (2):116-120.
14. Cheng, K.P.S & Sun M.N. 1998. Effect of Strand Spacing and Twist Multiplier on Cotton Siro-Spun Yarn. *Textile Research Journal* 68 (7): 520-527. DOI: 10.1177/004051759806800709
15. Gokarneshan, N., Anbumani, N. & Subramaniam, V. 2007. Influence of strand spacing on the interfibre cohesion in siro yarns, *The Journal of The Textile Institute*, 98:3: 289-292.
16. Soltani P. & Johari, M.S. 2012. A study on siro-, solo-, compact-, and conventional ring-spun yarns. Part I: structural and migratory properties of the yarns, *The Journal of The Textile Institute* 103(6): 622-628. DOI: 10.1080/00405000.2011.595567
17. Gowda, R.V. M., Sivakumar, M., Kannan, M. S. S. 2004. Influence of process variables on characteristics of modal siro-spun yarns using Box-Behnken response surface design. *Indian Journal of Fibre & Textile Research* 29: 412-418.
18. Yıldız B. S. & Kilic, M. 2017. An Investigation on Properties of Siro-spun Yarns. *Annals of University Oradea Fascicles of Textile and Leatherwork* 18:131-136.
19. Ortlek, H.G., Kilic, G., Bilgin, S. 2011. Comparative study on the properties of yarns produced by modified ring spinning methods. *Industria Textila* 62(3):129-133.
20. Lui, Y., Wang, Y. & Gao, W. 2019. Wicking Behaviours Of Ring And Compact-Siro Ring Spun Yarns With Different Twists. *AUTEX Research Journal*, 19(1) .
21. Su, X., Gao, W., Liu, X., Xie, C., Xu, B. 2015. Research on the Compact-Siro Spun Yarn Structure. *Fibres & Textiles in Eastern Europe* 111(3): 54-57.
22. Matsumoto, M., Matsumoto, Y., Kanai, H., Wakako, L., Fukushima, K. 2014. Construction of Twin Staple-core Spun Yarn with two Points of Yarn Formation in One Twisting Process. *Textile Research Journal* 84(17):1858-1866.
23. Matsumoto, Y., Kanai, H., Wakako, L., Morooka, H., Kimura, H., Fukushima, K. 2010. Exploratory Work on the Spinning Condition of the Structure of Staple-core Twin-spun Yarns. *Textile Research Journal* 80(11): 1056-1064.
24. Matsumoto, Y., Kimura, H., Yamamoto, T., Matsuoko, T., Fukushima, K. 2009. Characteristics of Novel Triplet Spun Yarns made from Fibers of Differing Fineness. *Textile Research Journal* 79 (10): 947-952.
25. Demir, M. and Kilic, M. 2017. Investigating Possibilities of Three-Strand Yarn Production. *Fibres and Textiles* 24(1): 30-35.
26. Demir, M. and Kilic, M. 2020. Development of Three-roving Ring Yarn Production System, *Indian Journal of Fibre & Textile Research* 45: 450-456.
27. Soltani, P. And Johari, M. S. 2012. The effect of spinning parameters on mechanical and physical properties of core-spun yarns produced by the three-strand modified method (TSMM). *Fibers and Polymers*, 13(7), 923-927.
28. Pourahmad, A. and Johari, M. S. 2009. Production of core-spun yarn by the three-strand modified method. *The Journal of The Textile Institute*, 100(3), 275-281.
29. Demir, M., Kilic, M. 2019. A modified Twist spinning-three-roving Yarn Spinning. In: *International Conference TexTeh IX Advanced Textiles for a Better World*. Bucharest, Romania, 24-25 October 2019.
30. Demir M, 2021. Design and development of three strand Yarn Production System, PhD Thesis, Available from YOKSIS database (691009)
31. Demir, M., Kilic, M., Sayin, S., Kiral, Z., Balduk, F., & Denge, K. K. (2021). Design of three-strand compact spinning system and numerical flow-field simulation for different structures of air-suction guides and suction inserts. *Textile Research Journal*, 91(15-16), 1795-1814.
32. Martindale, J.G. 1945. A New Method of Measuring the Irregularity of Yarns with Some Observations on the Origin of Irregularities in Worsted Slivers and Yarns. *Journal of Textile Institute* 36(3): 35-47.
33. Grosberg, P. and Iype, C. 1999. *Yarn Production – Theoretical Aspects*. Cambridge: Woodhead Publishing
34. Dyson, E. 1974. Some Observations on Yarn Irregularity. *Journal of Textile Institute*. 65(4):215-217.
35. Hearle, J.W.S., Lord, P.R. and Senturk, N. 1972. Fibre Migration in Open-End- Spun Yarns. *Journal of Textile Institute* 63(11):605-617. DOI: 10.1080/00405007208630383
36. Hua, T., Tao, M.X., Cheng, K.P.S, Xu, B.G. 2010. Effects of Geometry of Ring Spinning Triangle on Yarn Torque: Part II: Distribution of Fiber Tension within a Yarn and Its Effects on Yarn Residual Torque. *Textile Research Journal* 80(2): 116-123 .
37. Gupta, B. S. (Ed.) 2008. *Friction in textile materials*. Cambridge, UK: Woodhead Publishing
38. Pastore, C. M. & Kiekens, P. 2001. *Surface characteristics of fibers and textiles*. USA: Marcel Dekker Inc. Publishing Limited.
39. Kaynak, H.K., Babaarslan, O., Avcı, M.E, Doğan, F.B. 2017. Effects of spinning technology on deneim fabric performance. *Industria Textila* 68(3):197-203.



Strength and Elasticity Properties of Denim Fabrics Produced from Core Spun Yarns

Gonca Balcı Kılıç  0000-0001-8541-9254

Dokuz Eylül University / Faculty of Engineering / Department of Textile Engineering / Tınaztepe Campus, Buca, İzmir, Türkiye

Corresponding Author: Gonca BALCI KILIC, gonca.balci@deu.edu.tr

ABSTRACT

In parallel to the development of new fiber and yarn technologies, different fibers and yarns have been used in denim fabric production and breaking the market dominance of 100% cotton yarn in the denim market. In recent years, the use of elastane fibers for denim fabric production has rapidly increased thanks to their movement comfort. This study examines the strength and elasticity properties of denim fabrics containing core yarns. For this purpose, different weft yarns were used in the production of denim fabrics. While 100% cotton ring yarn was used as warp for all fabrics, cotton ring, cotton OE-rotor, cotton / PBT-elastane dual-core, cotton / elastane core and cotton-PET / elastane core yarns were used as weft. Within the scope of the study, tensile strength, tearing strength and bursting strength tests were carried out on denim fabrics. In addition, denim fabrics containing core spun yarns were tested for elasticity in the weft direction, which is the direction of core yarns used. When the results were examined, it was seen that tensile strength and breaking elongation are higher for the fabrics containing core yarn in general. Fabrics produced with dual-core yarns have the highest tearing strength values. In addition, the bursting strength values of fabrics containing core yarn are higher than fabrics without core yarn. It was seen that the elasticity values of denim fabrics produced using core yarn are generally above 50%. However, the highest growth values were seen in the fabrics with the highest elasticity.

1. INTRODUCTION

Denim fabrics, which were first produced in the 17th century, began to be widely used in the textile industry with the mass production in the middle of the 19th century [1,2]. Denim fabrics were preferred especially by farmers and for workwear used in mining industry in the first years of their production due to their high strength and high abrasion resistance. Due to the changing fashion perception over time and other features such as aesthetics and wearing comfort added to denim fabrics, the clothes produced from these fabrics have had a significant market share worldwide and still maintain their popularity. In parallel with the development of new fiber and yarn technologies, different fibers and yarns have also been used in the structure of denim fabrics, which used 100% cotton yarn at the beginning of their production [3]. In recent years, elastane fibers have taken their place among the fibers widely used

in denim fabric production, especially due to the movement comfort they provide. The use of elastane core yarn in the fabric structure is one of the main processes applied to give elasticity properties to denim fabrics. In denim fabrics, elastane core yarns can be used in only one direction (weft or warp), as well as in both directions. In recent years, with the production of dual-core (double core) yarns, the use of these yarns in denim fabrics has become widespread. Core yarns, also called complex, compound, composite or hybrid yarn, can be defined as a combination of filament and staple fibers. For the production of core yarns, the filaments are fed into the yarn axis as “core” and staple fibers are used to wrap the core filaments as sheath [4,5]. Thanks to its core yarn structure, it is possible to benefit from the high-performance properties of the filaments (core) such as elasticity, movement comfort and strength, depending on the properties of the filaments, as well as the handle properties such as warmth, softness and comfort properties

To cite this article: Balci Kilic. G. 2024. Strength and Elasticity Properties of Denim Fabrics Produced from Core Spun Yarns. *Tekstil ve Konfeksiyon*, 34(1), 32-43.

ARTICLE HISTORY

Received: 25.02.2022

Accepted: 24.01.2023

KEYWORDS

Denim fabric, core yarn, dual-core yarn, fabric strength, elasticity, growth

like moisture absorption and air permeability of the staple fibers (sheath).

Although core yarn production is possible in different spinning technologies such as friction spinning, OE-rotor spinning, air-jet spinning and ring spinning, ring spinning is the most widely used spinning technology for core yarn production. The most important point for core-spun yarn production in all spinning technologies is positioning the filament at the center axis of the yarn. Core yarn can be produced by suitable modification on a conventional ring spinning machine. A feeding device (core spun attachment) is mounted on top of the front rollers. The core filament (or core yarn) passes the core spun attachment and is fed directly into the front roller, while the wrapping (sheath) fibre strand passes the back, middle and front roller [5,6] Due to the advantages of the composite structure, after the core yarns found a wide area of use, various studies were carried out to improve the properties of the core yarns and dual-core yarns were introduced in the 2000s. In the production of dual-core yarn, two separate filaments which have different performance properties are fed to the yarn axis. Generally, a polyester-based filament is preferred as the first core because of its high strength properties, while a polyurethane-based filament is preferred as second core due to its high elasticity properties. Today, the use of core (single and double core) yarns in denim fabric production is quite high and the number of studies in this field is increasing day by day. With the use of core yarn technology in denim construction, researchers firstly aimed to examine the effect of single-core yarns on the properties of denim fabrics [7-13]. In parallel with the developments in core yarn technology, studies focused on examining the effect of using dual-core yarn in denim fabric structure [14-16] and comparatively examining [17-23] the effects of single and dual-core yarns on the performance and elasticity properties of denim fabrics.

In the literature, there are limited studies on comparison for ring, OE-rotor, core-spun, and dual-core spun yarns on denim fabrics' strength and elasticity properties. In this study, ring, OE-rotor, core-spun (two different sheaths), and dual-core spun yarns at the same linear density (Ne 24/1) were produced. These yarns used as weft yarns to make different denim fabrics at the same construction and

weaving machine. The same yarn (Ne 24/1, ring) is used as warp in all fabrics. Within the scope of this study, the strength properties of denim fabrics were examined in terms of tensile, tearing and bursting strengths, which are the most important strength parameters for fabrics. Furthermore, elasticity properties were measured by using the two most widely used different test methods and the results were examined comparatively. In addition, elasticity and hysteresis behaviors of denim fabrics containing core yarn under low stresses were also analyzed. It is thought that this study will contribute to the literature in terms of analysing the bursting strength of denim fabrics under the effect of multi-directional forces and comparing two commonly used elasticity test methods. Within the scope of the study, it is also aimed to examine the contribution of the second core to the mechanical and elasticity properties by comparing two different core yarns (with different sheath fibers) and dual-core yarn.

2. MATERIAL AND METHOD

2.1 Material

Within the scope of the study, denim fabrics containing different types of core yarns were produced. Cotton ring yarns were used as warp and cotton ring, cotton OE-rotor, cotton / PBT-elastane dual-core, cotton / elastane core, and cotton-PET / elastane core yarns were used as weft. Figure 1 shows the production of dual-core yarns. Properties of the fibers and yarn production parameters are shown in Table 1. Physical and mechanical properties of yarns are shown in Table 2. The properties of denim fabrics produced with fancy twill (Figure 2) weave structure are given in Table 3.



Figure 1. Cotton / PBT-elastane dual core ring yarn production

Table 1. Properties of the fibers and yarn production parameters

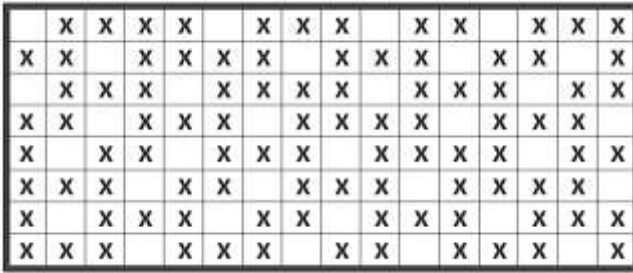
Parameter	Specification
Cotton fiber	Staple length: 27.8 mm, Fineness: 4.45 mic., Tenacity: 27.8 gf/tex, Elongation: 6.9%
PBT fiber	24F55dtex
Elastane	78 dtex
Polyester (used in sheath blend)	1,3 dtex 38 mm
Elastane draft ratio	3.5
Production Parameters	Sliver: Ne 0.12, Roving: Ne 0.70, Yarn twist: 900 T/m

Table 2. Physical and mechanical properties of yarns

Sample Code	CVm %	Thin Places -50%	Thick Places +50%	Neps +200 %	H	sH	Breaking load (cN)	Breaking elongation (%)
Ring	14.46	1.5	207.5	256.5	5.21	1.25	362.54	8.05
OE-rotor	14.77	27.5	88.0	307.0	4.74	1.19	259.08	7.92
Cotton+Core (Elastane)	9.51	0.0	6.0	6.5	4.77	0.88	349.22	10.14
Cotton+Dual Core (Elastane-PBT)	11.41	0.0	61.0	57.5	4.79	1.11	393.66	16.23
Cotton/PET+Core (Elastane)	14.25	1.0	190.5	127.5	6.18	1.35	366.18	12.82

Table 3. Production parameters of denim fabrics

Parameter	Definition
Warp Yarn	Ne 24/1 ring 100% cotton
	Ne 24/1 ring 100% cotton
	Ne 24/1 OE-rotor 100% cotton
Weft Yarn	Ne 24/1 dual core-spun Sheath: 100% cotton Core: Elastane (78 dtex)+PBT (55 dtex)
	Ne 24/1 core-spun Sheath: 100% cotton Core: Elastane (78 dtex)
	Ne 24/1 core-spun Sheath: 50% cotton, %50 polyester Core: Elastane (78 dtex)
Weave Structure	5/1/1/1 3 Fancy Twill Step 4
Reed Count	70/4
Loom width (cm)	215
Warp Setting (ends/cm)	34
Weft Setting (picks/cm)	25

**Figure 2.** Weave pattern for 5/1/1/1 fancy twill

2.2 Method

In the study, unit weight, warp and weft densities and thickness values were measured to determine the post-production structural properties of denim fabrics. Fabric unit weight tests were carried out according to TS EN 12127 [24] and warp and weft densities were measured by TS 250 EN 1049-2 [25] standards. Fabric thickness measurements were made with R&B Fabric Thickness Tester under 5 g/cm² pressure according to TS 7128 EN ISO 5084 [26]. In order to examine the effect of different weft yarns used in denim fabrics on the dimensional properties of the fabrics, dimensional stability test was conducted (TS EN ISO 3759) [27]. For the analysis of dimensional properties, fabric width measurements were also carried out before and after washing. To determine the mechanical properties of the fabrics, tensile and tear strength tests were performed on the Instron 4411 multi-purpose strength tester according to TS EN ISO 13934-1 [28] and TS EN ISO 13937-2 [29] standards, respectively. The bursting strength of denim fabrics was also analyzed within the scope of the study. As it is known, unlike other

strength tests, fabric is exposed to multidirectional force effects in bursting strength tests. Considering the purpose and usage area of denim fabrics containing elastane core, one of the main performance features expected from these fabrics is providing comfort of movement. Especially in the knee part of denim trousers, the fabric is under the effect of multi-directional forces, and the bursting strength test is one of the best tests to simulate forces in daily use. In the study, bursting strength tests were performed with the James Heal Truburst2 device according to the hydraulic method (diaphragm method) as described in TS EN ISO 13938-1 standard [30]. The measurement area for bursting strength tests performed with the diaphragm method is 50 cm². During the test, the fluid (air) pressure applied to the fabric placed on the elastic rubber (diaphragm) is increased regularly to reach the average bursting strength determined in the preliminary trials in 20±5 seconds, and as a result, the fabric bursting strength (kPa) and height at burst (mm) values are determined. Elasticity is another very important performance feature for elastane core denim fabrics. Elasticity properties of denim fabrics are commonly determined according to ASTM D3107-07 [31] and BS EN 14704-1 [32] standards. In this study, tests were carried out in accordance with both test methods in order to determine the elasticity and growth properties of fabrics and the results were analyzed. According to ASTM D3107-07 standard, the sample width is reduced to 50 mm by removing the thread along the length from the opposite edges of the fabric cut in certain sizes (60 mm x 560 mm). At least 250 mm long reference points are marked on the sample, centering the center point as much as possible (O1) (Figure 3.a). A 1.36 kg (3 lb) block is attached to the tip of the cut specimen and tension is applied three times for 5

seconds. After the fabric is exposed to the applied tension for the fourth time for 30 minutes, the distance (A) between the reference points is measured and recorded (Figure 3.b) and the elasticity value of the fabric (%) is determined according to Equation (1). In order to determine the permanent elongation (growth) value of the fabric, the tension on the fabric is removed and the fabric is laid on a flat surface without tension and the distance (B) between the reference points is measured (Figure 3.c). The growth values at the end of the specified periods (such as 30 minutes, 1 hour, 2 hours etc.) are calculated according to Equation (2).

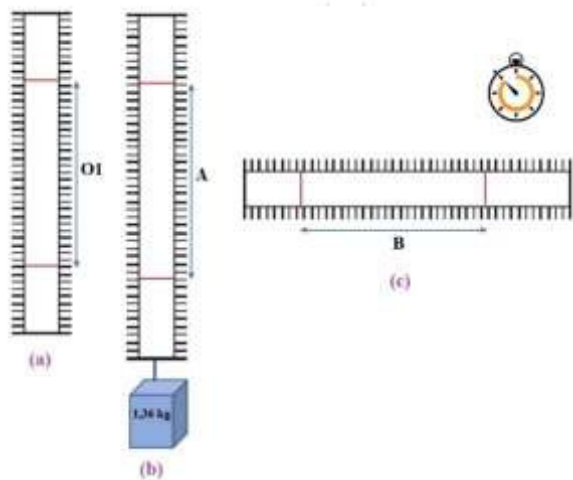


Figure 3. Calculation of fabric elasticity and growth (ASTM D3107-07)

$$\text{Elasticity (stretch)}(\%) = \left(\frac{A - O_1}{O_1} \right) \times 100 \quad \text{Equation (1)}$$

$$\text{Growth}(\%) = \left(\frac{B - O_1}{O_1} \right) \times 100 \quad \text{Equation (2)}$$

Where O_1 denotes the distance between the reference points, A denotes the distance between reference points after a load has been applied to the sample for a specified period of time and B denotes the distance between the reference points for the specified times after the load on the sample is removed.

According to BS EN 14704-1 Method A, the sample cut in dimensions of 50 mmx300 mm is placed between the jaws of the strength tester. The measuring length is 200 mm, and the test speed is 100 mm/min. Reference points showing the measurement length are marked on the sample and placed between the jaws. A load of 6 N/cm is applied to the sample for 5 cycles. Then the sample is placed on a flat surface and the distance between the reference points is measured after a certain time (1 min and 30 min). Elasticity (%) and growth (%) values are calculated in accordance with the standard.

In order to compare the elasticity test methods, the elasticity (%) value calculated according to the ASTM D 3107-07 standard was also calculated according to the BS

EN 14704-1. In addition, elastic recovery (%) values for both methods were calculated and analyzed.

In the study, elasticity (mm/N), stiffness (mm), plasticity (μm) and hysteresis (J) parameters were measured using the EMTEC TSA (Tissue Softness Analyzer) device to determine the elasticity and hysteresis behavior of denim fabrics under low stress. Table 4 and Figure 4 gives the parameters that EMTEC TSA device measures.

The tests in the study were carried out under standard atmospheric conditions (20 ± 2 °C temperature and $65 \pm 4\%$ relative humidity) specified in TS EN ISO 139. According to the standards, five fabric samples were tested for all tests.

3. RESULTS AND DISCUSSION

Within the scope of the study, the effect of different weft yarns on the properties of denim fabrics was investigated. Statistical analyzes were performed using the SPSS 24 program with a confidence interval of 95%.

3.1 Structural Properties (Unit Weight, Weft and Warp Density and Fabric Thickness)

The unit weights of denim fabrics before and after washing are given in Figure 5. When Figure 5 is examined, while there was no significant difference between the unit weights of denim fabrics produced using cotton (ring and OE-rotor) weft yarns, the differences between the unit weights of denim fabrics produced using core and dual-core weft yarns are quite high and statistically significant ($p=0.00$). When elastane core yarn is used as weft yarn in denim fabrics, an increase of 16%-26% was observed in fabric unit weights. The results are in line with the studies by Erbil et al. (2021) and Üte (2019). The reason of this situation is that the shrinkage values of the fabrics produced from core yarns containing elastane are quite high after washing as seen in Figure 6. The highest difference in unit weights belongs to denim fabrics produced from cotton+elastane single-core weft yarns, which has the highest shrinkage values.

The weft and warp density (/cm) and thickness (mm) values of denim fabrics after washing are given in Table 5. When examined, it is seen that warp density and fabric thickness values of denim fabrics produced from cotton ring and OE-rotor weft yarns are lower than fabrics produced from core yarns ($p=0.00$). The main reason for this is the lower packing density values of core yarns [18,34]. Therefore, since these yarns can be compressed more due to air gaps between fibers and the forces caused by the fabric shrinkage they are exposed to after fabric production, they will show a denser placement in the fabric structure.

Table 4. Explanations of the parameters measured by EMTEC TSA [33]

Parameter	Definition
D	Stiffness or “in-plane stiffness” or “stretch” (lower value = higher stiffness)
E	Elasticity (mm/N) the higher the value, the more elastic is the material, the lower the value, the less flexible.
H	Hysteresis (J) the higher the hysteresis, the more energy is generated during the recovery of the material.
P	Plasticity or “Fitting” (µm) the closer the value to zero “0”, the better the recovery of the material. P gives an information about the recovery characteristics of a fabric: to what extent does a material bounce back into its original position after deformation with a defined load.

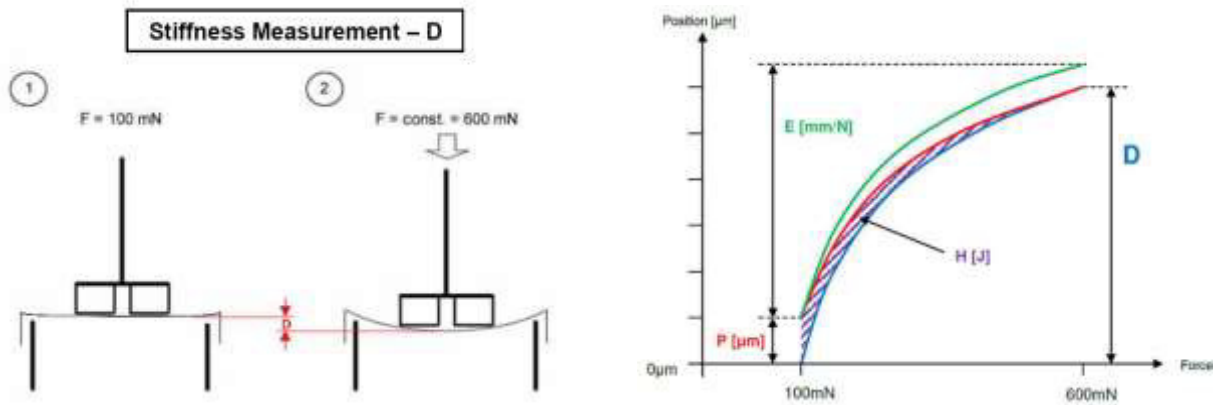


Figure 4. Measurement of the stiffness, elasticity, hysteresis and plasticity values [33]

Table 5. Density and thickness values of denim fabrics

Sample code	Weft density (/cm)	Warp density (/cm)	Fabric thickness (mm)
Ring	24.4	39.8	0.54
OE-rotor	24.4	38.8	0.57
Cotton+Dual Core (Elastane-PBT)	24.6	56.8	0.79
Cotton+Core (Elastane)	24.6	55.8	0.76
Cotton/PET+Core (Elastane)	24.6	55.8	0.75

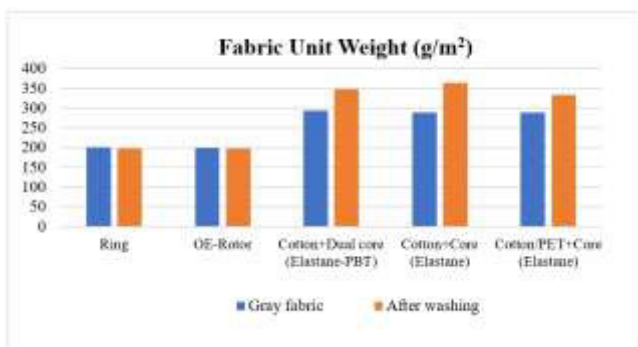


Figure 5. Fabric unit weights (g/m²) before and after washing

3.2 Dimensional Properties

When the dimensional change values of denim fabrics are examined, it is seen that denim fabrics containing single-core and dual-core weft yarn are quite higher than denim fabrics containing 100% cotton ring and 100% cotton OE-rotor weft yarn, as in unit weight test results (Figure 6). Positive dimensional stability test results indicate the fabric

elongation for the measured test direction, and negative results indicate shrinkage for the measured test direction, and it is seen that there is shrinkage in both directions for all fabrics in general (except for the cotton ring and cotton OE-rotor warp direction). It is seen that the dimensional change (shrinkage) in the weft direction is quite high (between 11-18%) in denim fabrics produced from elastane core yarns (for both single-core and dual core yarns) as weft yarn. The shrinkage value in fabrics produced from cotton-elastane core yarns is higher than in fabrics produced from cotton/PET+elastane core yarns and dual-core yarns. When the results are analyzed statistically, it is seen that this difference is statistically significant ($p < 0.05$).

Usable fabric width is one of the most important parameters for mass production of garments. When the widths of denim fabrics produced using the same weaving production parameters are examined, it is seen that the fabric width of the denim fabrics produced using 100% cotton (ring and OE-rotor) weft yarn is considerably higher than the denim fabrics produced using core (single and double) weft yarn (Figure 7) ($p = 0.00$). This situation can be explained by the

lower packing density and higher compressibility of core yarns [18]. When the shrinkage values after washing in denim fabric widths are examined, it is seen that the highest shrinkage value belongs to denim fabrics produced from single-core cotton-elastane yarns. The fabric width shrinkage values are in parallel with the dimensional stability values in the weft direction ($R=0.99$).

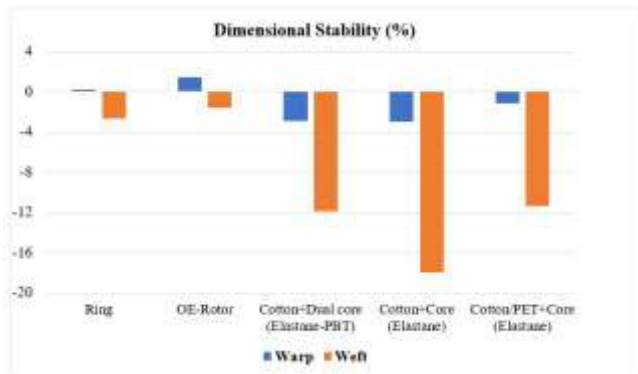


Figure 6. Dimensional stability of denim fabrics in warp and weft direction (%)

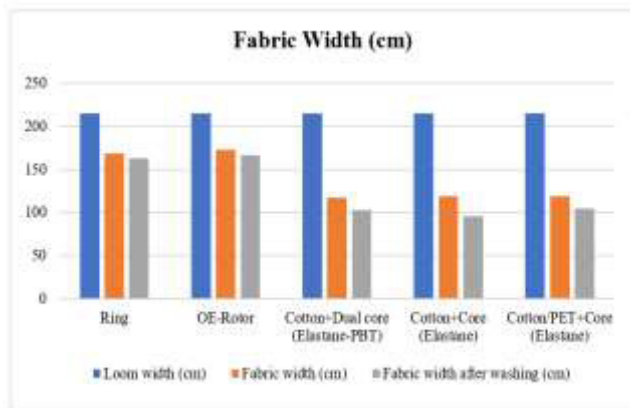


Figure 7. Denim fabric widths before and after washing

3.3 Tensile Strength and Breaking Elongation

The tensile strength (N) and breaking elongation (%) of denim fabrics produced using different weft yarns are shown in Figure 8. In warp direction, while the tensile strength values of denim fabrics containing elastane core yarn changes between approximately 675-795 N, breaking elongation values are 24-27%. In weft direction, the values for these fabrics are 245-345 N and 89-103%, respectively.

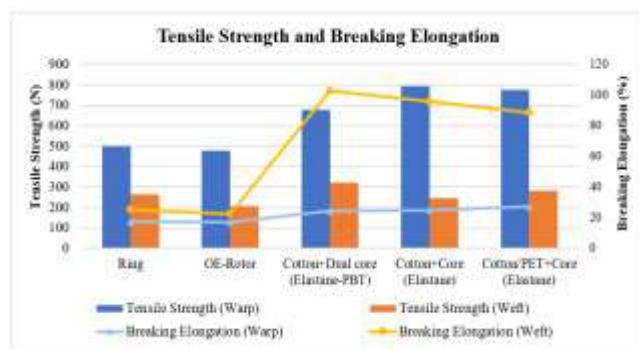


Figure 8. Tensile strength and breaking elongation of denim fabrics

When the tensile strength values of denim fabrics in the warp direction are examined, it is seen that fabrics containing elastane core weft yarn have higher values than fabrics containing both of 100% cotton ring and 100% cotton OE-rotor weft yarn. The reason of this situation is the increase of warp density in denim fabrics containing core yarn as seen in Table 5. When the strength and elongation values in the weft direction, which is the direction in which different weft yarns are used, are examined, it is seen that the differences are lower than in the warp direction. The fact that small differences between the tensile strength values in the weft direction can be explained by the loss of staple fibers in the yarn cross-section [18] and the lower differences between weft densities. It is seen that the highest tensile strength and breaking elongation values in the weft direction belong to denim fabrics produced using dual-core yarn, while the lowest values belong to denim fabrics produced using 100% cotton OE-rotor yarn. The second core in dual-core yarns supports the increase in strength. Tensile strength test results in the weft direction are parallel with yarn strength test results as seen in Table 2 [35]. In addition, fabric tensile strength test results are compatible with previous studies [17-18]. When the effect of using different weft yarns on tensile strength and breaking elongation is analyzed statistically, it is seen that it is statistically significant for both directions (weft and warp) ($p<0.05$). SNK test results have revealed that tensile strength values for warp and weft directions have been separated into five groups according to material in Table 6 and Table 7. When the SNK test results for breaking elongation are examined, it is seen that they have been divided into three groups for warp direction and they have been divided into three groups for weft direction (Table 8 and Table 9).

Table 6. SNK results for tensile strength values of denim fabrics (warp direction)

Material	N	1	2	3	4	5
OE-rotor	5	480.22				
Ring	5		499.76			
Cotton+Dual Core (Elastane-PBT)	5			676.22		
Cotton/PET+Core (Elastane)	5				774.18	
Cotton+Core (Elastane)	5					793.78
	Sig.	1.000	1.000	1.000	1.000	1.000



Table 7. SNK results for tensile strength values of denim fabrics (weft direction)

Material	N	1	2	3	4	5
OE-rotor	5	205.76				
Cotton+Core (Elastane)	5		244.36			
Ring	5			264.64		
Cotton/PET+Core (Elastane)	5				284.18	
Cotton+Dual Core (Elastane-PBT)	5					323.44
Sig.		1.000	1.000	1.000	1.000	1.000

Table 8. SNK results for breaking elongation values of denim fabrics (warp direction)

Material	N	1	2	3
OE-rotor	5	17.16		
Ring	5	17.48		
Cotton+Dual Core (Elastane-PBT)	5		24.31	
Cotton+Core (Elastane)	5		24.89	
Cotton/PET+Core (Elastane)	5			27.28
Sig.		0.517	0.246	1.000

Table 9. SNK results for breaking elongation values of denim fabrics (weft direction)

Material	N	1	2	3	4	5
OE-rotor	5	22.50				
Ring	5		25.32			
Cotton/PET+Core (Elastane)	5			88.61		
Cotton+Core (Elastane)	5				95.70	
Cotton+Dual Core (Elastane-PBT)	5					102.72
Sig.		1.000	1.000	1.000	1.000	1.000

3.4 Tearing Strength

The tearing strength values of elastane core denim fabrics are equal to approximately 45 N in warp direction for all fabrics, while it changes between 26-42 N in weft direction (Figure 9). Performing statistical analysis for the tearing strength values of the denim fabrics showed that differences are not statistically significant for warp direction but statistically significant for weft direction in which different yarns were used. When pairwise comparisons are made in the weft direction, it is seen that there is no significant difference between the tearing strength values of denim fabrics produced using single core weft yarn (cotton+elastane and cotton/PET+elastane) ($p>0.05$). Tearing strength values in weft direction of denim fabrics

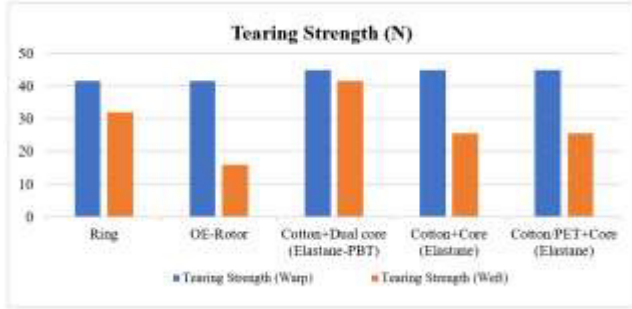
produced from dual-core yarns are higher than single-core (cotton+elastane and cotton/PET+elastane) fabrics because the second core supports the yarn breaking strength, and this difference is statistically significant ($p<0.05$). SNK results for the tearing strength of fabrics (for warp and weft direction) are seen in Table 10 and Table 11. For warp direction, tearing strength of fabrics have been divided into two groups. It was determined that fabrics produced from ring and OE-rotor weft yarns are in the same group, while fabrics containing elastane yarns are in the other group. For weft direction, tearing strength of fabrics have been separated into four groups. It was determined that fabrics produced from both single-core yarns are in the same group and that each of other fabrics are in different groups for weft direction.

Table 10. SNK results for tearing strength values of denim fabrics (warp direction)

Material	N	1	2
Ring	5	41.60	
OE-rotor	5	41.60	
Cotton/PET+Core (Elastane)	5		44.80
Cotton+Core (Elastane)	5		44.80
Cotton+Dual Core (Elastane-PBT)	5		44.80
Sig.		1.000	1.000

Table 11. SNK results for tearing strength values of denim fabrics (weft direction)

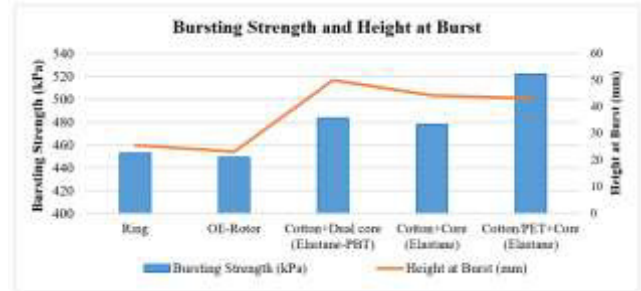
Material	N	1	2	3	4
OE-rotor	5	15.99			
Cotton/PET+Core (Elastane)	5		25.60		
Cotton+Core (Elastane)	5		25.60		
Ring	5			32.00	
Cotton+Dual Core (Elastane-PBT)	5				41.59
Sig.		1.000	1.000	1.000	1.000

**Figure 9.** Tearing strength of denim fabrics

3.5 Bursting Strength

Bursting strength (kPa) and height at burst (mm) values of denim fabrics are given in Figure 10. From Figure 10, it is seen that the bursting strength values of all fabrics produced using core (single and dual) yarn are different and higher than fabrics produced from 100% cotton yarn (ring and OE-rotor). The effect of weft yarn type on bursting strength is also statistically significant ($p < 0.05$). SNK test results for bursting strength and height at burst are given in Table 12 and Table 13, respectively. SNK test results have revealed that bursting strength values have been separated into three groups. It was determined that denim fabrics produced from ring and open-end rotor weft yarns are in one group, cotton+elastane and cotton+dual-core yarns are in the other group and cotton/PET+elastane yarn is in the last group. The highest bursting strength values belong to the fabrics

produced from single-core cotton/PET+elastane weft yarns, and the highest bursting height values belong to the fabrics produced from dual-core weft yarns which have the highest elongation values in the tensile strength test as seen in Figure 8. The reason why the bursting strength test results are not completely parallel with the breaking strength test results is that force is applied to the fabric in both directions in bursting strength tests. For this reason, both weft and warp yarns contribute greatly to the results in bursting strength tests. According to the tensile strength test results, the fabric with the highest total of weft and warp breaking strength is the fabric produced from cotton/PET+elastane single-core weft yarns, and similarly, this fabric has the highest bursting strength value. When the correlation between the total tensile strength (weft+warp) values and bursting strength values is examined, it is seen that the correlation coefficient is statistically significant ($R=0.85$).

**Figure 10.** Bursting strength and height at burst of denim fabrics**Table 12.** SNK results for bursting strength values of denim fabrics

Material	N	1	2	3
OE-rotor	5	448.96		
Ring	5	452.92		
Cotton+Core (Elastane)	5		478.20	
Cotton+Dual Core (Elastane-PBT)	5		483.74	
Cotton/PET+Core (Elastane)	5			522.02
Sig.		0.702	0.594	1.000

Table 13. SNK results for height at burst values of denim fabrics

Material	N	1	2	3	4
OE-rotor	5	23.06			
Ring	5		25.62		
Cotton/PET+Core (Elastane)	5			43.12	
Cotton+Core (Elastane)	5			44.28	
Cotton+Dual Core (Elastane-PBT)	5				49.96
Sig.		1.000	1.000	0.177	1.000



3.6 Elasticity and Growth

Elasticity is one of the most desired performance properties for denim fabrics containing elastane. In elasticity tests, elasticity (stretch) value shows the elongation (%) that occurs in the fabric under the load, and growth (%) value shows the permanent elongation that occurs in the fabric after the applied load is removed at the end of the determined time. Figure 11 and Figure 12 give the elasticity (%) and growth (%) values obtained in tests performed according to ASTM D3107-07 and BS EN 14704-1 standards. When the elasticity values are examined, it is seen that the highest values for both methods belong to the fabrics produced from cotton+elastane single-core weft yarns, while the lowest values belong to the fabrics produced from cotton/PET+elastane single core weft yarns. While the elasticity values of denim fabrics containing core weft yarn vary between 62% and 84% according to ASTM D 3107-07 standard, these values vary between 43% and 54% according to BS EN 14704-1 standard. This difference between elasticity values is due to the method differences. While the load (1.36 kg=13.34 N) applied to the fabric for 30 minutes according to ASTM D 3107-07 standard, the load (6 N/cm= 30 N) is applied to the fabric in 5 cycles according to the BS EN 14704-1 standard, and therefore the exposure time of the fabric to the applied load is also reduced. It is thought that this situation causes the lower elasticity results obtained in the BS EN 14704-1 test method. The elasticity values obtained by both methods show that the denim fabrics used in the study provide the movement elasticity (power stretch) [1,36]. When the growth (%) values are examined, it is seen that parallel results are obtained for both methods, as in the elasticity results. For both methods and all time periods (1 min, 30 min, 2 hours), the highest growth values belong to the denim fabric with the highest elasticity values, and the lowest permanent elongation values belong to the denim fabric with the lowest elasticity values. The difference between elasticity and growth values of core denim fabrics is statistically significant ($p < 0.05$). SNK test results for elasticity and growth values according to ASTM D3107-07 and BS EN 14704-1 standards are given in Table 14-Table 19. According to SNK test results for elasticity and growth values for ASTM D 3107-07 standard, each fabric takes place in different groups (Table 14-Table 16). SNK results

for elasticity and growth (30 min) according to BS EN 14704-1 standard have been divided into two groups (Table 17 and Table 19). It was determined that denim fabrics produced from cotton+elastane and cotton+dual-core weft yarns are in the same group, while denim fabric with single core cotton/PET+elastane weft yarns is in the other group. Within the scope of the study, elastic recovery values for 30 minutes were also calculated using elastic elongation and permanent elongation values. For both methods, it is seen that the elastic recovery values of the core denim fabrics are in the range of 90%-92% and there is no statistically significant difference between the elastic recovery values for the denim fabrics examined in the study ($p > 0.05$). The results of elasticity, growth and elastic recovery are compatible with previous studies [5,37].

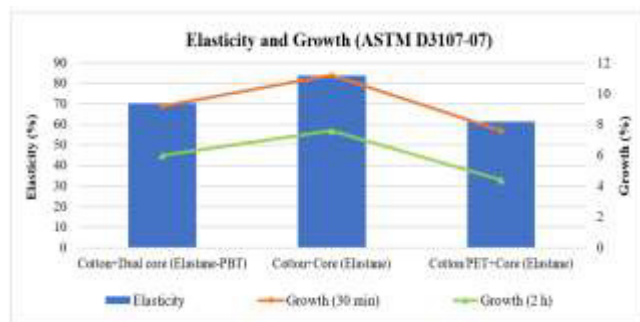


Figure 11. Elasticity (%) and growth (%) values in weft direction of denim fabrics (ASTM D3107-07)

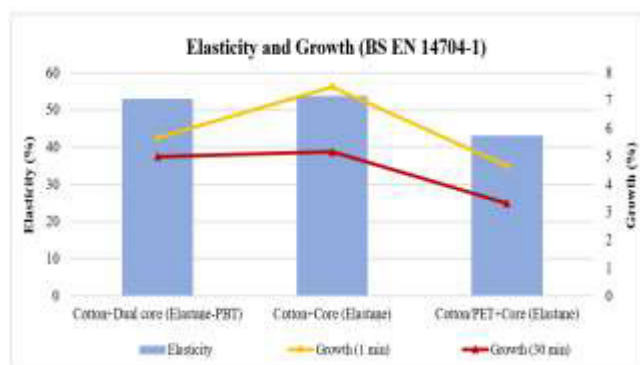


Figure 12. Elasticity (%) and growth (%) values in weft direction of denim fabrics (BS EN 14704-1)

Table 14. SNK results for elasticity values of denim fabrics (ASTM D3107-07)

Material	N	1	2	3
Cotton/PET+Core (Elastane)	5	61.60		
Cotton+Dual Core (Elastane-PBT)	5		70.40	
Cotton+Core (Elastane)	5			84.00
Sig.		1.000	1.000	1.000

Table 15. SNK results for 30 min. growth values of denim fabrics (ASTM D3107-07)

Material	N	1	2	3
Cotton/PET+Core (Elastane)	5	7.60		
Cotton+Dual Core (Elastane-PBT)	5		9.20	
Cotton+Core (Elastane)	5			11.20
Sig.		1.000	1.000	1.000

Table 16. SNK results for 2 hours growth values of denim fabrics (ASTM D3107-07)

Material	N	1	2	3
Cotton/PET+Core (Elastane)	5	4.40		
Cotton+Dual Core (Elastane-PBT)	5		6.00	
Cotton+Core (Elastane)	5			7.60
Sig.		1.000	1.000	1.000

Table 17. SNK results for elasticity values of denim fabrics (BS EN 14704-1)

Material	N	1	2
Cotton/PET+Core (Elastane)	5	43.03	
Cotton+Dual Core (Elastane-PBT)	5		52.74
Cotton+Core (Elastane)	5		53.63
Sig.		1.000	0.560

Table 18. SNK results for 1 min. growth values of denim fabrics (BS EN 14704-1)

Material	N	1	2	3
Cotton/PET+Core (Elastane)	5	4.68		
Cotton+Dual Core (Elastane-PBT)	5		5.67	
Cotton+Core (Elastane)	5			7.50
Sig.		1.000	1.000	1.000

Table 19. SNK results for 30 min. growth values of denim fabrics (BS EN 14704-1)

Material	N	1	2
Cotton/PET+Core (Elastane)	5	3.33	
Cotton+Dual Core (Elastane-PBT)	5		5.00
Cotton+Core (Elastane)	5		5.17
Sig.		1.000	0.682

3.4 Elasticity and Hysteresis under Low Stress

Elasticity (mm/N), stiffness (mm), hysteresis (J) and plasticity (μm) values of denim fabrics containing elastane under low stress are given in Table 20. When Table 20 is examined, it is seen that the elasticity and stiffness values of denim fabrics containing different core yarn constructions in the weft direction are quite close to each other and the lowest values belong to the fabrics produced from cotton+elastane single-core yarns. For these parameters, the differences between fabrics are not statistically significant ($p>0.05$).

When the hysteresis and plasticity values are examined, it is seen that the highest values belong to the fabrics produced from cotton+elastane single-core yarns and the differences between the fabrics are statistically significant ($p<0.05$). This means that fabric produced from cotton+elastane single-core yarns consumes more energy when returning to original size, that is, its recovery ability is less. It is thought that the higher growth values of the fabrics produced from cotton+elastane single-core yarns in the tests performed with standard test methods (ASTM D 3107-07 and BS EN 14704-1) support this result.

Table 20. Elasticity parameters measured under low stress

Sample code	Elasticity (E) (mm/N)			Stiffness (D) (mm)			Hysteresis (H) (J)			Plasticity (P) (μm)		
	Face	Back	Mean	Face	Back	Mean	Face	Back	Mean	Face	Back	Mean
Cotton+Dual Core (Elastane-PBT)	1.88	1.86	1.87	1.88	1.95	1.92	42.7	48.1	45.40	-60.8	-86.6	-73.7
Cotton+Core (Elastane)	1.80	1.82	1.81	1.86	1.91	1.89	50.7	56.6	53.65	-72.0	-91.0	-81.5
Cotton/PET+ Core (Elastane)	1.85	1.87	1.86	1.89	1.94	1.92	45.2	52.3	48.75	-59.8	-84.2	-72.0



4. CONCLUSION

Strength and elasticity properties are the most important performance parameters expected from denim fabrics. This study investigated the effect of different weft yarns (ring, OE-rotor, single-core and dual-core) on elasticity and strength properties of denim fabrics. In this context, the strength properties of denim fabrics were analyzed by breaking, tearing and bursting strength tests, and their elasticity properties were analyzed using the two most widely used test methods (ASTM D3107-07 and BS EN 14704-1) and under low stress. In addition, the effect of using different weft yarn structures on the structural and dimensional properties of fabrics was also evaluated. The main results of the study can be summarized as follows: The use of elastane core yarn in the weft direction has significantly increased the density in this direction and fabric unit weight. It was remarkable that 16%-26% fabric unit weight increased for single-core and dual-core weft yarn structure, in parallel with previous studies. It was seen that the dimensional change (shrinkage) in the weft direction is quite high (between 11-18%) in denim fabrics produced from single-core and dual core yarns. When the results were analyzed in terms of tensile strength and elongation, it was seen that the highest values in the weft direction belong to denim fabrics produced using dual-core yarn, while the lowest values belong to denim fabrics produced using 100% cotton OE-rotor yarn. For the tearing

strength, it was seen that there was no statistically significant difference for warp direction which has the same yarn construction for all fabrics, but there was a statistically significant difference in weft direction in which different yarn structures are used. The tearing strength values in weft direction of the denim fabrics produced from dual-core yarns were higher than the fabrics produced from single-core yarns, as in the tensile strength test results, due to the second core support the breaking strength. Bursting strength results, like other strength test results, show that fabrics with elastane core yarn structure have quite different behavior compared to other fabrics (cotton ring and cotton OE-rotor). On the other hand, bursting strength test results were not completely parallel with other strength test results. The reason for this is that the fabric is under the effect of multi-directional forces in the bursting strength test. Therefore, both weft and warp yarns contribute simultaneously to the bursting strength of fabrics. When the elasticity values are examined, for ASTM D 3107-07 standard: 62%-84%, and for BS EN 14704-1 standard: 43%-54%. This difference is due to the difference between test methods. For both methods, it is seen that the elastic recovery values of denim fabrics are: 90%-92%. The elasticity results show that the denim fabrics produced from single and dual-core yarns used in the study have power stretch, and thus provide movement elasticity and comfort.

REFERENCES

1. Kurban NS, Babaarslan O. 2019. Literature review on the properties of super stretch denim fabrics. *Journal of Textiles and Engineer* 26(113), 104-115.
2. İTKİB. 2012. Türkiye'nin denim kumaş ve konfeksiyon dış ticareti üzerine istatistikî bilgiler 2011 ve Dünya denim pantolon pazarına bakış. İTKİB Genel Sekreterliği AR-GE ve Mevzuat Şubesi.
3. Paul R. 2015, Denim and jeans: an overview. In P.R. Editor (Ed.), *Denim: Manufacture, Finishing and Applications*. United Kingdom: Woodhead Publishing, 1-11.
4. Lawrence CA. 2003. *Fundamentals of Spun Yarn Technology*. New York: CRC Press LLC.
5. Chen T. 2011. Compound yarns. In R. H. G. Editor (Ed.), *Specialist Yarn and Fabric Structures: Developments and applications*. United Kingdom: Woodhead Publishing, 1-20.
6. Gowda RVM. Advances in yarn spinning and texturizing. In R. A. and A.D. Editors (Ed.), *Technical textile yarns: Industrial and Medical Applications*. United Kingdom: Woodhead Publishing, 56-90.
7. Mezarciöz S, Oğulata RT, Nergis A. 2020. Investigation of elasticity and growth properties of denim fabrics woven with core and siro spun yarn. *Tekstil ve Konfeksiyon* 30(4), 312-320.
8. Shaw VP, Mukhopadhyay A. 2021. Impact of abrasion on strength, elasticity and elastic recovery properties of stretch-denim fabric. *International Journal of Clothing Science and Technology*, online published.
9. Sarioğlu E, Babaarslan O. 2017. A comparative strength analysis of denim fabrics made from core-spun yarns containing textured microfilaments. *Journal of Engineered Fibers and Fabrics* 12(1), 22-32.
10. Sarioğlu, E, Babaarslan O. 2019. Porosity and air permeability relationship of denim fabrics produced using core-spun yarns with different filament finenesses for filling. *Journal of Engineered Fibers and Fabrics* 14, 1-8.
11. Özdil, N. 2008. Stretch and bagging properties of denim fabrics containing different rates of elastane. *Fibres & Textiles in Eastern Europe* 16(1) 66, 63-67.
12. El-Ghezal S, Babay A, Dhoub S, Cheikhrouhou M. 2009. Study of the impact of elastane's ratio and finishing process on the mechanical properties of stretch denim. *The Journal of the Textile Institute* 100(3), 245-253.
13. Sinha SK, Bansal P, Maity S. 2017. Tensile and elastic performance of cotton/lycra core spun denim yarn. *Journal of the Institution of Engineers (India): Series E* 98(1), 71-78.
14. Daşan Y, Babaarslan O. 2020. Stretch and physical properties of weft stretch denim fabrics containing elastane and filament yarn. *Journal of Textile Science & Fashion Technology* 4(4), 1-10.
15. Ertaş OG, Zervent Ünal B, Çelik N. 2016. Analyzing the effect of the elastane-containing dual-core weft yarn density on the denim fabric performance properties. *The Journal of The Textile Institute* 107(1), 116-126.
16. Yildirim N, Akgül E, Türksoy HG. 2021. Selection of dual-core yarn production parameters for denim fabric by using MULTIMOORA method. *The Journal of The Textile Institute* 1-9, online published.- web sitesi adresi/DOI yok
17. Bedez Ute T. 2019. Analysis of mechanical and dimensional properties of the denim fabrics produced with double-core and core-spun weft yarns with different weft densities. *The Journal of the Textile Institute* 110(2), 179-185.
18. Erbil Y, Babaarslan O, Islam M R, Sirlibaş S. 2021. Performance of core & dual-core cotton yarn structures on denim fabrics. *Journal of Natural Fibers* 1-14, online published. web sitesi adresi/DOI yok
19. Sarioğlu E. 2019, June. the effect of core-spun yarn type and layout of these yarns in the fabric on stiffness properties of denims. In Ö.Ç.

- Editor (Ed.) Proceedings of the 5th International Conference on Engineering and Natural Science (408-413), Prague, Czech Republic.
20. Bedez Ute, T, Kadoglu, H. 2019. The effect of single and dual-core yarns produced with different core materials on the elasticity and recovery properties of denim fabrics. *Textile & Leather Review* 2(4), 174-182.
 21. Sabry M, Bakry M. 2017. The Effect of Different Weft Yarn Production Technique on the Pilling Property of Jeans Fabrics. *International Design Journal* 7(3), 161-169.
 22. Türksoy HG, Yıldırım N, Ertek Avcı M. 2021. Comparative evaluation of some comfort properties of denim fabrics including dual-core yarns containing wool and elastane yarn. *The Journal of the Textile Institute* 1-8, online published. web sitesi adresi /DOI yok
 23. Baykuş D, Oğulata, RT. 2019. Effects of using core weft yarn on elasticity and residual extension properties of denim fabrics. *Journal of Textiles and Engineer*, 26(116), 372-380.
 24. TS EN 12127. Textiles- Fabrics- Determination of mass per unit area using small samples. Turkish Standards Organization, Turkey, 1999.
 25. TS 250 EN 1049-2. Textiles-Woven fabrics-Construction-Methods of analysis-part 2 determination of number of threads per unit length. Turkish Standards Organization, Turkey, 1996.
 26. TS 7128 EN ISO 5084. Textiles-Determination of thickness of textiles and textile products. Turkish Standards Organization, Turkey, 1998.
 27. TS EN ISO 3759. Textiles - Preparation, marking and measuring of fabric specimens and garments in tests for determination of dimensional change. Turkish Standards Organization, Turkey, 2012.
 28. TS EN ISO 13934-1. Textiles- Tensile properties of fabrics- Part 1: Determination of maximum force and elongation at maximum force using the strip method. Turkish Standards Organization, Turkey, 2013.
 29. TS EN ISO 13937-2. Textiles- Tear properties of fabrics- Part 2: Determination of tear force of trouser- shaped test specimens (Single tear method). Turkish Standards Organization, Turkey, 2002.
 30. TS EN ISO 13938-1. Textiles - Bursting properties of fabrics - Part 1: Hydraulic method for determination of bursting strength and bursting distension. Turkish Standards Organization, Turkey, 1999.
 31. ASTM D3107-07. Standard test methods for stretch properties of fabrics woven from stretch yarns. American Society for Testing and Materials, USA, 2019.
 32. BS EN 14704-1. Determination of the elasticity of fabrics - Part 1: Strip tests. British Standards Institution, United Kingdom, 2006.
 33. Emtec. 2022. Tissue Softness Analyzer User Manual. Germany: Emtec Electronic GmbH.
 34. Erbil Y, Islam R, Babaarslan O, Sırlıbaş S. 2020. Effect of structural changes on the cotton composite yarn properties. *Journal of Natural Fibers*, 1-9, online published. web sitesi adresi /DOI yok
 35. Balci Kilic G. 2018. Analysing the physical and mechanical properties of core-spun yarns, *Annals of the University of Oradea Fascicle of Textiles, Leatherwork* 19(2), 13-18.
 36. Wang X, Liu X, Hurren C. 2008. Physical and mechanical testing of textiles. In J. H. Editor (Ed.) *Fabric Testing*. United Kingdom: Woodhead Publishing, 90-124.
 37. Babaarslan O, Sarioğlu E, Çelik Hİ, Artek Avcı M. Denim Fabrics Woven with Dual Core-Spun Yarns. In M. K. S. Editor (Ed.) *Engineered Fabrics*. United Kingdom: IntechOpen

Simultaneous Coloring and Antibacterial Finishing to Cotton Through Environmentally-Friendly Way

Burcu Sancar Beşen¹  0000-0001-5120-268X

Pınar Parlakyiğit¹  0000-0001-9235-6239

Erkan Yılmaz²  0000-0002-0947-3096

¹Adıyaman University, Faculty of Engineering, Department of Textile Engineering, Adıyaman/Turkiye

²Adıyaman University, Faculty of Pharmacy, Department of Pharmacognosy, Adıyaman/Turkiye

Corresponding Author: Burcu Sancar Beşen, bbesen@adiyaman.edu.tr

ABSTRACT

The present paper aimed to color 100% cotton fabrics while also ensuring antibacterial activity in an eco-friendly manner. For this purpose, cationized and pre-mordanted fabrics were dyed by using everlasting flower extract as a natural dye source. After dyeing process, antibacterial activity, CIEL^a*b* color values, color strength (K/S), and fastness properties (washing, perspiration, rubbing) of the dyed fabrics were investigated, as well as the bursting strength of the dyed and undyed fabrics was also examined. The results showed that it was possible to ensure simultaneous coloring and antibacterial activity on the cotton fabrics by using a methanol extract of the everlasting flower as a natural dye source. In addition, applying the cationizing and mordanting processes to cotton fabrics before dyeing provided higher antibacterial activity, better fastness properties, and a darker color.

ARTICLE HISTORY

Received: 11.11.2022

Accepted: 24.03.2023

KEYWORDS

Everlasting flower (*Helichrysum armenium* subsp. *araxinum*), natural dye, antibacterial activity, cationizing, mordanting

1. INTRODUCTION

Due to the public's enhanced environmental awareness and health concerns, sustainable, ecologic, nontoxic, and biodegradable products have recently gained more popularity [1]. Normally, textile dyeing and finishing processes include a number of steps in which hazardous chemicals are used. Scientists and textile industry firms have labored to reduce pollution caused by synthetic dyes and toxic chemicals currently used in textile applications [2,3]. Interest in the potential use of natural dyes has been growing, because of being safe, non-toxic, non-carcinogenic and biodegradable, having high compatibility with the environment, and being available in a range of natural shades as compared with synthetic dyes [3-6].

Natural dyes mainly contain various natural bioactive compounds, such as phenolic acids, flavonoids, alkaloids, terpenoids, essential oils, and natural color. These bioactive compounds have antimicrobial, antioxidant, anti-inflammatory activities and they can be used for hygiene, medical and pharmacological applications [2,4,7].

Antimicrobial textile materials have gained considerable popularity all over the world [4,8], since the textile

materials provide suitable environment for growth and multiplication of pathogenic microbes, leading to unpleasant odor, dermal infection, weakening of the substrate, discoloration, allergies, and other related diseases [7]. Various methods have been developed or are under development to give antimicrobial activity to textiles [5]. Although synthetic antimicrobial agents such as triclosan, metal and their salts, organometallics, phenols, etc. show good inhibition against bacteria, using natural eco-friendly agents such as natural dyes can eliminate their environmental risks [4]. For the reasons mentioned, with an ecological view, extract of everlasting flower (*Helichrysum armenium* DC. subsp. *araxinum* (Kirp.) Takht) was used as natural dye and antimicrobial agent in the present study.

The genus *Helichrysum*, belonging to the family of Asteraceae, consists of a few hundred species that are widespread throughout the world [9]. Plants of the genus *Helichrysum* are fertile producers of a host of secondary metabolites, including flavonoids, acetophenones, phloroglucinol, pyrones, triterpenoids and sesquiterpenes [10]. *Helichrysum* species are commonly used in Turkey and other parts of the world for their various biological properties, such as anti-inflammatory, antioxidant, and antimicrobial activities

To cite this article: Sancar Beşen B, Parlakyiğit P, Yılmaz E. 2024. Simultaneous Coloring and Antibacterial Finishing to Cotton Through Environmentally-Friendly Way. *Tekstil ve Konfeksiyon*, 34(1), 44-50.

[11]. Albayrak et.al (2010) showed the antibacterial activities of methanol extract of *Helichrysum armenium* subsp. *araxinum* against *Aeromonas hydrophila*, *Bacillus brevis*, *B. cereus*, *Klebsiella pneumoniae*, *Pseudomonas aeruginosa*, and *Staphylococcus aureus* bacteria [11].

In the literature, there are a lot of studies about coloring of some textile materials with natural sources. When the studies are focused, it can be seen that most of them have interested in dyeing of cationic textile materials such as wool, silk and polyamide [1,3-8,12-14] since the cationic fibers can be dyed easier than anionic ones. Although cotton is the most preferred natural fiber [15], there are limited studies about natural dyeing of cotton materials [16,17]. A cationization process should be applied to the cotton materials before natural dyeing in order to achieve better dyeing.

The most common methodology for cationization is to introduce amino groups into the fiber [18]. There have been various reported cationic agents for the modification of cotton in the literature, such as polyamide-based epichlorohydrin type of polymers, dendritic polymers, quaternary ammonium-based compounds, glycidyltrimethyl ammonium chloride (Glytac), choline chloride, N-methylolacrylamide, and biopolymers like chitosan [18,19], starch and their derivatives, keratin hydrolysate from chicken feather, horn and hoofs [19]. In the present study, chitosan, one of the biopolymers, was preferred for cationization. A renewable polysaccharide-based cationic biopolymer, chitosan (CH), is the deacetylated derivative of chitin [20] and is an important alternative to commonly used compounds to functionalize cotton because of its protonated amino groups [21]. Chitosan is inexpensive, abundant, non-toxic, biocompatible, and eco-friendly material [21,22].

Due to the low affinity of most natural dyes to textile fibers, mordants are used to increase their affinity and color fastness [12]. Mordants are commonly metallic salts such as tannic acid, alum, chrome alum, sodium chloride [24] which can be fixed on the cationic fibers and interact with dye through coordination bonds [4,12]. Mordanting can be achieved in three ways as pre-mordanting (before dyeing), simultaneously mordanting, and post-mordanting (after dyeing). In this study, the pre-mordanting process was carried out with using aluminum potassium sulphate as mordant agent due to being non-harmful to the environment.

In the experimental study, it was aimed to ensure simultaneous coloring and antibacterial activity to 100% cotton fabrics in an eco-friendly way. For this purpose, the methanol extract of the everlasting flower was used as a natural dye source. The cationized, pre-mordanted 100% cotton knitted fabrics were dyed with the extract. After the dyeing process, CIEL*a*b* color values, color strength values, fastness properties (washing, perspiration, rubbing), and antibacterial activity of the dyed fabrics were

investigated, as well as the bursting strength tests were also applied to dyed and undyed fabrics.

2. MATERIAL AND METHOD

2.1. Material

Chitosan (medium molecular weight, Sigma-Aldrich), aluminium potassium sulphate dodecahydrate ($KAl(SO_4)_2 \cdot 12H_2O$, Merck), Rucon LFF (cross-linker, Rudolf Duraner) methanol (Isolab), rotatory evaporator (Scilogex), ultrasonic bath (Isolab), and water bath (Isolab) were used. The $KAl(SO_4)_2$ was chosen as mordanting agent since it is known as green agent [25]. The chemicals were used without any further purification.

The aerial parts of the everlasting plant used in the study were collected from Bingöl Metan Mountain in Turkey on June, 2021. The photo of the plant can be seen in Figure 1. The collected sample were dried in the shade and stored in a clean and dry environment. Plant identity was verified by Dr. Ömer Kılıç and the prepared herbarium sample is kept in Hacettepe University Faculty of Pharmacy Herbarium with the number HUEF-21042.



Figure 1. *Helichrysum armenium* subsp. *araxinum* in its habitat

100% cotton knitted fabric (Ne 30/1, 1*1 rib knit, 212 g/m²) was used in the experiments. The fabric was scoured and bleached by the supplier (İskur Group, Kahramanmaraş). A laboratory-type fulard (Termal), an IR dyeing machine (Termal), and a steamer (Ataç) were also used.

2.2. Method

2.2.1. Preparation of everlasting flower extract

The powder of the everlasting flower was extracted with methanol via the maceration process. The ratio of plant:solvent was determined as approximately 1:10 (w/v) in the water bath at 40 °C. The maceration process was

repeated three times for three hours for each one, and the combined solutions were filtered through filter paper, and they were then evaporated to dryness under vacuum at 40 °C with a rotary evaporator. In order to preserve the structure of such chemical substances in the plant, the temperature was not exceeded by 40 °C during both extraction and evaporation.

The photo of the produced extract is given in Figure 2. The yield of the extract was calculated as 13.79%.



Figure 2. The methanol extract of everlasting flower

A stock solution of the everlasting flower extract was prepared in distilled water at the concentration of 20 mg/ml by using ultrasonic bath. The prepared stock solution was stored in the freezer at -24 °C for further usage.

2.2.2. Cationization process of the cotton fabrics

The cotton fabrics were cationized with chitosan. The concentration of chitosan was chosen at two different levels as 10 g/L and 20 g/L and it was applied to cotton samples by pad-dry-cure method. In order to prepare the application solution, the chitosan was dissolved in a %1 (w/v) acetic acid solution, and 50 g/L cross-linker agent was added to the solution. The fabric samples were squeezed to 96% pick up at fulard, then dried at 100 °C and cured for 2 minutes at steamer at 110 °C. Some of the fabric samples were saved without cationizing to investigate the effect of the cationization process on the results.

2.2.3. Mordanting process

The pre-mordanting process was carried out with 5 g/L concentration of $KAl(SO_4)_2$ at 98 °C for 60 minutes with a liquor ratio of 1:10 by using IR dyeing machine. After the process, the samples were rinsed with cold water and dried at 100 °C. In order to research the effect of the mordanting process on the results, some of the fabric samples were saved without mordanting.

2.2.4. Dyeing process

The different pretreated fabric samples (only cationized, only mordanted, both cationized and mordanted, and neither cationized nor mordanted) were dyed. The dyed

fabric samples can be seen in Table 1. The dyeing processes were carried out with the stock extract solution with a liquor ratio of 1:5 at 40 °C for 30 minutes by using an IR dyeing machine. After the dyeing, the samples were washed with cold water for 10 minutes and then dried at the room temperature.

Table 1. The dyed fabric samples

Sample Number	Chitosan concentration (g/l)	Mordant concentration (g/l)
1	0	0
2	10	0
3	20	0
4	0	5
5	10	5
6	20	5

2.3. The research methods

Bursting strength: The test was applied to dyed and undyed samples according to the ISO 13938-2:2019 standard [26] as three replications and the average of the results was calculated.

CIEL^a*b* color value and color strength (K/S) value:

The CIEL^a*b* values and the reflectance (R) values at wavelengths ranging from 400 to 700 nm of the dyed samples were measured. The measurements were carried out under D65 daylight and an aspect of 10° with a spectrophotometer (Datacolor SF 600 model). The results were measured over three replications, and the average of the results was calculated. The K/S values were calculated using the Kubelka-Munk equation by using the R-value at the wavelength (410 nm) at which each fabric sample had maximum absorption.

Color fastness test: In order to investigate the color fastness results of the dyed samples, fastness tests to washing [27], acidic and alkaline perspiration [28], and wet and dry rubbing [29] were carried out.

Antibacterial activity: The antibacterial activities of the everlasting flower extract and the fabric samples were investigated against Gram-negative bacteria (*Escherichia coli* ATCC 8739) and Gram-positive bacteria (*Staphylococcus aureus* ATCC 6538), since they are the major microorganisms responsible for 25% of hospital infections and popular test organisms which are resistant to common antimicrobial agents [30]. The tests were carried out in Ege University's Microbiological Analysis Laboratory (Egemikal). While the antibacterial activity of the extract was investigated through the disc diffusion method, it was researched via the AATCC 100 method for fabrics. The tests were applied as three replications.

3. RESULTS AND DISCUSSION

The antibacterial activity results of the stock solution of everlasting flower extract assessed according to the disc

diffusion method against *S. aureus* and *E. coli* bacteria are given in Figure 3. The inhibition zones formed by the extract solution against *S. aureus* and *E. coli* are 11.2 and 8 mm, respectively. Thus, it is possible to say that the prepared stock extract solution had antibacterial activity against both tested bacteria species.

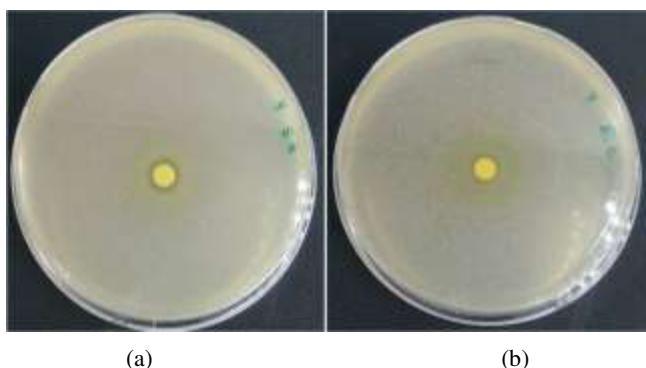


Figure 3. The antibacterial activity results of everlasting extract

The antibacterial activity results of the dyed samples assessed according to the AATCC 100 method against *E. coli* and *S. aureus* bacteria can be found in Table 2. The results show that the fabrics gained antibacterial activity against both *E. coli* and *S. aureus* bacteria. The fabric sample that was not subjected to cationizing and mordanting processes had less activity against *E. coli* than other samples since it had less dye. As *E. coli* is a more resistant bacteria than *S. aureus*, the result was observed more specifically for *E. coli*. As a result, it can be said that it is possible to provide both coloring and antibacterial activity simultaneously to a cotton fabric with a natural dyeing process through applying cationizing and mordanting processes before dyeing.

The bursting strength results of the fabric samples before and after dyeing can be seen in Figure 4. The bursting strength of the untreated raw fabric was 390,8 KPa, as shown in Figure 4, and the strength of the fabrics decreased after the cationizing and mordanting processes. However, the decline was not crucial and occurred at 14%. Generally, the increase in the chitosan concentration had no negative effect on the strength property. In addition, the dyeing process had a negligible effect on the strength properties of the samples, since no harsh chemicals were used in the natural dyeing process.

Table 3 shows the CIEL*a*b* color values as well as the color strength (K/S) values of the dyed samples. It is commonly known that while the L* value indicates the lightness and darkness, the b* value gives information about the yellowness and blueness, and the a* value is about the reddish and greenish tones of the fabric samples in the CIEL*a*b* color system. The L* value changes between 0 and 100, and the color becomes lighter as the L* value increases. The increase in the a* and b* values indicates that the color is becoming more reddish and yellowish, respectively. In addition, the increase in the K/S value means that the fabric is darker. When the results in Table 3 are focused, it can be clearly seen that both the application of the cationizing process and the use of mordants increased the dye uptake. Furthermore, the increase in the mordant concentration also increased the depth of color. In addition, the b* value increased significantly, especially when the mordant was used. This circumstance shows that the use of mordant had an effect on the shade of the fabric samples. The application of the mordant process after the chitosan treatments caused the color to have greater depth and strength. Thus, it is possible to say that in order to have a naturally colored fabric with a darker shade, it is necessary to apply both the cationizing and mordanting processes.

Table 2. % Reduction in bacteria after 24 hours

Sample number	<i>E. coli</i>			<i>S. aureus</i>		
	0.hour	24. hours	% Reduction	0.hour	24. hours	% Reduction
Untreated fabric	560000	Reproduction	-	263000	Reproduction	-
1	560000	45000	91.96	263000	100	99.96
2	560000	610	99.89	263000	50	99.98
3	560000	3380	99.40	263000	970	99.63
4	560000	1430	99.74	263000	75	99.97
5	560000	650	99.88	263000	80	99.97
6	560000	50	99.99	263000	300	99.89

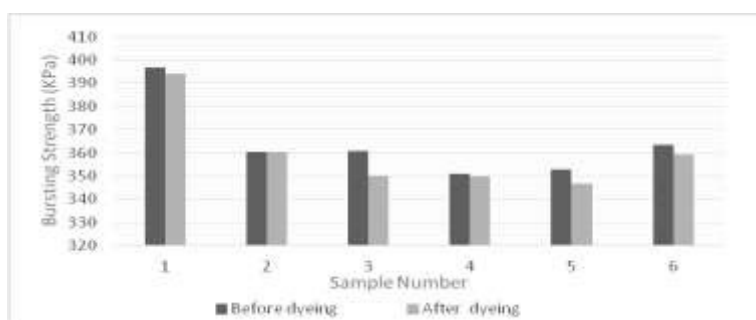


Figure 4. The bursting strength results of the fabric samples before and after dyeing

The results of washing, perspiration (acidic and alkaline), and rubbing (dry and wet) fastness of dyed samples are given in Table 4. Generally, the wash fastness of the fabric samples with dark colors has shown more staining than those with light colors. For that reason, the highest fastness

results were obtained for the samples to which neither the cationizing nor mordanting processes were applied, since they had less dye. Besides, the washing and perspiration fastness results got better when the mordanting process was applied to the fabric samples before the dyeing process.

Table 3. The results of CIEL*a*b* color values and color strength (K/S) values

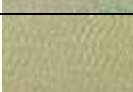
Sample number	Photos	L*	a*	b*	K/S
Undyed fabric		90.44	-0.07	1.87	-
1		79.02	-3.91	25.95	3.19
2		71.09	-3.79	27.98	6.97
3		70.35	-2.67	33.07	9.89
4		77.43	-3.95	45.67	7.96
5		71.13	-4.51	40.91	11.22
6		67.84	-2.95	42.89	11.84

Table 4. The results of color fastness of dyed samples

Sample number	Fading	Washing						Perspiration										Rubbing				
		As	Co	PA	PES	PAC	WO	Acidic					Alkaline					Wet	Dry			
								As	Co	PA	PES	PAC	WO	As	Co	PA	PES			PAC	WO	
1	5	4/5	3/4	4/5	4/5	4/5	4/5	4/5	3/4	3/4	4/5	4	4	4/5	2/3	3/4	4	4	4	4	4	4/5
2	4	4	2/3	4	4	4	4	4	3	3	4/5	4	4	4	2/3	3	4	4	4	3/4	3/4	4
3	3/4	4	2/3	4	4	4	4	4/5	3	3	4	4	3	4	1/2	2/3	4	4	4	3	3/4	4
4	4	4/5	3	4/5	4/5	4/5	4/5	4/5	3	3	4	4	4	4	2/3	3	3/4	3/4	3/4	3/4	3/4	4
5	4/5	4	3	4	4/5	4/5	4/5	4/5	3	3	4/5	4/5	4	4	2/3	3	4	4	4	3/4	3	4
6	4	4/5	3	4	4/5	4/5	4	4/5	3	3	4	4	3/4	4	2/3	2/3	3	3	3	3	3	4

4. CONCLUSION

The subject of applying dyeing process, which has crucial importance among the textile finishing process, with natural dyes and eco-friendly way has been more significant with increasing environmental awareness. For this reason, researchers have studied on coloring of the textile materials with different natural dye source. Furthermore, the vast majority of natural sources have antimicrobial activity, allowing for simultaneous coloring and antibacterial activity in textiles. In the present study, it was aimed to

provide simultaneous coloring and antibacterial activity to 100% cotton knitted fabrics with the everlasting flower extract. For this purpose, firstly, a methanol extract of the everlasting flower was prepared, and the antibacterial activity of the extract was examined. Then, the fabrics were cationized by using chitosan as a natural biopolymer and pre-mordanted with $KAl(SO_4)_2$ as a green mordanting agent. The treated fabrics were dyed with the prepared extract. Following the dyeing process, the fabrics' antibacterial activity, CIEL*a*b* color values, and color fastness to washing, perspiration, and rubbing were



evaluated. In addition, the bursting strength of the dyed and undyed fabrics was also measured. The results can be summarized as given below.

- The methanol extract of everlasting flower has antibacterial activity against both *S. aureus* and *E. coli* bacteria species.
- The bursting strength results are negatively affected by the cationizing and mordanting processes. However, the decline in the results is lower than 15% and not crucial. The increase in chitosan concentration has no crucial effect on the strength property, and the usage of both chitosan and mordant together have the most effect on the results.
- The applications of cationizing and mordanting processes increase the dye uptake, and treated fabrics dye with darker shade. In addition, the mordanting

process have positive effect on the fastness properties of the samples.

- The dyed samples after cationizing and mordanting processes gain high antibacterial activity against both *S. aureus* and *E. coli* bacteria.

As a conclusion, the %100 cotton fabrics can be colored with everlasting flower extract with gaining antibacterial activity. In order to achieve dyeing process with high antibacterial activity, good fastness, and dark color, the cationizing and mordanting processes are recommended before dyeing.

Acknowledgements

We are grateful to Prof. Dr. Ömer Kılıç (Adiyaman University Faculty of Pharmacy) for helpful assistance in botanical description.

5. REFERENCES

1. Koçak, ÖF, Yılmaz, F. 2022. Use of *Alpinia Officinarum* Rhizome in Textile Dyeing and Gaining Simultaneous Antibacterial Properties *Journal of Natural Fibers* 19(5), 1925–1936.
2. Rehan, M, Ibrahim, GE, Mashaly, HM, Hasanin, M, Rashad, HG, Mowaf, S. 2022. Simultaneous dyeing and multifunctional finishing of natural fabrics with Hibiscus flowers extract *Journal of Cleaner Production* 374 <https://doi.org/10.1016/j.jclepro.2022.133992>.
3. Zhang, B, Wang, L, Luo, L, King, MW. 2014. Natural dye extracted from Chinese gall e the application of color and antibacterial activity to wool fabric *Journal of Cleaner Production* 80, 204-210
4. Ghaheh, FS., Mortazavi, SM, Alihosseini, F, Fassihi, A, Nateri, AS, Abedi, D. 2014. Assessment of antibacterial activity of wool fabrics dyed with natural dyes *Journal of Cleaner Production* 72, 139-145
5. Mirjalili, M, Karimi, L. 2013a. Antibacterial Dyeing of Polyamide Using Turmeric as a Natural Dye, *AUTEX Research Journal*, 13(2) 51-56
6. Safapour, S, Sadeghi-Kiakhani, M, Eshaghloo-Galugahi, S. 2018. Extraction, Dyeing, and Antibacterial Properties of *Crataegus Elbursensis* Fruit Natural Dye on Wool Yarn *Fibers and Polymers* 19(7), 1428-1434.
7. Mirjalili, M, Karimi, L. 2013b. Extraction and Characterization of Natural Dye from Green Walnut Shells and Its Use in Dyeing Polyamide: Focus on Antibacterial Properties *Hindawi Publishing Corporation Journal of Chemistry* 2013, <http://dx.doi.org/10.1155/2013/375352>.
8. Shahid, M; Islam, S, Rather, LJ, Manzoor, N, Mohammad, F. 2019. Simultaneous shade development, antibacterial, and antifungal functionalization of wool using *Punica granatum* L. Peel extract as a source of textile dye *Journal of Natural Fibers* 16:4, 555-566.
9. Bahşi, M, Emre, MY, Emre, İ, Kurşat, M, Yılmaz, Ö. 2020. The determination of some biochemical contents of *Helichrysum armenium* DC. subsp. *araxinum* (Kirp.) Takht *Biological Diversity and Conservation* 13(1), 96-101.
10. Oji, K, Shafaghat, A. 2012. Constituents and Antimicrobial Activity of the Essential Oils from Flower, Leaf and Stem of *Helichrysum armenium*, *Natural Product Communications* 7(5), 671-674.
11. Albayrak, S, Aksoy, A, Sağdıç, O, Budak, Ü. 2010. Phenolic compounds and antioxidant and antimicrobial properties of *Helichrysum* species collected from eastern Anatolia, Turkey *Turkish Journal of Biology* 34(4), 463-473.
12. Ghoreishian, SM, Maleknia, L, Mirzapour, H, Norouz, M. 2013. Antibacterial Properties and Color Fastness of Silk Fabric Dyed with Turmeric Extract *Fibers and Polymers* 14(2), 201-207
13. Haji, A. 2012. Antibacterial Dyeing of Wool with Natural Cationic Dye Using Metal Mordants *Materials Science* 18(3), 267-270
14. Shabbir, M, Rather, LJ, Azam, M, Haque, QMR, Khan, MA, Mohammad, F. 2020. Antibacterial Functionalization and Simultaneous Coloration of Wool Fiber with the Application of Plant-Based Dyes *Journal of Natural Fibers* 17(3), 437-449
15. Gedik, G, Yavaş, A, Avingç, O, Şimşek, Ö. 2013. Cationized Natural Dyeing of Cotton Fabrics with Corn Poppy (*Papaver rhoeas*) and Investigation of Antibacterial Activity. *Asian Journal of Chemistry* 25(15), 8475-8483
16. Haji, A. 2013. Eco-Friendly Dyeing and Antibacterial Treatment of Cotton *Cellulose Chem. Technol.* 47 (3-4), 303-308
17. Kamel MM, Helmy HM, Meshaly HM, Abou-Okeil A. 2015. Antibacterial Activity of Cationised Cotton Dyed with Some Natural Dyes *J Textile Sci Eng* 5: 180. doi:10.4172/2165-8064.1000180
18. Correia, J, Rainert, KT, Oliveira, FR, Valle, RCSC, Valle, JAB. 2020. Cationization of cotton fiber: an integrated view of cationic agents, processes variables, properties, market and future prospects *Cellulose* 27, 8527–8550
19. Arivithamani, N., Dev, V.R.G. 2017. Cationization of Cotton for Industrial Scale Salt-Free Reactive Dyeing Of Garments *Clean Techn Environ Policy* 19, 2317–2326
20. Şahan, G, Demir, A. 2016. A Green Application of Nano Sized Chitosan in Textile Finishing *Tekstil ve Konfeksiyon* 26(4), 414-420
21. Yavuz, G, Zille, A, Seventekin, N, and Souto, AP. 2017. Structural Coloration of Chitosan-Cationized Cotton Fabric Using Photonic Crystals. *IOP Conf. Series: Materials Science and Engineering* 254, 102012 doi:10.1088/1757-899X/254/10/102012
22. Altınkaya E. 2021. Development of Multifunctional Bio-Based Cotton Composite *Tekstil ve Konfeksiyon* 31(4), 264-273
23. Arık, B, Seventekin, N. 2011. Evaluation Of Antibacterial and Structural Properties Of Cotton Fabric Coated By Chitosan/Titanium and Chitosan/Silica Hybrid Sol-Gel Coatings *Tekstil ve Konfeksiyon* 2, 107-115
24. Brahma, S., Islam, M.R., Shimo, S.S., Dina, R.B., 2019. Influence of Natural and Artificial Mordants on the Dyeing Performance of Cotton Knit Fabric with Natural Dyes *IOSR Journal of Polymer and Textile Engineering* 6(1), pp.1-6.
25. Karabulut, K. 2015. Giving Color, UV Protection and Antibacterial Activity In A Single Step To Knitted Cotton Fabrics Via Dyeing With Natural Dyes, MSc. Thesis, Namık Kemal University Graduate School of Natural and Applied Sciences, Tekirdağ, p.39.



-
26. ISO 13938-2:2019: Textiles — Bursting properties of fabrics- Part 2: Pneumatic Method for Determination of Bursting Strength and Bursting Distension
 27. TS EN ISO 105-C06: Textiles - Tests for Colour Fastness - Part C06: Colour Fastness to Domestic and Commercial Laundering
 28. TS EN ISO 105-E04: Textiles - Tests for Colour Fastness - Part E04: Colour Fastness to Perspiration
 29. TS EN ISO 105-X12: Textiles. Tests for Colour Fastness Colour Fastness to Rubbing
 30. Sancar Beşen, B. 2020. Tea Tree Oil/Ethyl Cellulose Microcapsule Loaded Antimicrobial Textiles AATCC Journal of Research 7(2), 1-6

Effect of UV Exposure on the Mechanical Properties of Polyurethane-Coated Fabrics

Memik Bünyamin Üzümcü¹  0000-0002-5741-1199

Burak Sarı²  0000-0003-3079-6153

Emrah Temel³  0000-0002-8520-2618

¹Gaziantep University, Department of Textile and Fashion Design, 27410, Gaziantep, Türkiye

²Bitlis Eren University, Department of Traditional Turkish Arts, 13100, Bitlis, Türkiye

³Ege University, Department of Textile Engineering, 35100, İzmir, Türkiye

Corresponding Author: Memik Bünyamin Üzümcü, buzumcu@gantep.edu.tr

ABSTRACT

Polyurethane materials can be used industrially in different ways, some of which can be used as textile materials or as auxiliary materials applied to textile materials. Polyurethane stands out as a widely used polymer for coating textile products used in outdoor applications, because of high stability at low temperature, flexibility, no or very little volatile organic component content, high water resistance, pH stability, excellent solvent resistance, weather resistance, and many other chemical and mechanical properties. In the study, cotton, PET, and viscose fabrics were coated with polyurethane and aged under UV light to investigate the causes and behavior of the mechanical degradation effects of UV on the coating material and fiber. The results indicate that the PU coating process improves the mechanical properties of textile materials while being exposed to UV rays impair the fabric structure. The deterioration in the structure of raw and coated fabrics with the effect of UV increased the air permeability. According to the results of DSC analysis, the increase in the time of UV exposure did not create significant differences in terms of thermal degradation temperatures in both cotton and viscose fabrics. The glass transition temperatures (T_g) increased with more exposure to UV rays, and the UV exposure time had a negative effect on the melting temperature (T_m) and enthalpy (ΔH) of coated PET fabrics.

1. INTRODUCTION

The innovative activities employed to improve textile products start from the selection and/or development of the raw materials, selection of the production system, and also include pre-production and post-production treatment processes. One such treatment process involves coating the textile surfaces with suitable polymers that confer desired properties [1]. for enhancing certain strength and permeability properties that cannot be achieved through traditional finishing methods, thereby rendering the textile material suitable for its intended use. Polyurethane (PU), one of the coating materials, finds application in various forms in the industry, such as fiber, foam, film, etc. [2]. PU can create effects that improve the electrical properties, mechanical strength, and weathering resistance of textile

materials when used as a coating material for them [3]. Due to its ability to increase weathering resistance, this polymer coating material emerges as an important alternative for outdoor products.

Polyurethane coatings are frequently used in the textile industry to improve the mechanical and physical properties of fabrics. Yang and Yu (2006) examined the effect of polyurethane coated fabrics on the mechanical performance and stated that the tensile strength and tear resistance increased greatly compared to uncoated fabrics, and this was due to the densely formed polyurethane layer on the surface [4]. According to the effect of PU and PVC coatings on various fabrics used in technical textile applications, Patel et al. (2015) revealed that coated fabrics showed greater water resistance, less air permeability and

To cite this article: Üzümcü M B, Sarı B, Temel E. 2024. Effect of UV Exposure on the Mechanical Properties of Polyurethane-Coated Fabrics. *Tekstil ve Konfeksiyon*, 34(1), 51-68.

better tensile strength compared to uncoated fabrics. It has been presented as a result that PU coatings are more suitable for technical textile applications due to their better mechanical and physical properties compared to PVC coatings [5]. In their study investigating the performance of PU and PU/silicone coated fabrics in both production and sewing capacities, Bulut and Sular (2013) determined that the coating process has a significant effect on the physical properties of the fabric, and an increase in tensile strength, tear strength and abrasion resistance occurs with both coating processes. However, it has been noted that adding silicone to PU coating gives better results than coating with PU alone [6].

The application of coatings to textile products has been a subject of great interest in recent years. This is especially true in the production process of both breathable and waterproof fabrics. Padleckiene and Petrulevičius (2009) stated that weight loss occurs with increasing wear and therefore the air permeability values of breathable coated fabrics decrease. Cho et al. (2004) revealed that shape memory polyurethane coated fabrics showed better water vapor permeability and mechanical strength compared to uncoated fabrics [8]. Jassal et al. (2004) investigated the use of polyurethanes to develop waterproof, breathable polymeric coatings. Using various types of polyurethane dispersions, they found that the resulting coatings exhibit remarkable water-resistant and breathable properties [9]. Mondal and Hu (2007) analyzed the effect of shape memory polyurethane coatings on the water vapor permeability of cotton fabrics and the coated fabrics exhibited better water vapor permeability [10]. Kara et al. (2018) found that the abrasion resistance of polyurethane coated polypropylene fabrics increased compared to uncoated fabrics, and the increase in coating weight caused a decrease in air permeability in so-coated fabrics. Some studies highlight the importance of understanding the microstructure of coated fabrics, and how it affects properties such as breathability. Güneşoğlu and Yüceer (2018) determined that the number and length of micro cracks in coated fabrics increased with the tensile stress applied to the fabric, the crack density decreased with increasing coating thickness, and the air permeability of the fabric increased with the increase in crack density [12]. Güneşoğlu et al. (2017) found that fabric treated with a chitosan treatment, which increases the hydrophilicity of fabrics and makes them more susceptible to cracking, has significantly higher air permeability than untreated fabric [13].

As it is known; light, heat, and oxygen have aging effects on textile materials due to their degrading properties. Since UV rays carried by sunlight have a photodegrading effect on textile surfaces, textile products, that are expected to be exposed to sunlight for a long time, must have a high UV resistance [14]. When exposing polymers to UV radiation, an undesirable result may occur. Specifically, this radiation could cause the breakdown of valuable polymer chains, thus resulting in free radicals. Due to the formation of these

potentially problematic radicals, the coating on an object may become brittle over time. This issue ultimately causes a loss in mechanical properties that were once present with the original coating. Some studies have explored the effectiveness of diversified polyurethane coatings, which includes isocyanate-based polyurethanes developed from various sources such as vegetable oil and palm oil. One particular research conducted by Das et al. (2017) investigated the consequences of UV aging on the performance characteristics of these two types of polymers. The results showed that providing vegetable oil or palm oil as a component into isocyanate-based polyurethane can enhance its UV resistance by incorporating antioxidants [15]. The effects of UV aging on polyurethane coatings and methods of increasing the resistance of polyurethane coated fabrics to UV radiation have been the focus of numerous studies. Zhang et al. (2019) determined that additives containing antimony-doped tin oxide (ATO) and titanium dioxide (TiO_2) used in polyurethane coatings improve the UV resistance of polyurethane coatings due to their ability to absorb UV radiation and convert it into heat [16]. Li et al. (2009) stated that zinc oxide nanoparticles increase the UV resistance of polyurethane coatings with their ability to absorb UV radiation and prevent free radical formation [17]. Mills et al. (2012) showed that the incorporation of silica nanoparticles into polyurethane coatings leads to increased UV resistance due to their ability to inhibit and reduce the formation of free radicals resulting from exposure to ultraviolet radiation [18]. Sabzi et al. (2009) examined how the surface modification of TiO_2 nanoparticles impacted the properties of polyurethane composite coatings when coupled with a silane coupling agent [19]. Van Tran et al. (2019) developed a new kind of polyurethane nanocomposite coatings that included silanized graphene as well as hexagonal boron nitride nanoadditives to make the coatings more resistant against the harmful effects of UV degradation. The researchers found that these new additives were effective in improving the overall UV resistance by absorbing UV radiation and preventing the formation of free radicals [20].

UV radiation is a major player in affecting the longevity and performance of textile products that come in contact with sunlight. It's particularly damaging for outdoor textiles; these could be tents, sportswear or any other kind of clothing mainly used outdoors because they are exposed to the sun for prolonged periods. As a result of extensive exposure to UV rays, textiles break down and lose their durability pretty quickly- which ultimately results in shorter product lifespans. In order to enhance the quality of textile products, it is essential to comprehend how UV exposure can impact various types of fabrics and their coatings. The main objective of this study is to investigate the effects of UV aging on the mechanical and physical properties of cotton, viscose, and PET woven fabrics coated with polyurethane. Specifically, the study aims to analyze the breaking strength, tear strength, elongation at break, and air permeability values of the coated fabrics after exposure to

UV-A radiation at an intensity of 35 W/m² for a range of 0-150 hours. Although previous researches have investigated the effect of polyurethane coating on the mechanical and permeability properties of fabrics, this study aims to fill this gap in the literature by examining the effect of UV aging on these properties. In addition, DSC analyzes of the coated fabrics were performed to better understand the thermal properties of the samples before and after UV exposure. The originality of this study is a comprehensive investigation of the effects of UV aging on both the mechanical and thermal properties of polyurethane coated fabrics made from different fibers commonly used in textile production. The results of this study will contribute to an understanding of the performance and durability of polyurethane coated fabrics when exposed to UV radiation.

2. MATERIAL AND METHOD

2.1 Material

In this study, three different raw woven fabrics (made from cotton, PET, and viscose) were utilized. These fabric types are commonly employed in textile production, and the objective was to examine their behavior under identical conditions, including the same coating and UV exposure time. The warp and weft yarns of these plain-woven fabrics had a linear density of Ne 30/1. The front faces of these fabrics were coated with PU (polyurethane) material, while the back faces were treated with fluorocarbon coating. The

PU coating material used was an aliphatic waterborne PU dispersion specifically recommended for formulating textile coatings for outerwear. The process steps for the coating are depicted in Figure 1.

2.2 Method

The physical properties of both the raw and coated fabric samples are provided in Table 1. To subject the fabric samples to UV aging, a Prowhite UV test cabin was utilized, with exposure durations of 50, 100, and 150 hours, and a UV parameter of 35 W/cm². The cabin temperature was maintained at 35°C. Subsequently, the mechanical and air permeability properties of the fabrics were analyzed. The testing procedures, along with the equipment and corresponding standards employed, are detailed in Table 2.

In addition to assessing the mechanical and permeability properties of the fabrics, surface and structural properties were examined using Thermo Scientific Apreo S Scanning Electron Microscopy (SEM) and TA DSC Q2000 Differential Scanning Calorimetry (DSC) equipment. SEM images were captured at magnifications of up to 5000x (HV: 3.00 KV, WD: 9.3-10.8 mm, spot size: 5.0) to evaluate the surface characteristics of the fabrics. DSC analyses were conducted in a nitrogen environment, with temperature intervals ranging from 0 to 350°C and a temperature rise rate of 10°C/min. Figure 2 presents SEM images of the raw and coated cotton, viscose, and PET fabrics

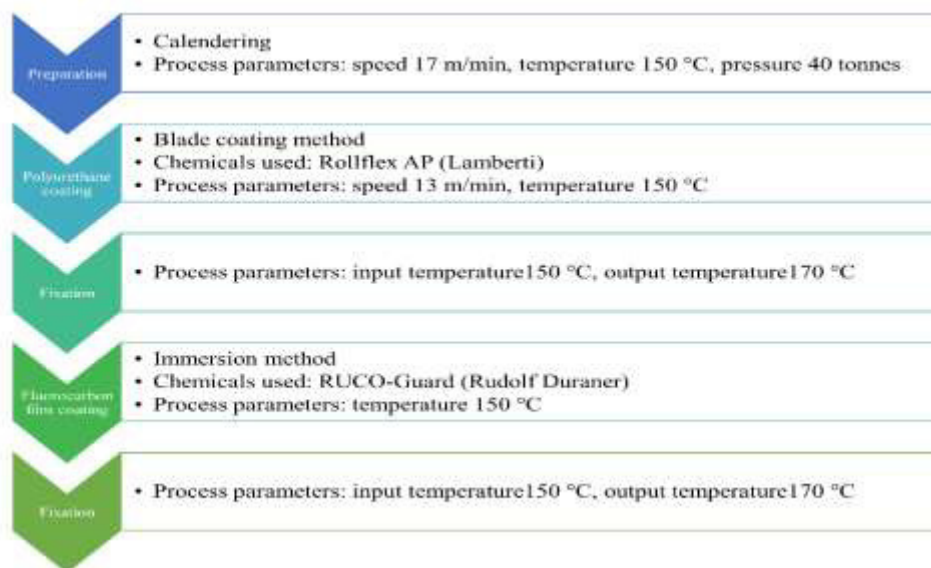


Figure 1. Coating process steps

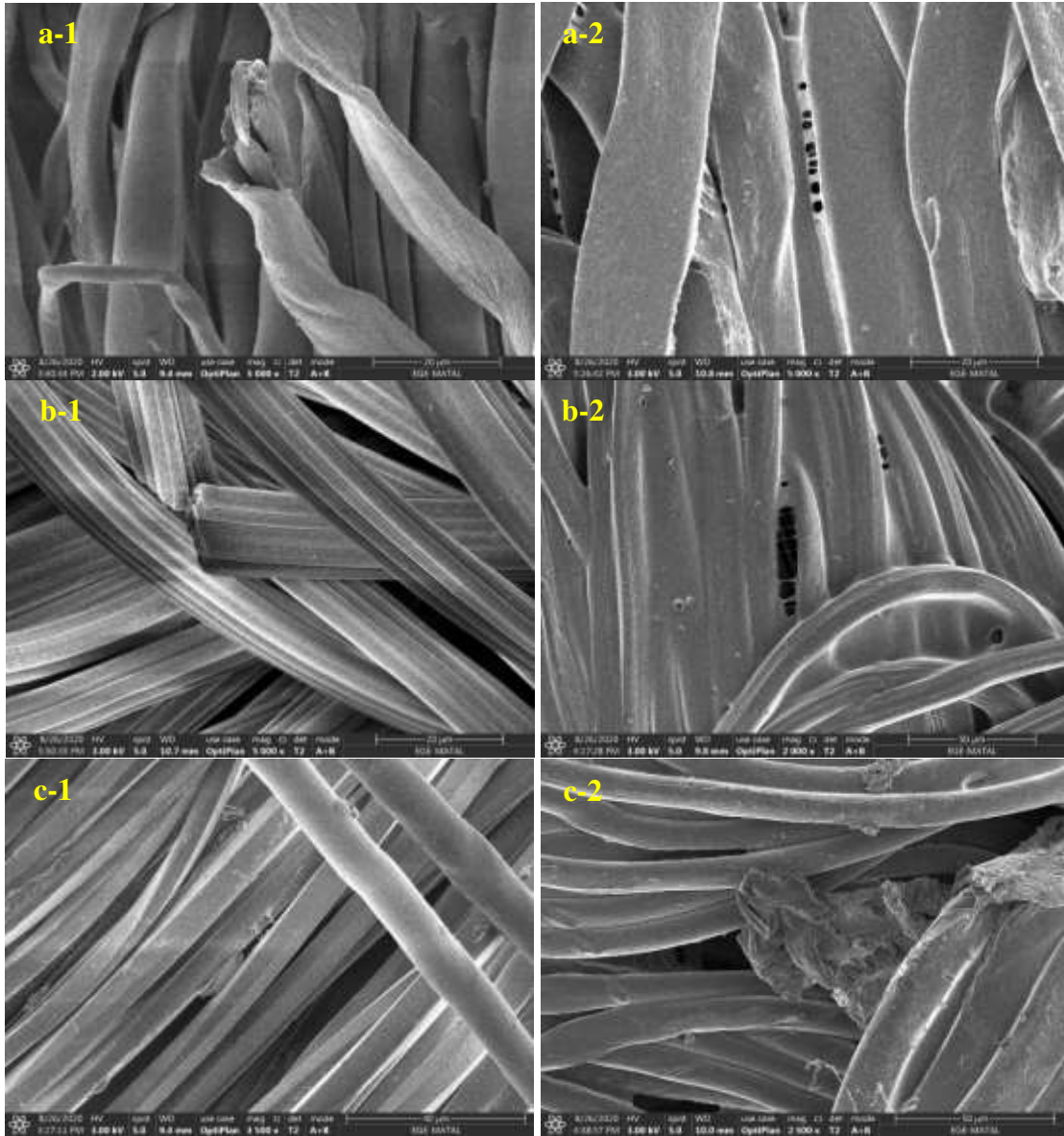
Table 1. Physical properties of fabric samples

Fabric material	Fabric codes	Warp density (warp/cm)	Weft density (weft/cm)	Thickness (mm)	Weight (g/m ²)
100% Cotton	Co	42	27	0.20	125
	Coat-Co	42	27	0.21	128.2
100% PET	PET	37	23	0.31	160.8
	Coat-PET	37	23	0.32	164.8
100% Viscose	Vis	30	23	0.22	116.4
	Coat-Vis	30	23	0.24	120.8



Table 2. The equipment and the standards of the tests

Fabric properties	Test equipment	Standards
Weight	-	EN ISO 12127
Thickness	SDL-Atlas M034A	EN ISO 5084
Density	-	EN 1049-2
Breaking strength and elongation	Zwick Z010 (Roell)	EN ISO 13934-1
Tear strength	Zwick Z010 (Roell)	EN ISO 13973-2
Air permeability	FX3300 (Textest)	EN ISO 9237

**Figure 2.** SEM images of raw (1) and coated (2) cotton (a), viscose (b), and PET (c) fabrics before UV exposure

The scope of this study was to investigate in detail the mechanical, thermal and air permeability properties of the UV resistance of fabrics with different fiber types. The mechanical and air permeability properties of fabrics with different fiber types, which are frequently used in textile production, were analyzed when exposed to UV. The results were analyzed in two different steps. In the first one, raw and coated fabrics of each fiber type were evaluated among

themselves. In this evaluation phase, UV-A type aging process was applied at 0 hours, 50 hours, 100 hours and 150 hours intervals. In order to determine the UV effect in general, a detailed analysis was made for each fiber type as raw fabric (RF), coated fabric (CF), raw fabric- UV exposed (RF-UV) and coated fabric-UV exposed (CF-UV) subgroups, regardless of the UV exposure time. One-way ANOVA analysis was done for statistical evaluations using IBM SPSS

Statistics 20 Software. The general effects were determined by interpreting the significance values (p), which are the decision-making factor in the ANOVA method, and in situations where the factor is significant ($\alpha=0.05$), post hoc tests were also carried out for further analysis.

3. RESULTS AND DISCUSSION

The main purpose of the study was to understand how different fibers commonly used in textiles are affected by UV-A rays when coated with the same PU coating under the same parameters. Therefore, several properties of the coated and raw fabrics were comparatively investigated, including breaking strength, breaking elongation, tear strength, and air permeability. Additionally, some of these fabrics were exposed to a UV aging process with different exposure times to understand the effect of exposure time. The strength and permeability results of the fabric samples are provided in Table 3.

3.1 Breaking strength

Significant decreases occur in the mechanical properties of the materials, because of the molecular level degradation caused by the effect of UV rays [21]. According to our

findings, it has been determined that as the UV exposure time increases, the breaking strength decreases for all sample groups (Figure 3 and Figure 4) which is consistent with previous studies [22-25]. The samples that were not exposed to the aging effect of UV treatment exhibited the highest strength values, as expected for coated fabrics, where the coating layer had an enhancing effect on the breaking strength [26,27]. In both types of cotton fabric samples, the highest tensile strength values were observed in the samples that were not subjected to UV treatment, while the lowest tensile strength values were observed in the samples treated for 150 hours. In the warp direction, considering the 150-hour samples of raw and coated cotton fabrics that were not exposed to any UV effect, a strength loss of around 50% was observed. For all PET fabrics, it was determined that while high rates of decrease occurred in raw fabrics for 100-150 hours, the breaking strength decrease in coated samples was more limited. Viscose fiber is known to have the lowest strength compared to other fibers used in the study [28]. The breaking strength, which was affected by the structural degradation caused by UV treatment, resulted in 60-75% strength decreases in the warp direction at the end of 150 hours in viscose fabrics.

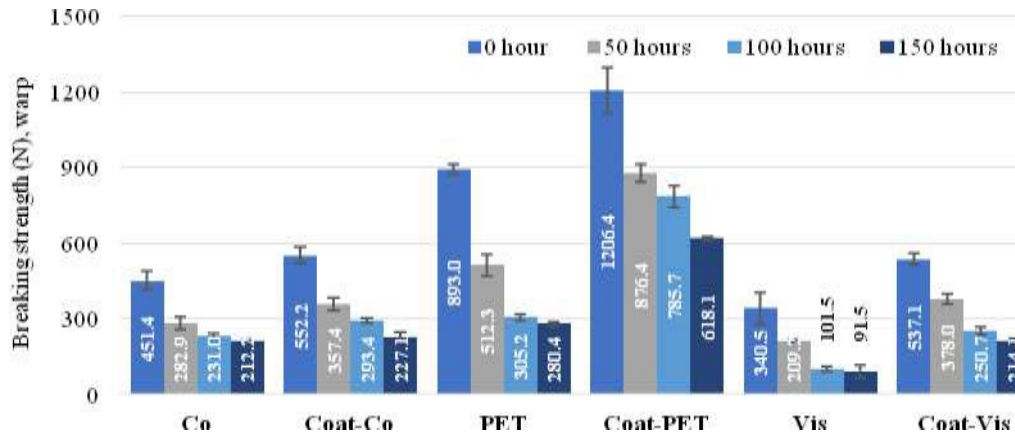
Table 3. Mechanical and air permeability results of the fabric samples (before and after UV exposure)

Fabric codes	UV aging duration	Breaking strength (N) (warp)	Breaking strength (N) (weft)	Breaking elongation (%) (warp)	Breaking elongation (%) (weft)	Tear strength (N) (warp)	Tear strength (N) (weft)	Air permeability (l/m ² /s)
Co	Unaged (0h)	451.39	366.85	7.51	24.41	7.37	10.80	632.80
	50 h	282.92	188.63	6.42	20.88	3.40	4.46	640
	100 h	230.95	144.35	5.80	18.21	2.42	3.30	627
	150 h	212.17	114.32	4.98	15.36	1.82	2.87	655
Coat-Co	Unaged (0h)	552.17	439.62	9.30	30.71	9.80	14.60	15.40
	50 h	357.37	234.08	8.10	26.42	5.14	7.41	17
	100 h	293.44	186.32	7.09	24.92	2.84	4.02	62.40
	150 h	227.08	130.92	6.01	23.36	1.17	2.96	207.40
PET	Unaged (0h)	892.99	485.08	24.80	47.32	21.58	30.69	208.60
	50 h	512.32	321.77	21.31	43.95	16.52	24.11	208.2
	100 h	305.22	122.34	18.85	42.25	12.80	18.19	213.4
	150 h	280.37	102.85	16.06	40.03	10.83	15.24	219.6
Coat-PET	Unaged (0h)	1206.40	711.72	13.70	35.75	41.62	57.24	55.80
	50 h	876.36	726.49	12.67	20.24	34.66	40.92	179
	100 h	785.72	648.49	11.79	19.16	25.08	31.70	201.20
	150 h	618.14	554.90	11.32	15.99	20.24	28.01	231.2
Vis	Unaged (0h)	340.51	210.50	20.91	40.02	8.62	11.53	563.80
	50 h	209.23	104.70	10.74	27.28	4.77	6.25	607
	100 h	101.53	29.95	7.26	17.84	1.55	3.48	630.80
	150 h	91.51	13.59	5.71	14.07	0.46	1.35	633.60
Coat-Vis	Unaged (0h)	537.12	328.32	22.49	28.23	9.53	13.52	18.80
	50 h	377.98	249.26	20.63	25.48	5.62	8.36	89.20
	100 h	250.67	186.19	18.05	22.18	3.36	6.15	145.80
	150 h	214.14	138.40	14.34	17.85	2.14	4.03	177.60



Table 4. ANOVA results for the effects of UV exposure time on breaking strength for all fabric types

Fabric Type	Warp direction		Weft direction	
	F Value	Significance	F Value	Significance
Co	61.659	.000*	67.165	.000*
Coat-Co	105.186	.000*	186.160	.000*
PET	378.279	.000*	17.257	.001*
Coat-PET	62.600	.000*	27.371	.000*
Vis	34.763	.000*	878.123	.000*
Coat-Vis	191.774	.000*	108.445	.000*

**Figure 3.** Breaking strength of the fabrics (warp direction)

In studies examining the mechanical properties of fabrics, it is generally observed that measurements taken in the weft direction, which contains fewer yarns compared to the warp direction, yield lower breaking strength values [29]. Similarly, it was found that the warp yarns of each fabric examined had higher linear densities than the weft yarns, resulting in lower breaking strength values in the weft direction. After exposure to UV, the breaking strength of all fabric samples decreased in both the warp and weft directions. In terms of UV exposure time, a strength loss of approximately 75% was detected in the breaking strength of cotton-containing fabrics in the weft direction when comparing samples with 0-150 hours of exposure. Although the inherent low strength potential of weft yarns resulted in more pronounced effects, especially in uncoated PET samples, the strength decrease in coated samples was also observed at lower rates, particularly in the weft direction, as reported in previous studies [22]. Similar to studies examining the UV effect on viscose fabrics [30], lower breaking strength values were measured in all viscose samples after UV exposure. Especially in raw viscose fabrics, a strength loss of up to 95% was observed at the end of 150 hours (Figure 4).

The results of the analyses independent of the UV exposure time indicated that the coating process was a significant factor in enhancing the tensile strength of all fabric samples (Table 5). The coating process provided an additional

surface layer on the fabric and increased resistance to forces acting on the fabric from various directions. In terms of tensile strength, the lowest values were observed in raw and coated cotton samples exposed to UV. The abrasive effect of UV treatment led to significant decreases in the tensile strength of cotton fabrics, with a higher decrease of approximately 60% in the weft direction. Conversely, in cotton fabric samples without UV exposure, the coating process resulted in significant increases in tensile strength, with strength values measured to increase by 25% in both directions. For PET fabrics, the lowest tensile strength was observed in raw samples treated with UV in both the warp and weft directions. In the warp direction, the coating process resulted in a 35% increase in strength and a 40% decrease was calculated with UV treatment. In the weft direction, the strength increased by 45% with coating and decreased by 37% with UV exposure. Notably, the coating process prevented strength decreases caused by UV, especially in the weft direction, which is problematic in terms of breaking strength. In viscose fabrics, higher strength values were obtained in the warp direction. The coating process led to a proportional increase of approximately 60% in both the weft and warp directions. Similarly, to other analyses, UV treatment resulted in strength decreases in both directions due to structural distortions. The decreases observed in raw viscose samples were higher in the weft direction, with a rate of 75%, compared to 60% in the warp direction (Figure 5).

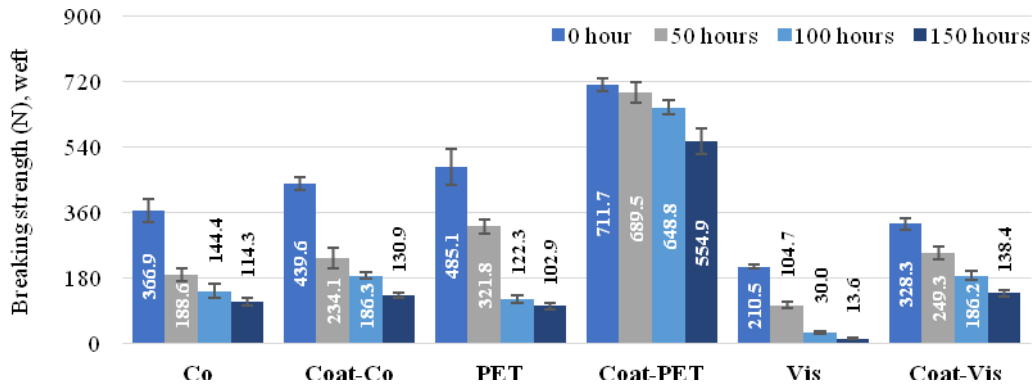


Figure 4. Breaking strength of the fabrics (weft direction)

Table 5. ANOVA results for the effects of UV exposure and coating process on breaking strength regardless of UV exposure time

Fabric Types	Warp direction		Weft direction	
	F Value	Significance	F Value	Significance
Co and Coat-Co	42.871	.000*	56.614	.000*
PET and Coat-PET	55.701	.000*	43.254	.000*
Vis and Coat-Vis	32.206	.000*	40.934	.000*

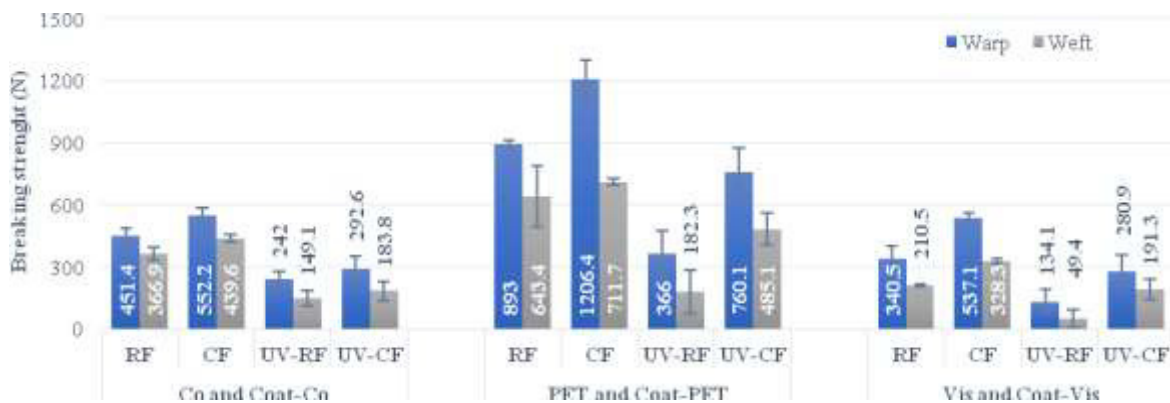


Figure 5. Breaking strength of raw and coated fabrics independent of UV exposure time for all fabric types

3.2 Breaking elongation

Similar to the breaking strength, it was observed that increasing UV exposure time had a detrimental effect on the breaking elongation values of all fabrics. Consistent with previous studies [24,25,31,32], fabric ruptures occurred at lower elongation values due to structural degradation caused by UV exposure. In the case of cotton fabrics, the highest elongation values were obtained in the warp and weft directions for samples that were not exposed to UV, while the lowest elongation values were observed at 150 hours, representing the most severe UV exposure. The increase in UV exposure time negatively affected the elongation at break of both raw and coated PET fabrics. Notably, different responses were observed depending on

the measurement direction for raw and coated PET fabrics. The decrease in elongation at break in the warp direction of raw PET fabrics progressed proportionally with the duration of UV treatment. However, the coated PET fabrics exhibited a limited abrasive effect in the warp direction, likely due to the fabric structure acquiring a more rigid form through the coating process. In the case of raw viscose fabrics, significant decreases in elongation at break were observed after 50 hours, aligned with the decline in tensile strength resulting from UV-induced structural degradation. Subsequent decreases were less pronounced as the exposure time prolonged. Coated viscose fabrics showed a parallel decrease in elongation at break with increasing UV exposure time (Figure 6).

Table 6. ANOVA results for the effects of UV exposure time on breaking elongation for all fabric types

Fabric Type	Warp direction		Weft direction	
	F Value	Significance	F Value	Significance
Co	19.059	.001*	32.521	.000*
Coat-Co	19.974	.000*	13.757	.002*
PET	19.013	.001*	15.317	.001*
Coat-PET	7.094	.012*	82.143	.000*
Vis	26.600	.000*	179.942	.000*
Coat-Vis	21.189	.000*	50.410	.000*

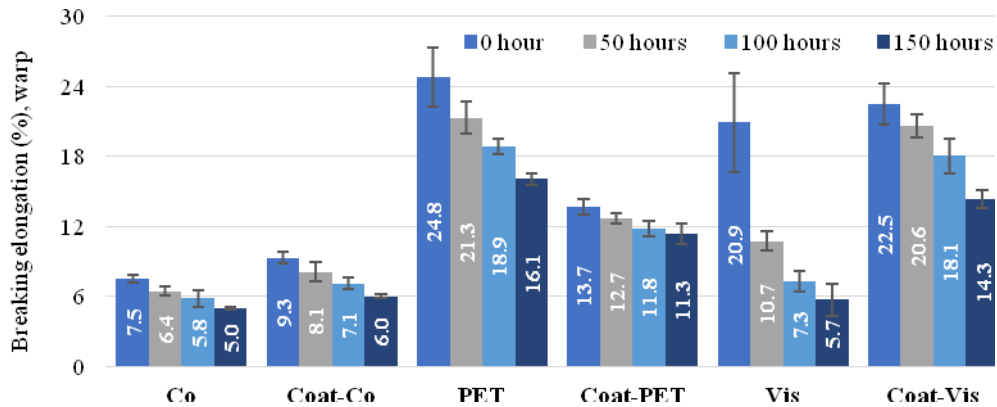


Figure 6. Breaking elongation of the fabrics (warp direction)

Due to the tensions experienced by warp yarns during their positioning in the fabric and the production process, it is observed that fabrics exhibit lower elongation values in the warp direction compared to the weft direction [33]. This trend was consistent across all fabric types, with higher elongation at break values observed in the weft direction. In raw cotton fabrics, the decrease in elongation at break in the weft direction was found to be proportional to the UV exposure time, whereas in coated cotton samples, the decrease in elongation at break values stabilized after 50 hours. The high breaking elongation values observed in raw PET fabrics can be attributed to the high tenacity and elongation characteristics of the yarn used [28]. In coated PET fabrics, the elongation at break values in the weft direction decreased significantly after 50 hours, and the rate of decrease stabilized, similar to coated cotton fabrics. After 150 hours, a 55% decrease in elongation at break was observed in the weft direction of coated PET fabrics. Raw viscose fabrics experienced a 65% decrease in elongation at break in the weft direction after 150 hours. In the case of coated viscose fabrics, the decrease in elongation at break in the weft direction was determined to be 35% after 150 hours (Figure 7).

According to the analyses conducted independently of the UV exposure time parameter, both coating and UV exposure were found to have a statistically significant effect on the elongation at break properties of all examined fabrics (Table 7). Furthermore, due to the inherent physical

characteristics of weft yarns in terms of stretchability, it was observed that weft yarns exhibited higher elongation at break values compared to warp yarns in all fabrics. The elongation at break results of cotton fabrics indicated that UV treatment played a significant role in reducing the elongation at break. However, it was determined that the effects caused by UV exposure were somewhat mitigated by coating the fabric surfaces. Conversely, in coated samples that were not exposed to UV, the elongation values were measured at the highest level, highlighting the stretchable nature of the coated fabric surface. The integration of coating and UV treatment in PET fabrics had a negative impact on the elongation at break. The lowest breaking elongation values were observed in samples that were both coated and exposed to UV, due to the hardening effect of the coating process [8] and the deterioration in the fabric structure caused by the UV exposure. Regarding the elongation at break results, the coating process led to a 45% decrease in elongation at break in the warp direction, while UV treatment resulted in a 25% decrease. In the weft direction, the coating process caused a 25% decrease, while UV treatment led to a 12% decrease. In terms of elongation at break in viscose fabrics, UV exposure had a significant effect. The viscose fabric samples exhibited the lowest elongation at break values due to UV exposure, with a 60% decrease in the warp direction and a 50% decrease in the weft direction. Although the coating process did not have a significant effect in the warp direction, it provided the

highest elongation values and mitigated the negative impact of UV exposure. In the weft direction, the coating process contributed to a decrease in elongation values by increasing

fabric density and reducing stretching abilities, resulting in a 30% decrease in elongation at break (Figure 8).

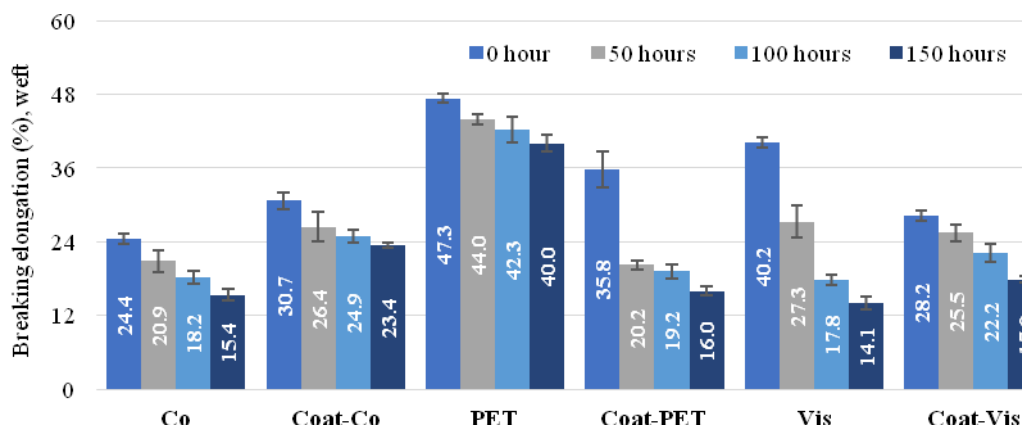


Figure 7. Breaking elongation of the fabrics (weft direction)

Table 7. ANOVA results for the effects of UV exposure and coating process on breaking elongation regardless of UV exposure time

Fabric Types	Warp direction		Weft direction	
	F Value	Significance	F Value	Significance
Co and Coat-Co	15.287	.000*	32.318	.000*
PET and Coat-PET	47.169	.000*	242.923	.000*
Vis and Coat-Vis	33.801	.000*	17.752	.000*

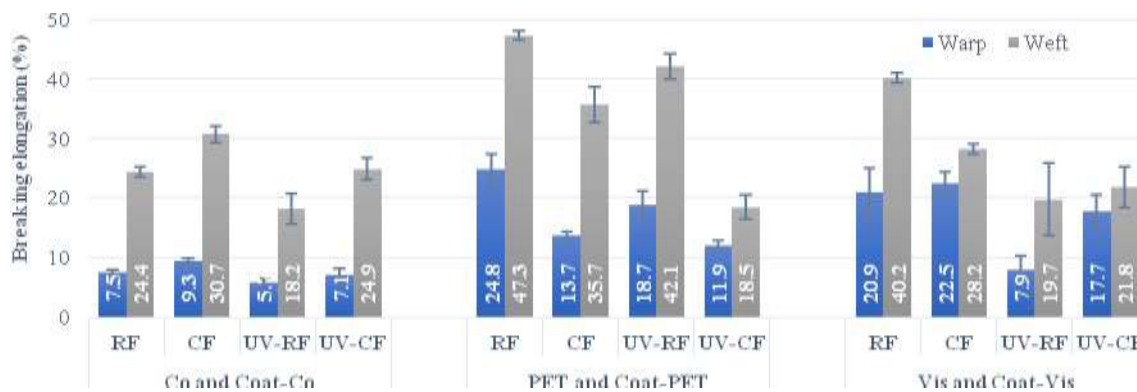


Figure 8. Breaking elongation of raw and coated fabrics independent of UV exposure time

3.3 Tear strength

The tear strength of a fabric is influenced by factors such as the breaking strength of the yarns that form the fabric and the mobility of the yarns within the fabric [34]. Consistent with previous studies in the literature [22,24,30-32], the degrading effect of UV exposure on the fabric structure has a negative impact not only on the breaking strength but also on the tear strength properties. The tear strength results of all fabrics revealed statistically significant differences attributed to the effect of UV exposure (Figure 9 and Figure 10). Similar to the breaking strength, according to the tear

strength test results, the lowest values in all cotton fabric samples were determined in the samples exposed to 150 hours of UV treatment. Due to the damage caused by UV effect in the fabric structure, there were decreases in tear strength in both warp and weft directions. It was determined that PET fabrics without UV exposure had the highest tear strength values due to the abrasive effect of UV in raw and coated fabric samples. In both PET fabric groups, the tear strength reduction rates were parallel to the exposure time and 50% decreases were measured when compared to the 150-hour samples and 0-hour samples. The increase in UV exposure time also had a negative effect on



viscose fabrics and the lowest tear strength values were determined after 150 hours. Strength reductions of up to 95% in the warp direction after 150 hours due to UV were calculated for raw viscose fabrics. Especially in both viscose fabrics, the decreases after 50 hours were higher.

Due to the higher mobility of weft yarns compared to warp yarns in the fabric, they tend to move and stay closer to each other in the region of tearing under the influence of tear forces [34, 35]. Consistent with previous studies [36-38], higher tear strength values were observed in the weft direction for all fabric types. In both raw and coated cotton fabrics, approximately 80% loss in tear strength was determined in samples exposed to UV in both warp and weft directions. The effects of coating and UV exposure on PET fabrics exhibited a similar trend in both directions. While tear strength values in the weft direction were relatively higher for viscose fabrics, reductions of 70% and 90% were observed in the weft direction for raw and coated viscose fabrics, respectively, after 150 hours of UV exposure (Figure 10).

In the evaluation conducted independently of the UV exposure time, it was determined that both the coating process and UV exposure had a statistically significant impact on the tear strength of all fabrics, as shown in Table

9. Despite the beneficial effect of the coating process, it was found that the strength of all fabric types was significantly reduced due to UV exposure. In the case of cotton fabrics, the tear strength decreased by 70% in both warp and weft directions under the influence of UV. However, for the fabric samples not exposed to UV, the coating process led to a significant improvement in tear strength. Measurements conducted in both warp and weft directions showed strength increases of 35%. The positive impact of the coating process was evident in the tear strength results of PET fabrics, with nearly 100% increases observed in both directions. A comparison between the RF and UV-CF PET fabrics revealed an increase in tear strength due to the coating process, despite the abrasive effect of UV treatment. However, the effect of UV resulted in a decrease of 35-40% in tear strength for PET fabrics in both directions. Regarding fabric samples containing viscose, the tear strength-reducing effects of UV treatment were observed. Raw viscose fabrics experienced decreases of 70% in both directions as a result of UV treatment. Even in coated viscose samples, reductions of up to 60% were observed. While there was a 15% increase in tear strength in the weft direction due to the coating process, it remained relatively low.

Table 8. ANOVA results for the effects of UV exposure time on tear strength for all fabric types

Fabric Type	Warp direction		Weft direction	
	F Value	Significance	F Value	Significance
Co	314.933	.000*	179.418	.000*
Coat-Co	138.256	.000*	137.657	.000*
PET	29.201	.000*	42.716	.001*
Coat-PET	50.775	.000*	137.627	.000*
Vis	289.149	.000*	179.388	.000*
Coat-Vis	107.766	.000*	67.140	.000*

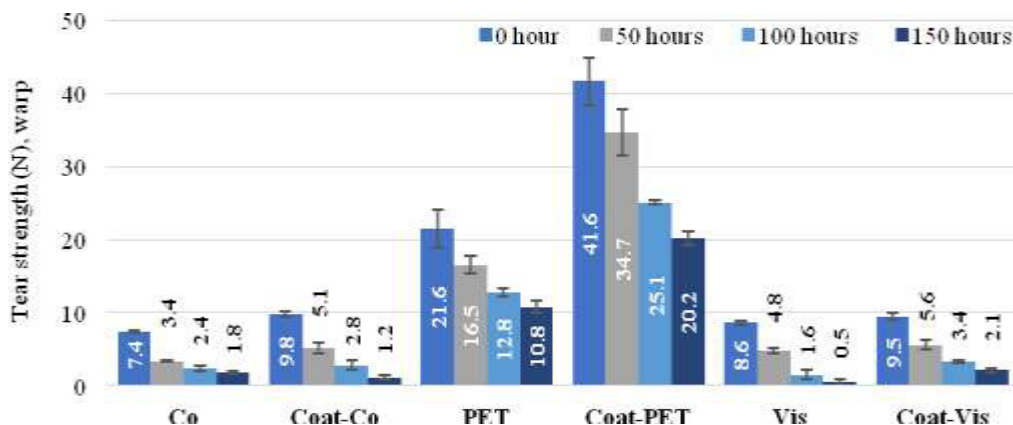


Figure 9. Tear strength of the fabrics (warp direction)

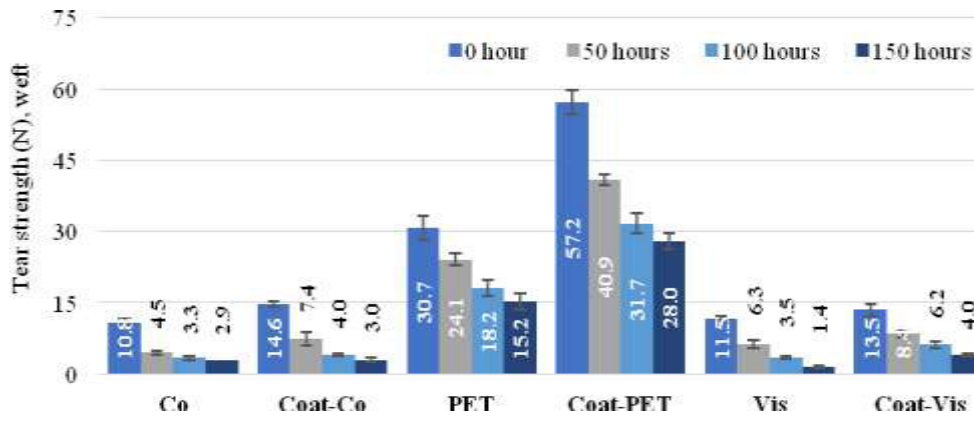


Figure 10. Tear strength of the fabrics (weft direction)

Table 9. ANOVA results for the effects of UV exposure and coating process on tear strength regardless of UV exposure time

Fabric Types	Warp direction		Weft direction	
	F Value	Significance	F Value	Significance
Co and Coat-Co	35.012	.000*	54.077	.000*
PET and Coat-PET	30.618	.000*	50.777	.000*
Vis and Coat-Vis	22.731	.000*	26.826	.000*

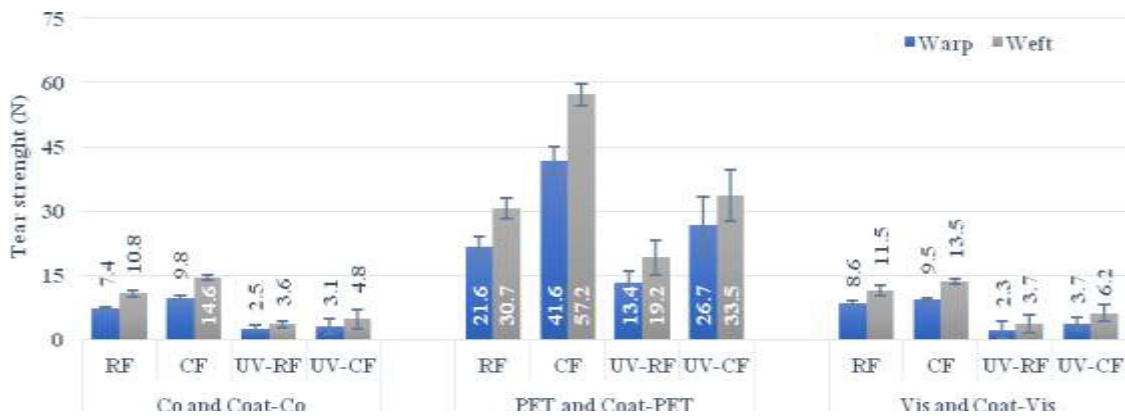


Figure 11. Tear strength of raw and coated fabrics independent of UV exposure time

3.4 Air permeability

According to the results of the statistical analysis regarding air permeability, it was observed that the UV exposure time did not have a significant effect on the air permeability of raw cotton and raw PET samples (Table 10). However, the effect of UV exposure time on raw viscose fabrics and all coated fabric types was found to be statistically significant, as indicated in Table 10. In the case of raw viscose fabrics, an increase in air permeability was observed with UV exposure during the initial 50 hours, and this increase was maintained at a constant level thereafter. After 50 hours of UV exposure, a 7% increase in air permeability was observed, while at the end of 150 hours, the air permeability showed a 12% increase compared to the air permeability of the raw viscose fabrics at 0 hours (Figure 12).

Table 10. ANOVA results for the effects of UV exposure time on air permeability for all fabric types

Fabric Type	F Value	Significance
Co	2,179	.079
Coat-Co	292,951	.000*
PET	0,754	.536
Coat-PET	71,269	.000*
Vis	10,594	.000*
Coat-Vis	108,275	.000*

The results of the air permeability tests revealed that the changes in the fabric surface structure due to increased UV exposure time were most pronounced in the coated fabric samples. In woven fabrics, air flow passes perpendicularly through the gaps between the warp and weft yarns [39]. Consistent with previous studies [40-43], it was observed that the coating process restricted the fabric's porosity, which is responsible for allowing vertical air movement

[44]. Consequently, the fabrics that were not exposed to UV exhibited significantly low air permeability properties (Figure 12). In coated cotton fabrics, the coating effect remained relatively stable within the first 50 hours of UV exposure. However, after 100 and 150 hours, there was a significant increase in air permeability values. For coated PET fabrics, the abrasive effect of UV exposure became apparent after 50 hours, and the highest air permeability values were observed after 150 hours. Notably, deep cracks and ruptures (indicated by red arrows) appeared in the

fibers and coated layer of coated PET fabrics after 150 hours of UV exposure, resulting in air permeability values similar to those of raw PET fabrics (Figure 13). In the case of coated viscose samples, the covering effect produced by the coating surface, which reduces permeability, underwent significant changes with increased UV exposure time. The most permeable coated viscose fabric structure, in terms of air permeability, was observed after 150 hours of UV exposure.

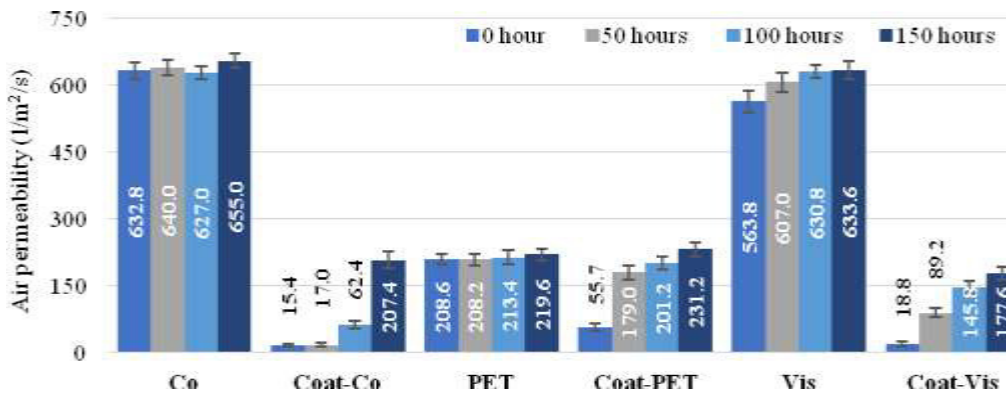


Figure 12. Air permeability of the fabrics

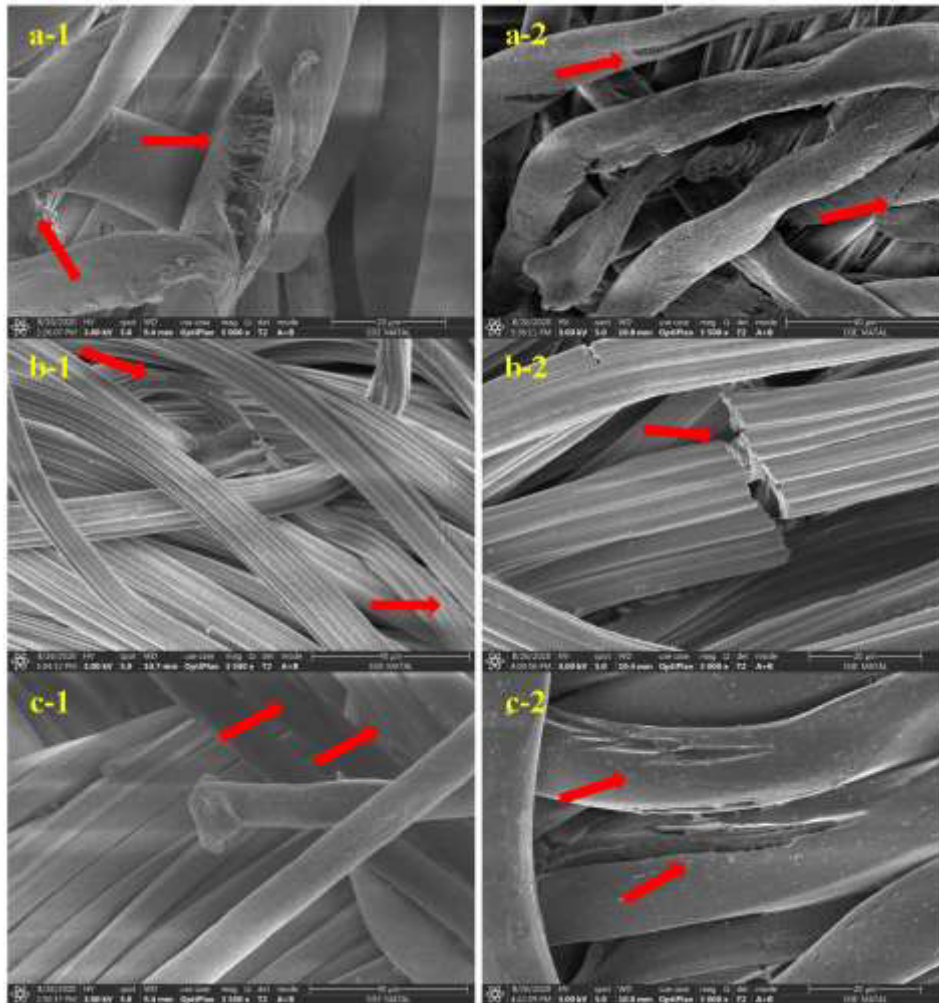


Figure 13. Deep cracks and ruptures observed on the raw cotton (a-1), coated cotton (a-2), raw viscose (b-1), coated viscose (b-2), raw PET (c-1), and coated PET (c-2) fabrics after 150 hours of UV exposure

The results of the air permeability test analysis for all fabrics, regardless of UV exposure time, indicated that the coating process had the greatest impact on the fabric's vertical air permeability. It was observed that the coating process significantly reduced the air permeability values. In the case of coated cotton fabrics, although the coating effect led to decreased permeability values, it was hypothesized that the surface abrasion effect of UV might create new air passage channels. This effect was not observed in raw cotton fabrics, where both UV-exposed and non-exposed samples exhibited similar air permeability properties. Regarding the air permeability analysis of PET fabrics, it was determined that the coating process had a primary effect, while the interaction between the coating and UV treatment had a secondary effect. The air permeability values in coated PET fabrics decreased by 75%. However, in the UV-CF group of PET fabrics, where the coating effect was expected to be dominant, the covering effect was not detected. The UV exposure seemed to diminish the impact of the extra surface created by the coating, and the distortions caused by UV on the coating surface allowed for the reestablishment of gaps required for vertical air movement. In the case of viscose fabrics, both the coating and UV treatment had significant effects, leading to statistically distinct groups based on air permeability levels. The CF group of viscose fabrics exhibited very low air permeability. However, UV exposure caused deterioration in the coating surface and fabric structure, resulting in the formation of new spaces for air movement. A comparison between RF and UV-CF fabrics of viscose revealed a 75% reduction in air permeability due to the coating process, despite UV exposure (Figure 14).

Table 11. ANOVA results for the effects of UV exposure and coating process on air permeability regardless of UV exposure time

Fabric Type	F Value	Significance
Co and Coat-Co	357.042	.000*
PET and Coat-PET	73.403	.000*
Vis and Coat-Vis	916.286	.000*

3.5 DSC Analyses

DSC analyses were performed on PU-coated fabrics within the temperature range of 0-350°C. The DSC analysis results of the coated fabrics were examined for two groups: cellulosic fabrics (cotton and viscose) and PET fabrics, after 0-150 hours of UV exposure. It was observed that the DSC graphics of the cellulosic fabrics exhibited a distribution similar to previous studies in the literature [45]. The first noticeable endothermic peak was attributed to moisture present in the fibers, and the moisture evaporation peak values (T_{peak}) were measured to be around 65°C in untreated (UV) cellulosic fabrics [46]. It was determined that the increase in UV exposure time of coated cotton and viscose fabrics (Figure 15 and Figure 16) increased the moisture evaporation peak temperatures (T_{peak}) and evaporation offset temperatures (T_{offset}). The literature suggests that the moisture management properties of fibers change due to the oxidation of hydroxyl side groups in cellulosic fibers under the influence of UV radiation [47]. Notably, the coated viscose fabrics exhibited higher values at both temperature values of the first endothermic peak after 150 hours of UV exposure (Table 12). Cellulosic fibers, which contain more moisture in their structure, generally exhibit higher evaporation temperature values [48]. It is presumed that these temperature differences arose due to the higher moisture-holding capacity of viscose fibers (12-14%) compared to cotton fibers (7-8%) [46].

The second peak in the DSC graphs of cellulosic fabrics corresponds to the onset of thermal degradation of the fibers [49], which is consistent with previous studies in the literature [50-52]. The onset temperature value (T_{onset}) of cotton fabrics not exposed to UV was observed to be 327.92°C, while for viscose fabrics, it was 306.77°C (Figure 15, 16). This difference can be attributed to the higher degree of polymerization and crystallinity of cotton fibers, which leads to a higher onset temperature for thermal degradation compared to viscose fibers [46,51]. Furthermore, it was found that the coated cotton fabrics exhibited higher onset thermal degradation temperature values compared to the coated viscose fabrics. Although the effects of UV exposure on the mechanical properties of cellulosic fabrics were evident, the increase in UV exposure time did not result in significant differences in terms of thermal degradation temperatures for both cotton and viscose fabrics (Table 12).

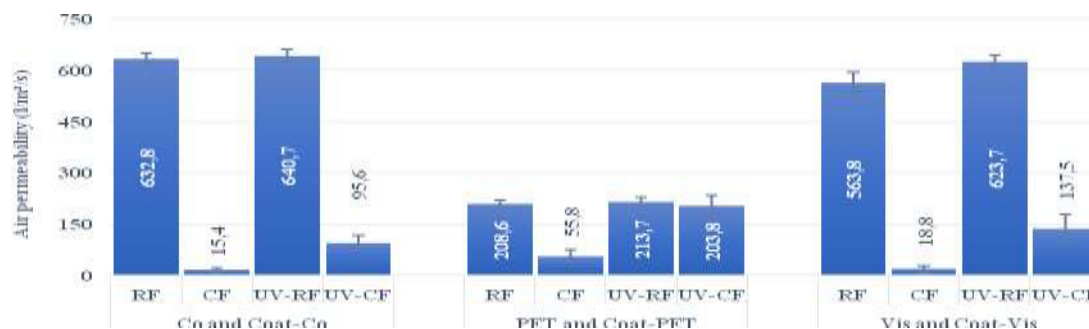


Figure 14. Air permeability of raw and coated fabrics independent of UV exposure time

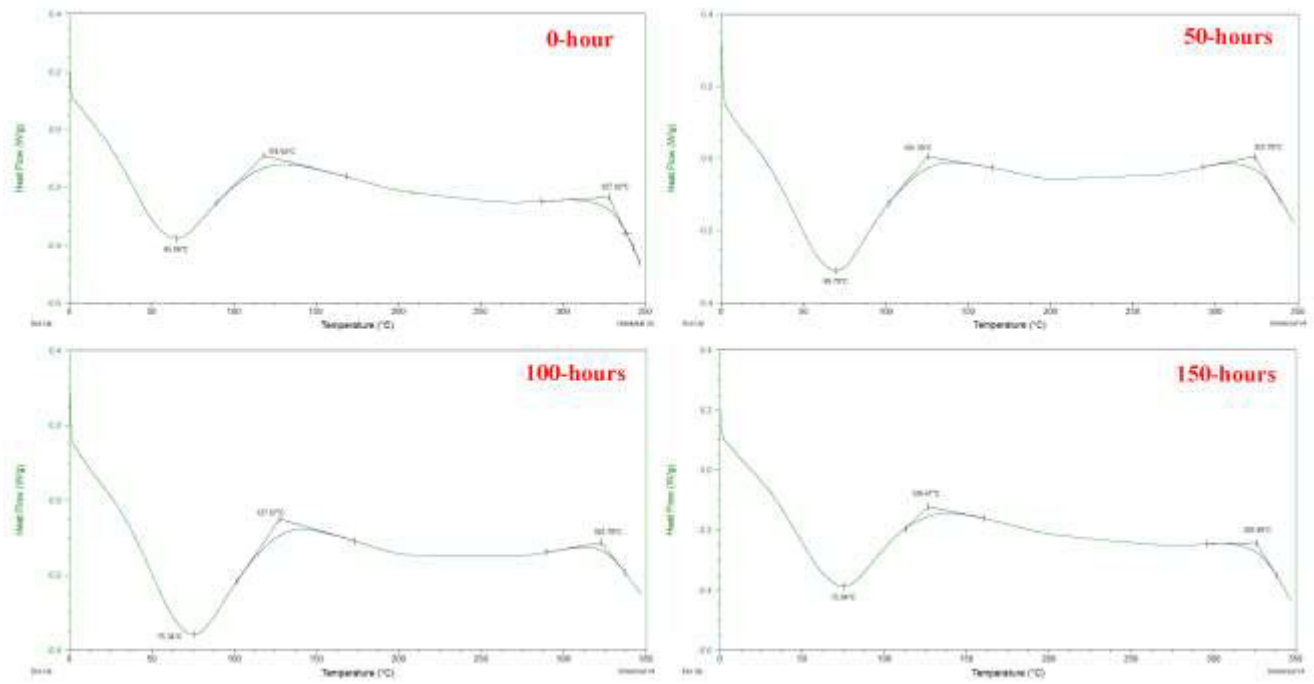


Figure 15. The DSC graphs of coated cotton fabrics

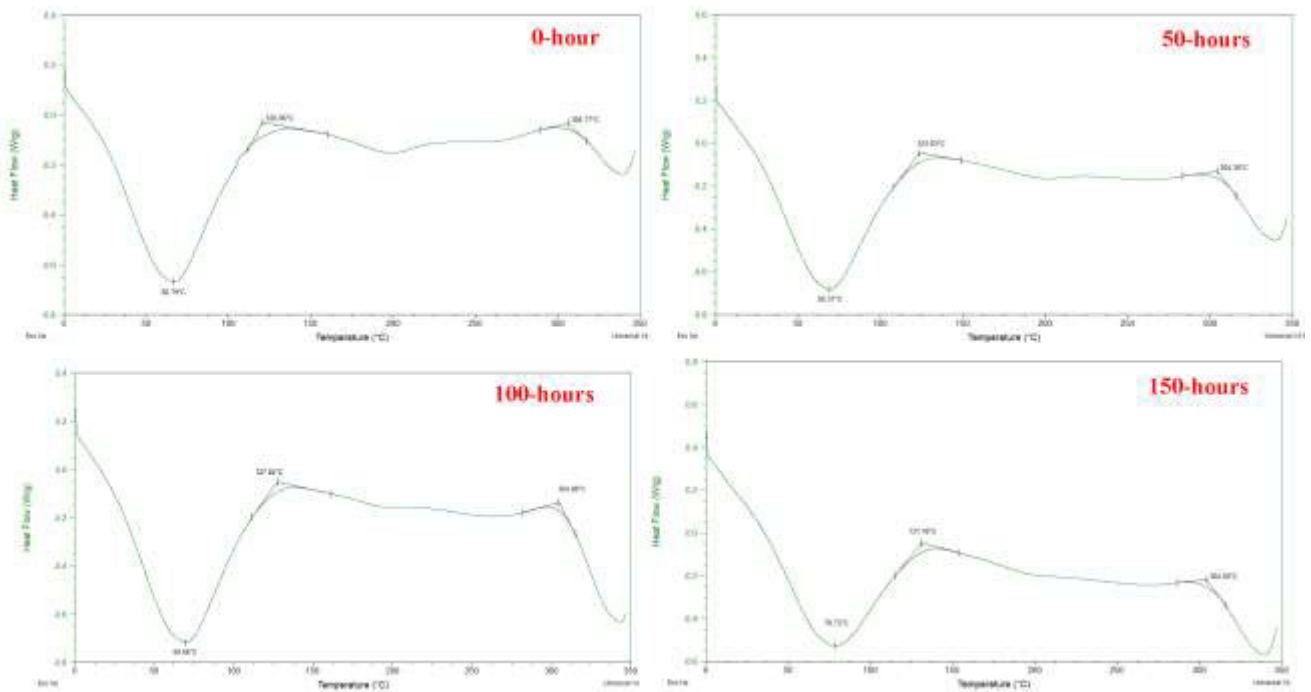


Figure 16. The DSC graphs of coated viscose fabrics

Table 12. Moisture evaporation and thermal decomposition in DSC analyses of cellulosic fibers

UV-Exposure Time	Moisture Evaporation Peak (T_{peak} / °C)		End point of Evaporation (T_{offset} / °C)		Start of Thermal Decomposition (T_{onset} / °C)	
	Coat-Co	Coat-Vis	Coat-Co	Coat-Vis	Coat-Co	Coat-Vis
0 hours	65.06	66.79	118.04	120.86	327.92	306.77
50 hours	69.79	69.31	125.39	123.83	323.78	304.36
100 hours	75.34	69.66	127.67	127.65	322.78	304.88
150 hours	75.04	78.72	126.47	131.16	325.99	304.60

The first peak in the DSC graphs of coated PET fabrics corresponds to the glass transition temperature (T_g), as reported in previous studies [53-55]. The observed changes in T_g values, which increased significantly after 50 hours of UV exposure, indicate the effect of UV aging on PET fabrics (Table 13). Previous studies have also shown an increase in T_g temperatures with prolonged exposure to UV rays [56,57]. This change is attributed to a slight increase in the crosslinking density induced by the UV effect [58-60].

The other notable region in the DSC analysis of coated PET fabrics corresponds to the melting temperatures (T_m), as mentioned in previous studies [61,62]. Consistent with earlier researches [63,64], an increase in UV exposure time was found to have a negative impact on the melting temperature (T_m) and enthalpy (ΔH) values of coated PET fabrics (Table 13). UV exposure leads to photodegradation and photooxidation, causing damage to basic bond structures such as ester bonds and a decrease in molecular weight. As a result of these degradations, PET fibers exhibit lower melting points and reduced enthalpy values [65,66].

4. CONCLUSION

Coating conventional fabrics with a suitable layer offers numerous functional properties, particularly enhanced

resistance against physical impacts. In the context of textile products designed for outdoor use, the photodegradation effect caused by UV rays stands as a significant concern. In this study, the effects of UV exposure on the mechanical properties of different polyurethane-coated fabrics types were investigated. The results demonstrated that UV exposure time caused significant decreases in the breaking strength, breaking elongation, tear strength, and air permeability of the fabric samples.

The breaking strength of all fabric types decreased as the duration of UV exposure increased. Coated fabrics exhibited higher strength values compared to raw fabrics, indicating the enhancing effect of the coating layer. Cotton fabrics showed the highest tensile strength in samples without UV treatment, while the lowest values were observed in samples exposed to 150 hours of UV. PET fabrics experienced high rates of strength decrease in raw samples, but the decrease was more limited in coated samples. Viscose fabrics had the lowest strength and showed significant strength reductions after UV exposure.

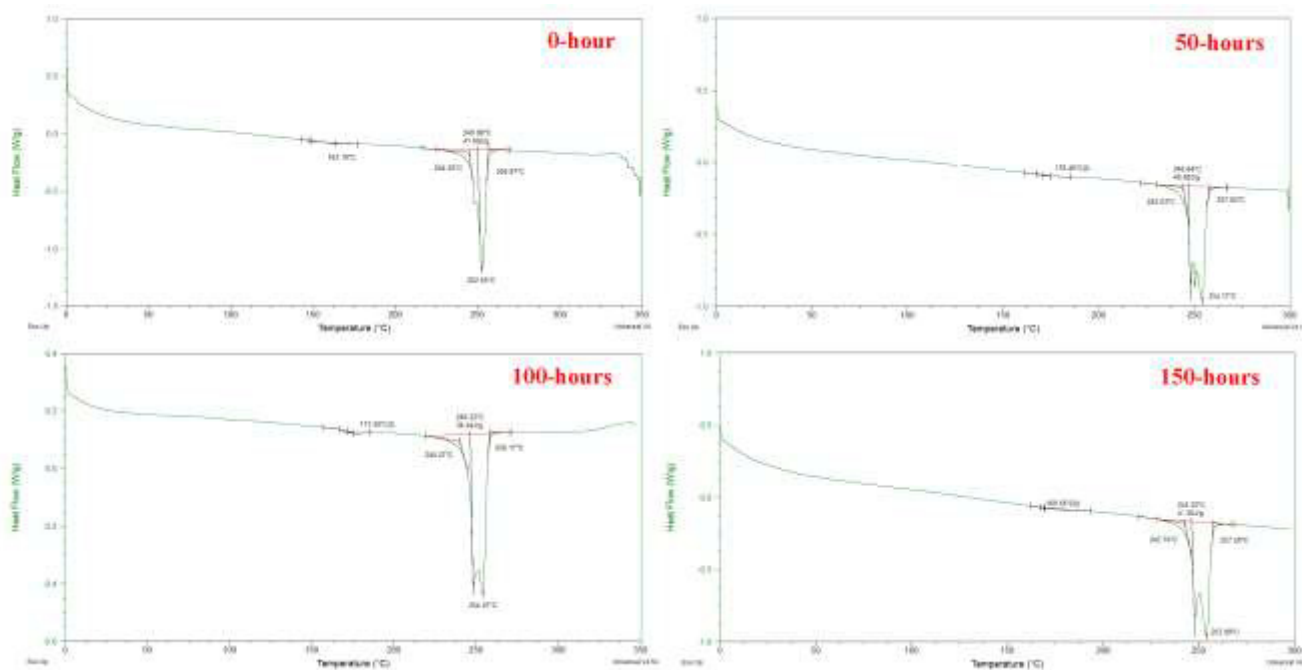


Figure 17. The DSC graphs of coated PET fabrics

Table 13. Glass transition temperatures and melting temperatures of coated PET fibers

UV-Exposure Time	Glass Transition Temperature (T_g /°C)	Melting Temperature (T_m /°C)	ΔH (Jg ⁻¹)
0 hours	163.10	249.98	41.00
50 hours	170.46	246.64	40.08
100 hours	171.50	246.22	34.44
150 hours	169.56	246.32	34.72



Breaking elongation, which measures the ability of a fabric to stretch before breaking, was also affected by UV exposure. Increasing exposure time resulted in lower elongation values for all fabrics. Similar to breaking strength, the decrease in elongation was more pronounced in the warp direction compared to the weft direction. Coating the fabrics and UV exposure both had a significant impact on elongation at break properties. Coating the fabrics increased elongation values, while UV exposure decreased elongation. Cotton fabrics showed a decrease in elongation at break values with UV exposure, but the coating process mitigated the negative effects. PET fabrics exhibited a decrease in elongation values with both coating and UV exposure. Viscose fabrics showed a significant decrease in elongation at break with UV exposure, but the coating process helped maintain elongation values.

The tear strength of the fabrics was also influenced by UV exposure. UV exposure led to decreases in tear strength in both warp and weft directions for all fabric types. The decrease in tear strength was more pronounced in the weft direction compared to the warp direction. Coated fabrics generally exhibited higher tear strength values compared to raw fabrics, but still experienced reductions in tear strength with UV exposure. Cotton fabrics showed an approximately 80% loss in tear strength with UV exposure. PET fabrics showed parallel reductions in tear strength with increasing exposure time. Viscose fabrics had the lowest tear strength values after 150 hours of UV exposure.

Air permeability, which measures the fabric's ability to allow air to pass through, was affected by UV exposure and the coating process. UV exposure had a significant effect on air permeability for raw viscose fabrics and all coated fabrics. Raw viscose fabrics showed an increase in air permeability with UV exposure, while coated fabrics exhibited changes in porosity and increased air permeability after extended UV exposure. The coating process generally reduced air permeability values, but UV exposure caused changes in the coated fabric samples, leading to higher air permeability.

According to the results of the analyses performed independently of the UV exposure time, it was found that polyurethane coating and UV exposure had significant effects on the mechanical and air permeability of the fabrics. The coating process proved to be effective in enhancing the breaking strength of all fabric samples by providing an additional surface layer that increased resistance to external forces. However, UV treatment had an abrasive effect on the fabrics, leading to a significant decrease in breaking strength, especially in cotton fabrics. Nevertheless, the coating process helped mitigate the strength reduction caused by UV exposure, particularly in the weft direction where breaking strength was more vulnerable.

The elongation at break properties were also influenced by both the coating process and UV exposure. While UV

treatment generally reduced the elongation at break, the coating process resulted in higher elongation values, indicating the stretchable nature of the coated fabric surface. However, in PET fabrics, the integration of coating and UV had a negative impact, leading to lower breaking elongation values due to the hardening effect of the coating process and structural deterioration caused by UV exposure. The coating process had varying effects on the elongation at break of viscose fabrics, with increased elongation values in the warp direction but decreased values in the weft direction due to increased fabric density and reduced stretching abilities.

The tear strength of all fabric types was significantly reduced by UV exposure, while the coating process improved tear strength in fabric samples not exposed to UV. PET fabrics showed a remarkable increase in tear strength due to the coating process, despite the abrasive effect of UV treatment. However, the tear strength of PET fabrics was still negatively affected by UV exposure. Similarly, UV treatment caused reductions in tear strength for viscose fabrics, even in coated samples.

Regarding air permeability, the coating process had a significant impact on reducing vertical air permeability values. However, the surface abrasion effect of UV treatment in cotton fabrics created new air passage channels, which counteracted the coating effect. In PET fabrics, the coating process primarily decreased air permeability, but the interaction with UV treatment diminished the covering effect. UV exposure resulted in distortions on the coating surface, allowing for the reestablishment of gaps required for air movement. In the case of viscose fabrics, both the coating process and UV treatment had significant effects on air permeability, leading to distinct groups based on permeability levels.

The DSC analyses conducted on PU-coated fabrics provided valuable insights into the thermal behavior of different fabric types under UV exposure. The results revealed significant changes in moisture evaporation and thermal degradation characteristics, as well as glass transition and melting temperatures, due to UV aging. For cellulosic fabrics (cotton and viscose), the DSC graphs displayed typical patterns observed in previous studies. The first endothermic peak corresponded to moisture evaporation, and it was observed that UV exposure time increased the evaporation peak temperatures. This can be attributed to the oxidation of hydroxyl side groups in cellulosic fibers under the influence of UV radiation. Notably, coated viscose fabrics exhibited higher evaporation temperature values compared to coated cotton fabrics, which can be attributed to the higher moisture-holding capacity of viscose fibers. The second peak in the DSC graphs indicated the onset of thermal degradation, with cotton fabrics (327.92°C) exhibiting higher onset temperature values compared to viscose fabrics (306.77°C),

owing to their higher degree of polymerization and crystallinity. UV exposure had noticeable effects on the mechanical properties of cellulosic fabrics but did not result in significant differences in thermal degradation temperatures.

In the case of PET fabrics, the first peak in the DSC graphs corresponded to the glass transition temperature (T_g), which significantly increased after 50 hours of UV exposure. This

increase in T_g values is consistent with previous studies and can be attributed to the crosslinking density induced by UV aging. The DSC analysis also revealed changes in the melting temperatures (T_m) and enthalpy (ΔH) values of coated PET fabrics. Prolonged UV exposure had a negative impact on T_m and ΔH , indicating photodegradation, photooxidation, and damage to the molecular structure of PET fibers. These changes resulted in lower melting points and reduced enthalpy values.

REFERENCES

1. Sen A.K., 2007. *Coated textiles: principles and applications*. Boca Raton-Florida: CRC Press.
2. Clemitson, I.2012. *Polyurethane Casting Primer*. Boca Raton-Florida: CRC Press..
3. Arshad N, Zia K.M., Jabeen F., Anjum M.N., Akram N., Zuber M.2018. Synthesis, characterization of novel chitosan based water dispersible polyurethanes and their potential deployment as antibacterial textile finish, *Int. J. Biol. Macromol.*, May, Vol. 111, 485–492.
4. Yang F., Yu W.2006. Study on Mechanical Properties of PU Coated Fabric. *International Forum on Textile Science and Engineering for Doctoral Candidates*.
5. Patel J.P., Patel P.R., Mahera H.K., Patel P. 2015.Effect of PU And PVC Coating on Different Fabrics for Technical Textile Application. *IJSTE -International J. Sci. Technol. Eng.*, 1 (11), 279–284.
6. Bulut Y., Sular V.2013. Manufacturing and sewing performance of polyurethane and polyurethane/silicone coated fabrics. *Mater. Manuf. Process.*, 28 (1), 106–111.
7. Padleckiene I., Petrulis D. 2009. Effect of abrasion on the air permeability & mass loss of breathable-coated fabrics. *Fibres Text. East. Eur.*, 73 (2), 50–54.
8. Cho J.W., Jung Y.C., Chun B.C., Chung Y.C. 2004. Water vapor permeability and mechanical properties of fabrics coated with shape-memory polyurethane. *J. Appl. Polym. Sci.*, 92 (5), 2812–2816.
9. Jassal M., Khungar A., Bajaj P., Sinha T. J. M. 2004. Waterproof breathable polymeric coatings based on polyurethanes. *J. Ind. Text.*, 33 (4), 269–280.
10. Mondal S., Hu J.L. 2007. Water vapor permeability of cotton fabrics coated with shape memory polyurethane. *Carbohydr. Polym.*, 67 (3), 282–287.
11. Kara S., Yesilpinar S., Aksit A. 2018. Permeability properties and abrasion resistance of coated polypropylene fabrics. *Vlakna a Text.*, 25 (2), 40–47.
12. Güneşoğlu S., Yüceer M. 2018. A modeling study of micro-cracking processes of polyurethane coated cotton fabrics. *Text. Res. J.*, 88 (24), 2766–2781.
13. Gunesoglu S, Cerçi E., Topalbekiroglu M. 2017. The improved breathability of polyurethane coated cotton fabric via micro-cracking. *J. Text. Inst.*, 108 (10),1815–1821.
14. Rubeziene V., Varnaite S., Baltusnikaite J., Padleckiene I. 2012. "Effects of light exposure on textile durability," in *Understanding and Improving the Durability of Textiles*, Elsevier, 104–125.
15. Das, S., Pandey, P., Mohanty, S., & Nayak, S. K. 2017. Study of UV aging on the performance characteristics of vegetable oil and palm oil derived isocyanate based polyurethane. *Korean Journal of Chemical Engineering*, 34(2), 523–538.
16. Zhang, W., Yao, J., & Wang, S. 2019. Multifunctional outdoor fabrics with ATO and TiO₂ embedded PU coatings. *Pigment & Resin Technology*, 48(4), 344–352.
17. Li, J. H., Hong, R. Y., Li, M. Y., Li, H. Z., Zheng, Y., & Ding, J. 2009. Effects of ZnO nanoparticles on the mechanical and antibacterial properties of polyurethane coatings. *Progress in Organic Coatings*, 64(4), 504–509.
18. Mills, D. J., Jamali, S. S., & Paprocka, K. 2012. Investigation into the effect of nano-silica on the protective properties of polyurethane coatings. *Surface & Coatings Technology*, 209, 137–142.
19. Sabzi, M., Mirabedini, S. M., Zohuriaan-Mehr, J., & Atai, M. 2009. Surface modification of TiO₂ nanoparticles with silane coupling agent and investigation of its effect on the properties of polyurethane composite coating. *Progress in Organic Coatings*, 65(2), 222–228.
20. Van Tran, T., Abedin, F., Usta, A., & Asmatulu, R. 2019. Polyurethane nanocomposite coating with silanized graphene and hexagonal boron nitride as nanoadditives for improved resistance against ultraviolet degradation. *Journal of Composites Materials*, 53(10), 1387–1399.
21. Yousif, E., & Haddad, R. 2013. Photodegradation and photostabilization of polymers, especially polystyrene: Review. *SpringerPlus*, 2(1).
22. Zhang, Y., & Zhang, M. 2017. Aging properties of polyvinylidene fluoride-coated polyesters used in tensioned membrane structure: Effect of loading protocol environment. *Advances in Materials Science and Engineering*.
23. Jana, R. N., & Bhunia, H. 2010. Accelerated hygrothermal and UV aging of thermoplastic polyurethanes. *High Performance Polymers*, 22(1), 3–15.
24. Houshyar, S., Padhye, R., Nayak, R., & Shanks, R. A. 2016. Deterioration of polyaramid and polybenzimidazole woven fabrics after ultraviolet irradiation. *Journal of Applied Polymer Science*, 133(9), 1–7.
25. Pal, S. K., Thakare, V. B., Singha, G., & Verma, M. K. 2011. Effect of outdoor exposure and accelerated aging on textile materials used in aerostat and aircraft arrester barrier nets. *Indian Journal of Fibre & Textile Research*, 36(2), 145–151.
26. Abbott, N. J., Lannefeld, T. E., Barish, L., & Brysson, R. J. 1971. A study of tearing in coated cotton fabrics: Part III: The influence of fabric construction. *Journal of Coating and Fibrous Materials*, 1(3), 4–17.
27. Bulut, Y., & Sular, V. 2011. Effects of process parameters on mechanical properties of coated fabrics. *International Journal of Clothing Science and Technology*, 23(4), 205–221.
28. Morton, W. E., & Hearle, J. W. S. 2008. Tensile properties. In *Physical Properties of Textile Fibres* (pp. 274–321). Woodhead Publishing.
29. Özdemir, H., & Mert, E. 2013. The effects of fabric structural parameters on the tensile, bursting, and impact strengths of cellular woven fabrics. *Journal of the Textile Institute*, 104(3), 330–338.
30. Zuber, M., Zia, K. M., Bhatti, I. A., Ali, Z., Arshad, M. U., & Saif,



- M. J. 2012. Modification of cellulosic fibers by UV-irradiation. Part II: After treatments effects. *International Journal of Biological Macromolecules*, 51(5), 743–748.
31. Mengüç, G. S., Temel, E., & Bozdoğan, F. 2018. Sunlight exposure: The effects on the performance of paragliding fabric. *Industrial Textile*, 69(5), 381–389.
 32. Eichert, U. 1994. Residual tensile and tear strength of coated industrial fabrics determined in long-time tests in natural weather conditions. *Journal of Coated Fabrics*, 23, 311–327.
 33. Hu, J., & Xin, B. 2008. Structure and mechanics of woven fabrics. In *Structure and Mechanics of Textile Fibre Assemblies* (pp. 27-60). Woodhead Publishing.
 34. Scelzo, W. A., Backer, S., & Boyce, M. C. 1994. Mechanistic role of yarn and fabric structure in determining tear resistance of woven cloth: Part I: Understanding tongue tear. *Textile Research Journal*, 64(5), 291–304.
 35. Krook, C. M., & Fox, K. R. 1945. Study of the tongue-tear test. *Textile Research Journal*, 15(11), 389–396.
 36. Jahan, I. 2017. Effect of fabric structure on the mechanical properties of woven fabrics. *Advanced Research in Textile Engineering*, 2(2).
 37. Eryuruk, S. H., & Kalaoglu, F. 2015. The effect of weave construction on tear strength of woven fabrics. *Autex Research Journal*, 15(3), 207–214.
 38. Temel, E., Bozdoğan, F., & Mizmizlioglu, D. 2020. Structural investigation of UV aged tent fabrics. *Tekstil ve Konfeksiyon*, 29(3), 246–252.
 39. Çay, A., Vassiliadis, S., Rangoussi, M., & Tarakcioglu, I. 2007. Prediction of the air permeability of woven fabrics using neural networks. *International Journal of Clothing Science and Technology*, 19(1), 18–35.
 40. Pakdel, E., Daoud, W. A., Afrin, T., Sun, L., & Wang, X. 2017. Enhanced antimicrobial coating on cotton and its impact on UV protection and physical characteristics. *Cellulose*, 24(9), 4003–4015.
 41. Ugur, Ş. S., Sarıışık, M., & Aktaş, A. H. 2011. Nano-TiO₂ based multilayer film deposition on cotton fabrics for UV-protection. *Fibers and Polymers*, 12(2), 190–196.
 42. Broasca, G., Borgia, G., Dumitrascu, N., & Vranceanu, N. 2013. Characterization of ZnO coated polyester fabrics for UV protection. *Applied Surface Science*, 279, 272–278.
 43. Gunaydin, G. K. 2019. Effect of coating ratio and weft density on some physical properties of upholstery fabrics. *Industrial Textile*, 70(4), 379–385.
 44. Havlová, M. 2013. Air permeability and constructional parameters of woven fabrics. *Fibres and Textiles in Eastern Europe*, 98(2), 84–89.
 45. Hatakeyama, T., Nakamura, K., & Hatakeyama, A. 2000. Vaporization of bound water associated with cellulose fibres. *Thermochimica Acta*, 352(353), 233–239.
 46. Yang, P., & Kokot, S. 1996. Thermal analysis of different cellulosic fabrics. *Journal of Applied Polymer Science*, 60(8), 1137–1146.
 47. Wypych, G. 2020. *Handbook of UV Degradation and Stabilization* (3rd ed.). Toronto: ChemTec Publishing.
 48. Oliveira, F. R., et al. 2016. Tintorial behavior of curaua and banana fibers and dyeing wastewater treatment by porous alumina membranes. *Desalination and Water Treatment*, 57(6), 2750–2758.
 49. Shafizadeh, F., & Bradbury, A. G. W. 1979. Thermal degradation of cellulose in air and nitrogen at low temperatures. *Journal of Applied Polymer Science*, 23(5), 1431–1442.
 50. Fan, F., Zhang, W., & Wang, C. 2015. Covalent bonding and photochromic properties of double-shell polyurethane-chitosan microcapsules crosslinked onto cotton fabric. *Cellulose*, 22(2), 1427–1438.
 51. Xu, Y., Lu, Z., & Tang, R. 2007. Structure and thermal properties of bamboo viscose, Tencel and conventional viscose fiber. *Journal of Thermal Analysis and Calorimetry*, 89(1), 197–201.
 52. Giesz, P., Mackiewicz, E., Nejman, A., Celichowski, G., & Cieślak, M. 2017. Investigation on functionalization of cotton and viscose fabrics with AgNWs. *Cellulose*, 24(1), 409–422.
 53. Kong, Y., & Hay, J. N. 2002. Multiple melting behaviour of poly(ethylene terephthalate). *Polymer*, 44(3), 623–633.
 54. Peng, G., et al. 2008. Effects of nano ZnO on strength and stability of unsaturated polyester composites. *Polymer Advances in Technology*.
 55. Samyn, P. 2016. Tribological properties and thermomechanical analysis of unsaturated polyester fabric composite in oscillating line-contact sliding. *Tribology International*, 99, 127–139.
 56. Boubakri, A., Guermazi, N., Elleuch, K., & Ayedi, H. F. 2010. Study of UV-aging of thermoplastic polyurethane material. *Materials Science and Engineering: A*, 527(7–8), 1649–1654.
 57. Younis, A. A. 2016. Evaluation of the flammability and thermal properties of a new flame retardant coating applied on polyester fabric. *Egyptian Journal of Petroleum*, 25(2), 161–169.
 58. Pegoretti, A., & Penati, A. 2004. Effects of hygrothermal aging on the molar mass and thermal properties of recycled poly(ethylene terephthalate) and its short glass fibre composites. *Polymer Degradation and Stability*, 86(2), 233–243.
 59. Wang, M., et al. 2019. Fabrication of highly durable polysiloxane-zinc oxide (ZnO) coated polyethylene terephthalate (PET) fabric with improved ultraviolet resistance, hydrophobicity, and thermal resistance. *Journal of Colloid Interface Science*, 537, 91–100.
 60. Allen, N. S., Edge, M., Mohammadian, M., & Jones, K. 1994. Physicochemical aspects of the environmental degradation of poly(ethylene terephthalate). *Polymer Degradation and Stability*, 43(2), 229–237.
 61. Nejman, A., Kamińska, I., Giesz, P., & Cieślak, M. 2015. Thermal stability of polyester fabric with polyacrylic coatings. *Fibres & Textiles in Eastern Europe*, 23(4), 73–82.
 62. Yildiz, Z., Gungor, A., Onen, A., & Usta, I. 2016. Synthesis and characterization of dual-curable epoxyacrylates for polyester cord/rubber applications. *Journal of Industrial Textiles*, 46(2), 596–610.
 63. Abidi, H., et al. 2021. Accelerated weathering of textile waste nonwovens used as sustainable agricultural mulching. *Journal of Industrial Textiles*, 50(7), 1079–1110.
 64. Zhang, H., et al. 2006. Effects of solar UV irradiation on the tensile properties and structure of PPTA fiber. *Polymer Degradation and Stability*, 91(11), 2761–2767.
 65. Kijchavengkul, T., Auras, R., Rubino, M., Alvarado, E., Camacho Montero, J. R., & Rosales, J. M. 2010. Atmospheric and soil degradation of aliphatic-aromatic polyester films. *Polymer Degradation and Stability*, 95(2), 99–107.
 66. Sang T., Wallis C.J., Hill G., Britovsek G. J. P. 2020. Polyethylene terephthalate degradation under natural and accelerated weathering conditions. *Eur. Polym. J.*, 136 (June), 109873.

The Effects of Sustainability and Fast Fashion Factors on Apparel Buying Behavior

Derya Bilen¹  0000-0001-9658-9187
Turan Atılğan²  0000-0001-5136-0231
Seher Kanat²  0000-0001-8367-9773

¹Ege University, Graduate School of Natural and Applied Sciences, Izmir, Türkiye

²Ege University, Engineering Faculty, Department of Textile Engineering, Izmir, Türkiye

Corresponding Author: Seher Kanat, seher.kanat@ege.edu.tr

ABSTRACT

Nowadays, apparel sector, in which the importance of sustainability concept gradually increases, can directly and indirectly harm the environment and human health with production processes and wastes. Some of the wastes are occurred via the products which have completed their economic lives. In this regard, this research aims to analyze the effects of sustainability and fast fashion factors on apparel buying behavior. In accordance with this aim, a survey was conducted to consumers whose ages are 18 and over and who live in three biggest cities of Türkiye. Thus, it is revealed that how consumers are affected from sustainability and fast fashion factors during their apparel purchase process. Besides, suggestions are made to apparel brands and enterprises on the basis of the findings.

1. INTRODUCTION

The factors like environmental pollution, decrease in sources, easy access to information and increase in consumer awareness; lead the sectors and enterprises to be more sensitive to their environment and to give more importance to sustainability. Apparel sector, whose environmental damage is high, is one of the sectors, in which the importance of sustainability concept increases. Apparel sector can damage the environment both with production processes and with wastes of products that completed their lives. Especially, fast fashion concept, which gradually becomes popular in recent years and which is usually contradictory to sustainability, has caused an increase in damage. Therefore, also with the increasing pressure of consumers, apparel enterprises' sustainability activities increase day by day. Thus, this study aims to investigate the effects of sustainability and fast fashion factors on apparel buying behavior. The research guides the apparel brands and enterprises by revealing how consumers are affected from sustainability and fast fashion factors during their apparel buying processes.

To cite this article: Bilen D, Atılğan T, Kanat T. 2024. The Effects of Sustainability and Fast Fashion Factors on Apparel Buying Behavior. *Tekstil ve Konfeksiyon*, 34(1), 69-76.

ARTICLE HISTORY

Received: 17.02.2023

Accepted: 13.09.2023

KEYWORDS

Sustainability, apparel sector, fast fashion, consumer, buying behavior

Within the literature there are studies about sustainability, sustainability in apparel sector and fast fashion concept [1 - 17]. However, researches, which analyze the sustainability and fast fashion concepts on the basis of apparel sector and which investigates the effects of these concepts to each other, are limited [18 - 25]. Therefore, there isn't any study, which analyzes the interactions of these concepts on the basis of Turkish apparel sector which is a leading apparel exporter and which is one of the significant apparel markets. In this context, this research alters from other researches within the literature.

2. SUSTAINABILITY CONCEPT AND SUSTAINABILITY IN APPAREL SECTOR

Sustainability is defined as development that meets the needs of the present without compromising the ability of future generations to meet their own needs by World Commission on Environment and Development [7,11,22, 25,26].

Sustainability involves complicated and variable dynamics, which affects human welfare and living, which is both global

and local and whose ecologic, economic and sociopolitical dimensions intersect [25]. Nowadays, sustainability concept consists of three main factors as social, environmental and economic [7]. Long-term strategies for sustainable development are suggested on the basis of these three main factors. The environmental dimension of sustainability indicates that source use should be long-term by emphasizing source exhaustion and environmental degradation. Economic sustainability states a dynamic economy, which can exist for a long time and which has understood the importance of long-term employment. Social dimension of sustainability specifies the equality issue and the welfare of people and society [19].

In this context, the sustainability issues in apparel sector can be listed as; short and seasonal product life cycles, high product range, low product predictability, demand that is affected from many different factors, impulse buying behaviors of consumers, preference differences of consumers, emotional factors which affect the consumers' buying decisions and institutions' concentration on sustainable development [3].

3. FAST FASHION CONCEPT AND ITS RELATION WITH SUSTAINABILITY

Fast fashion is defined as a positioning strategy, which gives quick response by presenting frequently updated fashion products to current fashion trends [23]. Fast fashion is characterized by the transformation of fashionable design to products, which can be bought by the masses. This concept aims to attract consumers to stores as frequently as possible in order to increase the purchase frequency of fashionable styles [20].

Fast fashion is a quick response system, which presents affordable apparel collections that are based on current luxury fashion trends and which promotes throwing away. The cycle time between podium and consumers was six months. However, nowadays, it is declined to only a few weeks. Fast fashion enterprises improve themselves in fast cycles by presenting ready products with price tags, fast samples, small parties combined with high diversity, productive transportation and delivery. Retailers follow the new trends for ensuring consumers return and they buy products every week in order to present new products and replace inventories. Also, enthusiastic consumers check on fast fashion stores in every three weeks looking for new styles [25].

Fast fashion concept owes its specific properties and structure to requirements such as; shortened delivery times, faster inventory cycle and high order coverage ratios for consumer demands in high seasons. The concept possesses an extremely competitive structure, which presents the possible newest trend to consumers and which causes pressure on costs. Therefore, it requires a specific productivity level together with high responsiveness ability. High responsiveness to demand is obtained by the

implementation of strategies such as; just in time source supply, quick response systems and agile supply chain management. However, various ethical, employment and environmental issues are ignored in order to provide and protect this high responsiveness. Thus, an unsustainable structure is occurred [20].

At this point, fashion industry feels more pressure due to these sustainability issues, which are revealed by media and consumers. Therefore, many enterprises in fast fashion industry redesign their supply chains and embrace sustainable strategies in order to provide coordination between stakeholders and balance the economic, environmental and social performance. On the other hand, the enterprises in fast fashion industry lead to consumer behaviors rather than meeting the consumer demands. They succeed this with proper prices, high product range, presenting fashionable clothes for consumers under the age of 40 and supply chain's quick response. This business model improves economic performance by reducing risk and uncertainty of consumers' strategic choices. However, the industry commonly faces with environmental and social issues. These issues show the distinction between maximizing the economic benefits and social responsibility search [22].

The studies within the literature, which analyze the relations between fast fashion and sustainability, are focused on investigating social sustainability reports of fast fashion enterprises, analyzing the strategies of fast fashion enterprises for positioning sustainability, the effects of corporate social responsibility behavior on sustainability performance of fast fashion enterprises, analyzing consumer perception with regard to a specific fast fashion retailer's sustainability and the relations between sustainable fashion consumption and fast fashion [18-25]. When the studies, which analyze the effects of fast fashion and sustainability on apparel buying behavior, are investigated, it is seen that these effects are changed according to demographic factors such as gender, education level, age, income, apparel budget and etc. [1,16-19,24,27-32]. As it is indicated in the literature, young consumers generally do not show sustainable apparel consumption behaviors [1,18,24,27,28,32]. In addition to this, women are more interested in fashionable clothing with regard to men [18,28,31]. However, some studies indicate that, women are more environmentally concerned and give more importance to purchase sustainable clothes [16,17,30]. Moreover, it can be indicated that as the education level is increased, the purchase intention towards sustainable clothes is also increased [16,17]. Finally, it can be specified that income is positively related to sustainable apparel purchase. As the income levels and the apparel budgets of consumers are increased, the purchase intention towards sustainable clothes is also increased [17,19,29]. Thus, the following hypotheses are suggested:

H1: The effects of sustainability and fast fashion factors on apparel buying behavior alter according to women and men consumers.

H2: The effects of sustainability and fast fashion factors on apparel buying behavior alter according to the education level of consumers.

H3: The effects of sustainability and fast fashion factors on apparel buying behavior alter according to consumers' ages.

H4: The effects of sustainability and fast fashion factors on apparel buying behavior alter according to consumers' apparel budgets.

4. METHOD OF THE RESEARCH

This research aims to analyze the effects of sustainability and fast fashion factors on apparel buying behavior. It purposes to reveal how consumers in Türkiye are affected from sustainability and fast fashion factors during their apparel purchase process. Besides, it aims to make suggestions to apparel brands and enterprises on the basis of the findings.

In accordance with this aim, a survey was conducted to consumers whose ages are 18 and over and who live in three biggest cities of Türkiye (İstanbul, Ankara and İzmir) [33]. Consumers whose ages are 18 and over were incorporated in the research because the age of legal majority is 18 in Türkiye. Besides, İstanbul, Ankara and İzmir provinces were selected because they can represent the country-wide due to their cosmopolite structures and population densities.

According to data of Turkish Statistical Institute [34], Türkiye's population was 82.003.882 on 31.12.2018. The population, whose ages were 18 and over, was 59.083.460. Sample size was calculated as 384 at 95% confidence interval with 5% error margin. The individuals, who constitute the sample, were determined according to simple random sampling.

The survey was carried out between March 2020 and August 2020. Face to face interview and online survey techniques were used [33]. Survey form consists of 10 main and 34 sub-questions. Ege University's Ethical Board of Social and Human Sciences Scientific Research and Publication was ethically approved the survey on 29.08.2019 with 353 protocol number. 515 survey forms were incorporated in the research. The findings obtained were analyzed by using SPSS program.

5. FINDINGS OF THE RESEARCH AND THEIR ANALYSIS

Firstly, the questionnaire's reliability was calculated and the reliability co-efficient α was found as 0,904. According to this, the scale of the questionnaire is found to be highly reliable. Secondly the participants' demographic features were evaluated. It is found that they are generally well-educated young consumers who possess middle-income (Table 1).

Table 1. Distribution of participants according to their demographic features

Demographic Features	Frequency	Valid Percent
Age	18-25	22,9
	26-33	25,4
	33-41	19,2
	42-49	22,1
	50 and over	10,3
Gender	Women	58,1
	Men	41,9
Education status	High school and below	28,5
	University	60,8
	Postgraduate	10,7
Monthly income	500 \$ and below	62,7
	501 \$ - 875 \$	27,4
	876 \$ and over	9,9

Table 2. Distribution of participants according to their evaluation methods for end-of-life clothes

Evaluation methods for end-of-life clothes	Frequency	Valid Percent
I put them to garment collection boxes or donate to charity organizations for the use of needy people.	433	84,1
I throw them to waste.	35	6,8
I give them to enterprises or brands, which recycle garments.	28	5,4
I sell them to second hand garment stores.	19	3,7

Moreover, 33% of the participants live in İstanbul province, whereas 34% lives in Ankara and 33% lives in İzmir. In addition to these, 71% of the participants separate 20% or less from their monthly budgets for apparel expense. Besides, 75% of the participants generally purchase their garments from physical stores. Also, the participants indicate that they mostly give importance to quality (35%) in any apparel product. This factor is followed by; perfect fit to body (30%), price (18%), design (11%), fashionableness (3%) and being unharmed to human health and environment (3%) respectively.

84% of the participants specify that they put their end-of-life clothes to garment collection boxes or donate to charity organizations for the use of needy people (Table 2). In other

words, consumers contribute to reuse, which is a part of sustainability implementations. On the other hand, recycling of clothes or selling them as second hand clothes are unlikely options for Turkish consumers.

The survey includes 25 statements, which analyze the effects of sustainability and fast fashion factors on apparel buying behavior by using quinary likert scale. Participants were asked to select their agreement levels for each of these statements. In quinary likert scale I certainly agree was coded as 5, I agree as 4, I have no idea or I'm on the fence as 3, I don't agree as 2 and I certainly don't agree as 1. Firstly, the averages and standard deviations of the statements were calculated. The findings obtained are given in Table 3.

Table 3. The descriptive statistics of the statements and the results of the exploratory factor analysis

Factors	Statements	Rotated Loadings	Average	Standard Deviation	Averages of the Factors
Environmental sustainability factors	I give importance to buying apparel products, which possess ecolabels (organic, ecologic, Oeotex, recycled etc.)	0,809	3,55	1,039	3,75
	I give importance to buying environmentally friendly apparel products.	0,802	3,82	0,976	
	I give importance to buying apparel products, which possess organic raw material.	0,777	3,62	1,049	
	I give importance to buying apparel products, which possess recycled raw material.	0,766	3,38	1,009	
	I give importance to buying apparel products, which do not contain harmful chemicals/dyes.	0,699	3,96	0,991	
	I give importance to buying apparel products that are harmless to human health.	0,679	4,19	0,837	
Social, economic and environmental sustainability factors	The sustainability and environment policies of an apparel brand, from which I bought clothes, are important for me.	0,766	3,83	0,992	3,85
	Social responsibility projects of an apparel brand, from which I bought clothes, are important for me.	0,743	3,75	1,001	
	Ecological design activities of an apparel brand, from which I bought clothes, are important for me.	0,706	3,70	0,994	
	If an apparel brand, from which I bought clothes, shares its sustainability activities with public, it is important for me.	0,752	3,75	1,005	
	If an apparel brand, from which I bought clothes, possesses projects for reducing water and energy consumption, it is important for me.	0,713	3,76	1,041	
	The ethical and moral values of an apparel brand, from which I bought clothes, are important for me.	0,694	4,04	0,968	
	The environmentally friendly package use of an apparel brand, from which I bought clothes, is important for me.	0,601	3,78	1,039	
	If an apparel brand, from which I bought clothes, is harmless to human health and environment during its production, it is important for me.	0,581	4,05	0,960	
	I give importance to buying apparel products, which possess long economic lives.	0,459	4,34	0,789	
	I'm ready to pay more to environmentally friendly apparel products.	0,400	3,50	1,186	
Fast fashion factors	I buy clothes for my pleasure even if I do not need them.	0,850	2,92	1,389	2,94
	I buy clothes only for liking their design even if I do not need them.	0,840	2,97	1,356	
	I buy clothes only for being fashionable even if I do not need them.	0,829	2,48	1,294	
	The amount of clothes that I bought increases each year.	0,732	2,88	1,300	
	I closely follow the fashion trends via magazines and social media.	0,684	2,77	1,412	
	I put more clothes to garment collection boxes each year.	0,529	2,96	1,269	
	The fashionableness of an apparel brand, from which I bought clothes, is important for me.	0,487	3,58	1,198	
Second hand garment factor	I can use second hand garments.	0,923	2,75	1,381	2,65
	I buy second hand garments.	0,901	2,54	1,375	

According to the averages obtained, participants indicate that they give great importance to the economic lives of their bought clothes. They also specify that they give importance to buying clothes that are harmless to human health. Besides, they prefer buying clothes from environmentally friendly apparel brands, which follow ethical and moral values. Therefore, it can be said that consumers prefer to buy sustainable clothes (possessing durability and quality and/or being classical and timeless), because if a garment's economic life is long and it is environmentally friendly, it is accepted to be sustainable. Although, consumers do not indicate that the most important factor during their apparel shopping is sustainability, they demonstrate that they give importance to sustainability by paying attention to factors such as quality, long economic life and being harmless to human health and environment. All these findings are also compatible with the literature [12,18,28,35,37].

On the other hand, consumers are affected from other sustainability factors in intermediate level. These factors can be listed as; apparel products which do not contain harmful chemicals/dyes, apparel brands which possess sustainability and environmental policies, environmentally friendly apparel products, apparel brands which use environmentally friendly packages, apparel brands which possess projects for reducing water and energy consumption, apparel brands which possess social responsibility projects, apparel brands which share their sustainability activities with public, apparel brands which possess ecologic design activities, apparel products which involve organic raw material, fashionable apparel products, apparel products which possess ecolabels, being ready to pay more to environmentally friendly apparel products, apparel products which involve recycled raw material. As it can be understood from all these factors, consumers are affected from environmental, social and economic sustainability factors during their apparel shopping, but this influence level is not very high.

If the statements, which evaluate the sustainability and fast fashion factors together, are analyzed, it can be seen that, the consumers are not highly affected from fast fashion factors. In this context, it can be said that, they give importance to sustainability factors. Accordingly, most of the consumers do not buy clothes only because they like

their design or for their pleasure. Besides, they do not buy more clothes each year and they do not put more clothes to garment collection boxes or donate to charity organizations for the use of needy people. Similarly, most of the consumers do not closely follow the fashion trends. In spite of these, it is determined that most of the consumers do not prefer to buy or use second hand garments.

After the basic evaluation, the statements were analyzed by using exploratory factor analysis and gathered into four groups. Exploratory factor analysis is actualized in order to obtain brief statements instead of 25 statements. It was found that the sample is suitable and reliable for factor analysis (Kaiser-Meyer-Olkin measure of sampling is equal to 0,920 and the significance of Bartlett's Test of Sphericity is equal to 0,000). Principal components extraction was used for extracting factors with eigenvalues over 1 and the rotation of factor loading matrix was chosen as varimax. The standard loading of 22 statements are higher than 0,50 (they differ between 0,501 and 0,825) and the cumulative variance of 4 factors is equal to 63,268%. The loadings (scores) of the statements within Table 3 are taken from rotated component matrix (only three loadings are lower than 0,50). The obtained four factors are renamed (Table 3). Afterwards, hypotheses tests were actualized.

Four main hypotheses involve 16 sub-hypotheses due to the 4 factors and 4 demographic features. All sub-hypotheses were tested at 95% confidence interval. According to the obtained results, 6 hypotheses are accepted, whereas 10 hypotheses are rejected.

1 sub-hypothesis with regard to the first main hypothesis is accepted (Table 4). Women consumers' apparel buying behaviors are more affected from the fast fashion factors with regard to men consumers. Women consumers buy more apparel products with regard to men consumers, although they do not need them. Women consumers can buy apparel products only for their pleasure or liking their design or being fashionable. These findings are also compatible with the literature [18,28,31].

None of the sub-hypotheses are accepted with regard to the second hypothesis. According to this, the effects of sustainability and fast fashion factors on apparel buying behavior do not alter according to the education levels of consumers.

Table 4. Divergences between the effects of sustainability and fast fashion factors on apparel buying behavior of women and men consumers

Hypothesis 1a: The effects of fast fashion factors on apparel buying behavior alter according to women and men consumers.						
Gender	N	Average	Standard Deviation	t	df	p
Women	299	0,1486260	1,017021	4,078	483,089	0,000
Men	216	-0,2057370	0,940118			

3 sub-hypotheses with regard to the third main hypothesis are accepted (Table 5). As the age increases, the environmental sustainability effects on consumers' apparel buying behaviors are also increased. It can be said that the

increasing experience and awareness due to increasing age affect this result. Besides, fast fashion factors mostly affect the young consumers' buying behaviors (their ages are between 18 and 25). This group is followed by 26-33 age



group, 42-49 age group, 34-41 age group and 50 and over age group respectively. According to these findings it can be said that, as the age decreases, the fast fashion effects on consumers' apparel buying behaviors are also increased. Young consumers generally follow fashion and trends due to their high approval and admiration wishes. Besides, due to their limited incomes, they generally want to acquire fashionable and trendy clothes with affordable prices. Therefore, young consumers usually prefer to buy fast fashion products and support consumption rather than sustainability. Besides, these findings are compatible with the literature [1,18,24,27,28,32]. On the other hand second hand garment factor mostly affects the apparel buying behaviors of consumers, whose ages are between 26 and 33.

2 sub-hypotheses with regard to the fourth main hypothesis are accepted (Table 6). Fast fashion factors mostly affect the apparel buying behaviors of consumers, whose apparel budgets are between 41% and 50% within their monthly budgets. Also it is determined that, as the ratio of apparel budget within monthly budget is increased, the fast fashion effects on consumers' apparel buying behaviors are also increased. In other words, as the ratio of apparel budget within monthly budget is increased, the consumers' sustainability concerns are decreased. On the other hand, second hand garment factor mostly affects the apparel buying behaviors of consumers, whose apparel budgets are 10% or below within their monthly budgets. In other words, second hand garments are mostly preferred by consumers who possess the lowest apparel budgets.

Table 5. Divergences between the effects of sustainability and fast fashion factors on apparel buying behavior of consumers at different age groups

Hypothesis 3a: The effects of environmental sustainability factors on apparel buying behavior alter according to consumers' ages.							
Age	N	Average	Standard Deviation	F	df ₁	df ₂	p
18-25	118	-0,337080	1,091744				
26-33	131	-0,161378	0,915282				
34-41	99	0,121557	0,865202	9,198	4	510	0,000
42-49	114	0,218200	1,017577				
50 and over	53	0,452961	0,884586				
Hypothesis 3b: The effects of fast fashion factors on apparel buying behavior alter according to consumers' ages.							
Age	N	Average	Standard Deviation	F	df ₁	df ₂	p
18-25	118	0,221216	1,013788				
26-33	131	0,056327	1,015537				
34-41	99	-0,143405	0,893853	2,820	4	510	0,025
42-49	114	-0,072323	1,011420				
50 and over	53	-0,208309	1,025290				
Hypothesis 3c: The effects of second hand garment factor on apparel buying behavior alter according to consumers' ages.							
Age	N	Average	Standard Deviation	F	df ₁	df ₂	p
18-25	118	0,079098	1,011753				
26-33	131	0,197125	0,982062				
34-41	99	-0,140318	0,901209	2,847	4	510	0,024
42-49	114	-0,172715	0,999808				
50 and over	53	-0,0297363	1,118722				

Table 6. Divergences between the effects of sustainability and fast fashion factors on apparel buying behavior of consumers at different apparel budget groups

Hypothesis 4a: The effects of fast fashion factors on apparel buying behavior alter according to consumers' apparel budgets.							
Apparel budget	N	Average	Standard Deviation	F	df ₁	df ₂	p
%10 and below	198	-0,396464	0,949346				
%11-20	168	0,077316	0,926459				
%21-30	83	0,302731	0,953832				
%31-40	34	0,612187	0,922111	14,593	5	509	0,000
%41-50	23	0,615260	0,867706				
%51 and over	9	0,602083	1,086301				
Hypothesis 4b: The effects of second hand garment factor on apparel buying behavior alter according to consumers' apparel budgets.							
Apparel budget	N	Average	Standard Deviation	F	df ₁	df ₂	p
%10 and below	198	0,154842	1,083648				
%11-20	168	-0,012133	0,948712				
%21-30	83	-0,178094	0,911374				
%31-40	34	-0,004601	0,986470	2,737	5	509	0,019
%41-50	23	-0,477370	0,830428				
%51 and over	9	-0,300287	0,661761				

6. GENERAL EVALUATION AND SUGGESTIONS

The important research results and the suggestions that can be made on the basis of these results can be summarized as followed. First of all, it is determined that, consumers mostly give importance to quality and perfect fit in any apparel product. Besides, they give great importance to the economic life of their bought clothes. These findings are also compatible with the literature [12,28,35]. Therefore, apparel enterprises and brands, which want to attract consumers' attention and adopt sustainability factors, should design and produce qualified, durable, classic and timeless clothes.

According to another finding of the research, consumers donate their end-of-life clothes for the reuse of needy people. This finding is also compatible with the literature [36]. At this point, if the apparel enterprises and brands collect the used clothes from consumers and convey those to needy people after repairing and cleaning, it will be useful in terms of sustainability. Besides, the apparel enterprises and brands should collect the used clothes for recycling and promote awareness of consumers.

As it is indicated in the literature, consumers give importance to buying sustainable clothes and they prefer to buy clothes from apparel brands which follow ethical and moral values [12,18,37]. Similarly, according to our findings, consumers give importance to buying clothes which are harmless to human health. Besides, they prefer buying clothes from environmentally friendly apparel brands which follow ethical and moral values. Therefore, the apparel enterprises and brands should give importance to produce environmentally friendly garments. Besides, they should follow ethical and moral values and their production processes should be environmentally friendly.

As stated by our research results, consumers are not highly affected from fast fashion factors and they give importance to sustainability factors. Accordingly, most of the consumers do not buy clothes only because they like their design or for their pleasure. Besides, they indicate that they do not buy more clothes each year and they do not put more clothes to garment collection boxes or donate to charity organizations for the use of needy people. These findings are also compatible with the literature [12,18]. Therefore, the apparel enterprises and brands should give more importance to designing and producing qualified, durable, classic and timeless clothes rather than fashionable, unqualified, flimsy and affordable clothes.

According to our research results, although Turkish consumers give importance to sustainability, they do not prefer to use or buy second hand clothes. This finding is

also compatible with the literature [12]. At this point, the apparel enterprises and brands should follow marketing strategies which promote second hand garment use.

According to the literature, women are more interested in fashionable clothing with regard to men [18,28,31]. Similarly, according to our findings, women consumers' apparel buying behaviors are more affected from the fast fashion factors with regard to men consumers. In addition to this, women consumers' apparel buying behaviors (especially during buying fast fashion products) are less affected from sustainability factors with regard to men consumers. At this point, apparel enterprises and brands, which produce clothes for women, should design and produce more chic and stylish clothes in order to lead consumers towards sustainability. Moreover, apparel brands and enterprises, which produce clothes for men, should give more importance to sustainability factors and reflect this situation to their consumers.

As it is indicated in the literature, young consumers generally do not show sustainable apparel consumption behaviors [1,18,24,27,28,32]. Similarly, according to our findings, as the consumers' ages are increased, the environmental sustainability effects on consumers' apparel buying behaviors are also increased. Also, as the consumers' ages are decreased, the fast fashion effects on consumers' apparel buying behaviors are increased. Therefore, apparel brands and enterprises should inform young consumers about sustainability and increase the amount of timeless but chic clothes within their collections in order to lead them towards sustainability. Besides, apparel enterprises and brands, whose target groups are at their middle ages or over, should give more importance to sustainability factors and should reflect this importance to them.

According to the findings of our research, consumers are not ready to pay more to environmentally friendly apparel products. This finding is also compatible with the literature [5,28,37]. At this point, the apparel enterprises and brands should actualize their sustainability activities without reflecting an incremental cost to their products or with a slight incremental cost.

To sum up, this research contributes to the literature by revealing the interactions of sustainability and fast fashion concept on the basis of Turkish consumers. Also, it highlights and proves some of the previous findings within literature on the basis of Turkish consumers. However, the research also possesses some limitations. The survey can be conducted in more cities or different countries and thus, more comparisons can be made.

REFERENCES

1. Diddi S., Yan R.N., Bloodhart B., Bajtelsmit V., McShane K. 2019. Exploring young adult consumers' sustainable clothing consumption intention-behavior gap: a behavioral reasoning theory perspective. *Sustainable Production and Consumption* 18, 200-209.
2. Woodside A.G., Fine M.B. 2019. Sustainable fashion themes in luxury brand storytelling: the sustainability fashion research grid. *Journal of Global Fashion Marketing* 10(2), 111-128.
3. Ciasullo M.V., Cardinali S., Cosimato S. 2017. A strenuous path for sustainable supply chains in the footwear industry: a business strategy issue. *Journal of Global Fashion Marketing* 8(2), 143-162.
4. Khurana K., Ricchetti M. 2016. Two decades of sustainable supply chain management in the fashion business, an appraisal. *Journal of Fashion Marketing and Management* 20(1), 89-104.
5. Lenne O.D., Vandenbosch L. 2017. Media and sustainable apparel buying intention. *Journal of Fashion Marketing and Management* 21(4), 483-498.
6. Sirilertsuwan P., Ekwall D., Hjelmgren D. 2018. Proximity manufacturing for enhancing clothing supply chain sustainability. *The International Journal of Logistics Management* 29(4), 1346-1378.
7. Shen B. 2014. Sustainable fashion supply chain: lessons from H&M. *Sustainability* 6, 6236-6249.
8. Chang H.J., Watchravesringkan K.T. 2018. Who are sustainably minded apparel shoppers? An investigation to the influencing factors of sustainable apparel consumption. *International Journal of Retail & Distribution Management* 46(2), 148-162.
9. Noh M., Johnson K.K.P. 2019. Effect of apparel brands' sustainability efforts on consumers' brand loyalty. *Journal of Global Fashion Marketing* 10(1), 1-17.
10. Hu Z.H., Li Q., Chen X.J., Wang Y.F. 2014. Sustainable rent based closed loop supply chain for fashion products. *Sustainability* 6, 7063-7088.
11. Goworek H., Fisher T., Cooper T., Woodward S., Hiller A. 2012. The sustainable clothing market: an evaluation of potential strategies for UK retailers. *International Journal of Retail & Distribution Management* 40(12), 935-955.
12. Bick R., Halsey E., Ekenga C.C. 2018. The global environmental injustice of fast fashion. *Environmental Health* 17(92), 1-4.
13. Hvass K.K., Pedersen E.R.G. 2019. Toward circular economy of fashion: experiences from a brand's product take-back initiative. *Journal of Fashion Marketing and Management* 23(3), 345-365.
14. Hall J. 2018. Digital kimono: fast fashion, slow fashion?. *Fashion Theory* 22(3), 283-307.
15. Sandvik I.M., Stubbs W. 2019. Circular fashion supply chain through textile-to-textile recycling. *Journal of Fashion Marketing and Management*, 23(3), 366-381.
16. Stefko R., Steffek V. 2018. Key issues in slow fashion: current challenges and future perspectives. *Sustainability* 10, 1-11.
17. Tama D., Cüreklibatır Encan B., Öndoğan Z. 2017. University Students' attitude towards clothes in terms of environmental sustainability and slow fashion. *Tekstil ve Konfeksiyon* 27(2), 191-197.
18. McNeill L., Moore R. 2015. Sustainable fashion consumption and the fast fashion conundrum: fashionable consumers and attitudes to sustainability in clothing choice. *International Journal of Consumer Studies* 39, 212-222.
19. Park H., Kim Y.K. 2016. An empirical test of the triple bottom line of customer-centric sustainability: the case of fast fashion. *Fashion and Textiles* 3(25), 1-18.
20. Turker D., Altuntas C. 2014. Sustainable supply chain management in the fast fashion industry: an analysis of corporate reports. *European Management Journal* 32, 837-849.
21. Garcia-Torres S., Rey-Garcia M., Albareda-Vivo L. 2017. Effective disclosure in the fast fashion industry: from sustainability reporting to action. *Sustainability* 9, 1-27.
22. Li Y., Zhao X., Shi D., Li X. 2014. Governance of sustainable supply chains in the fast fashion industry. *European Management Journal* 32, 853-836.
23. Chang H.J., Jai T.M. 2015. Is fast fashion sustainable? The effect of positioning strategies on consumers' attitudes and purchase intentions. *Social Responsibility Journal* 11(4), 853-867.
24. Hill J., Lee H.H. 2015. Sustainable brand extensions of fast fashion retailers. *Journal of Fashion Marketing and Management* 19(2), 205-222.
25. Joy A., Sherry J.F., Venkatesh A., Wang J., Chan R. 2012. Fast fashion, sustainability and the ethical appeal of luxury brands. *Fashion Theory* 16(3), 273-295.
26. United Nations World Commission on Environment and Development. 1987. Our Common Future Report. Oxford University Press, New York, USA.
27. Grundmeier A.M. 2017. Why education can foster sustainability in the fashion market. *IOP Conference Series: Materials Science and Engineering* 254,1-6.
28. Park H., Min-Young L., Koo W. 2017. The four faces of apparel consumers: identifying sustainable consumers for apparel. *Journal of Global Fashion Marketing* 8(4):298-312.
29. Nguyen M.T.T., Nguyen L.H., Nguyen H.V. 2019. Materialistic values and green apparel purchase intention among young Vietnamese consumers. *Young Consumers* 20(4):246-263.
30. Arangdad S.R., Thoney-Barletta K., Joines J., Rothenberg L. 2019. Influence of demographics and motivational factors on US consumer clothing and shoes disposal behavior. *Research Journal of Textile and Apparel* 23(3):170-188.
31. Townsend K., Kent A., Sadkowska A. 2019. Fashioning clothing with and for mature women: a small-scale sustainable design business model. *Management Decision* 57(1):3-20.
32. Valaei N., Nikhashemi S.R. 2017. Generation Y consumers' buying behavior in fashion apparel industry: a moderation analysis. *Journal of Fashion Marketing and Management* 21(4):523-543.
33. Bilen D. 2021. The Effects of Fast Fashion Culture on Sustainability in Clothing Sector (Unpublished master's thesis). Graduate School of Natural and Applied Sciences, Department of Textile Engineering, 53 p.
34. Turkish Statistical Institute, 2019, Address Based Population Registration Statistics 2018, Population by Province, Single Age and Gender, Retrieved from http://www.tuik.gov.tr/PreTablo.do?alt_id=1059 (Date of access: August 2019)
35. Rahman O., Fung B.C.M., Chen Z., Gao X. 2017. A cross-national study of apparel consumer preferences and the role of product-evaluative cues. *Asia Pacific Journal of Marketing and Logistics* 29(4):796-812.
36. Joung H.M. 2014. Fast-fashion consumers' post-purchase behaviours. *International Journal of Retail & Distribution Management* 42(8):688-697.
37. Vehmas K., Raudaskoski A., Heikkilä P., Harlin A., Mensonen A. 2018. Consumer attitudes and communication in circular fashion. *Journal of Fashion Marketing and Management* 22(3):286-300.

Application of Neural Network for the Prediction of Loss in Mechanical Properties of Aramid Fabrics After Thermal Aging

Banu Özgen Keleş  0000-0001-9978-3268

Ege University, Emel Akın Vocational School, Izmir, 35040, Turkiye

Corresponding Author: Banu Özgen Keleş, banu.ozgen@ege.edu.tr

ABSTRACT

Aramid fabrics are used to produce most of the flame resistant protection clothes to fulfil the protection requirements. Even though aramid fibers have good thermal stability and flame resistance properties, fabrics used in protective clothing age and lose some of their essential functions under various environmental and operational conditions during their lifetime. These conditions cause serious limitations in the use of clothing. In this study, various woven fabrics produced from aramid (Nomex, Kevlar) fabrics were exposed to accelerated aging tests under varying temperature and time period in order to construct Neural Network models to predict weight loss and tensile strength loss percentages of the fabrics. The results of Artificial Neural Network models demonstrate that regression values are 0.98405 for weight loss percentages and 0.99935 for tensile strength loss percentages of the fabrics. Accordingly, the proposed Artificial Neural Network models were correctly constituted and the losses in determined fabric properties were successfully predicted.

1. INTRODUCTION

Since textiles are used in many technical fields apart from the fashion industry today, predicting performance properties of these textiles in design phase has become even more important. Since textile structures are highly complex, features of fiber and yarn affect characteristic of the final fabric and fabric properties determine the performance of the end product [1, 2]. These behaviors of textiles have led researchers to use different computational modeling methods for forecasting. Artificial neural networks (ANN) are very effective tools in solving many prediction-related problems in textiles such as classification and analysis of defects, prediction of characteristics of textiles, process optimization, identification, marketing and planning [3,4]. Artificial neural networks attempt to mimic capabilities of human brain. In order to form the network, a large number of artificial neurons are connected to each other by weights of variables. The knowledge that is gained from the system is processed with some simple connecting functions and the network learns from the previously acquired experimental results [4, 5]. It learns from examples through iterations

without any prior knowledge of relationship between variables under investigation. Unlike a computer, the network has the ability to process and learn patterns efficiently when properly trained [6]. Thus, artificial neural network modelling is a suitable tool to predict losses in performance properties of aramid fabrics.

The performance of materials used for protective clothing of workers at high risk of heat and flame exposure and firefighters, is critical for ensuring the safety of workers wearing them [7, 8]. They must also exhibit good mechanical performance to maintain the physical completeness of the clothing during service [9, 10]. However, during their lifetime, fabric structure of these garments degrades under the influence of many external factors like fire, extreme heat and hot water vapor. Furthermore, the loss in performance may not always be easily detected unless it has reached an extreme level. Therefore, it is of great importance to know and predict the mechanism underlying this aging process [11, 12].

Liu *et al.* [13] also indicated that predicting service life of firefighters' clothing before taking it out of service is

To cite this article: Özgen Keleş B. 2024. Application of Neural Network for the Prediction of Loss in Mechanical Properties of Aramid Fabrics After Thermal Aging. *Tekstil ve Konfeksiyon*, 34(1), 77-86.

necessary during the usage and maintenance of the uniform and they investigated the tensile strength of flame-retardant fabrics under fire exposure. They used regression analysis and ANN models to estimate the tensile strength of Kevlar/polybenzimidazole and polyimide/Kevlar fabrics. Lemmi *et al.* [14] investigated effects of aging temperature and time on the mechanical and surface structural properties of high tenacity polyester yarn. The investigation illustrated that aging time and temperature influenced the surface structure of fibers, tenacity and elongation properties of the yarn. In another study, thermal aging of high-performance fibers (Kevlar and PBI) was also investigated and tensile strength tests were carried out on aged and unaged samples. The tensile strength data was fitted using the Arrhenius model following two different approaches [15]. Some researchers [16, 17] used regression analysis to investigate the relationship between the tensile strength and reflection coefficient of flame-retardant fabrics and to estimate the tensile strength of these fabrics after heat exposure. The previous researches indicated that the multi linear regression (MLR) models could predict some properties of a fabric, however ANN model showed higher accuracy for prediction when compared with MLR model [13, 18, 19].

Factors like heat exposure time, temperature, and fabric type affect properties of fabrics after thermal aging process [20, 21, 22]. The temperature of the fabric during heat exposure procedure, such as glass transition, surface and degradation temperature can expound the thermal aging mechanisms in some degree. The loss in mechanical properties of the fabric may not be revealed visually and some measurements are essential to verify the losses after heat exposure [13]. Losses in weight and thickness of the fabrics occurred for aramid fabrics with the rise of heat exposure intensity and duration [23]. Thus, the best way to understand the damage occurred on the clothing is to predict the losses in the fabric mechanic properties without destruction by using modeling methods. For this purpose, woven fabrics with varying amounts of Kevlar and Nomex yarns were subjected to accelerated thermal aging processes for two different temperatures and four time periods. After the selected exposure durations, fabric tensile strength and weight values were measured and loss percentages of these fabric properties were calculated. Artificial neural network models were generated for the estimation of tensile strength and weight loss percentages.

The aim of this article is to predict the weight and strength loss percentages of aramid woven fabrics after accelerated thermal aging by using ANN models and to determine the best fit model to evaluate the service life of the fabrics. The models based on the developed neural network can describe and estimate the strength and weight loss of aramid fabrics under different conditions. The recommended models will be helpful for predicting service life of firefighter's clothing and ensuring the safety of workers wearing them.

2. MATERIAL AND METHOD

2.1 Material

Nm 50 Kevlar and Nomex yarns were procured from Erba Foreign Trade Ltd. Com. and woven fabrics were produced by using these yarns in various proportions. Plain woven fabric structure was selected for experiments since most ballistic and body protection fabrics made from Kevlar are manufactured as plain woven fabrics. Weft and warp densities for all fabric types were 20 weft/cm, 40 warp/cm, respectively. Five plain woven fabrics were manufactured for the experiments with varying Kevlar and Nomex contents: %100 Kevlar, %100 Nomex, %50 Kevlar/%50 Nomex, %33.3 Kevlar/%66.7 Nomex, %16.6 Kevlar/%83.4 Nomex.

2.2 Accelerated thermal aging test

Accelerated thermal aging tests were carried out with James Heal drying oven. 220°C and 300°C were selected for aging processes when the operating temperatures of Nomex and Kevlar were 200°C and 260°C, respectively. Since, it was reported that fire-fighters operate under 100–300°C standard conditions [15, 24]. The durations of cumulative exposures were 48, 240, 480, 720 hours for 220°C and 24, 48, 120, 240 hours for 300°C. The effects of accelerated aging process on weight and tensile strength loss were observed faster at high temperatures, thus the heat treatment durations for 220°C were chosen longer than the periods for 300°C [25].

2.3 Measurements of weight loss

Fabric samples were conditioned before weight measurements under standard atmospheric conditions and fabric weights were measured prior to thermal aging and after each selected exposure time. Percentage of variation in weight (%wl) after thermal aging was determined as:

$$\%wl = (\Delta w/w_0) \times 100 \quad (1)$$

where $\Delta w = w_0 - w_{\text{heat treated}}$, w_0 and $w_{\text{heat treated}}$ is the weight of a fabric sample before and after heat treatment, respectively.

2.4 Measurements of tensile strength loss

Zwick/Roell Z010 universal testing machine was used to determine tensile strength of aramid fabrics before and after accelerated thermal aging periods. The tests were performed with 10 kN load cell and the cross-head speed of testing machine was 100 mm/minute according to the ISO 13934-1 standard [26].

2.5 ANN modelling

In this study, multilayer perceptron ANN modelling was performed to estimate weight loss percentages and tensile strength loss percentages of Kevlar/Nomex woven fabrics. ANN is a powerful modelling tool to determine and exhibit

any type of connection between input and output variables. The ANN structure proposed for the estimation of fabric weight loss percentage and tensile strength loss percentage is shown in Figure 1. These networks consist of an input layer, hidden layer(s) and an output layer, respectively. The input variables were selected as Kevlar and Nomex yarn percentages in the fabrics, thermal aging temperature and aging duration. The output dependents were fabric weight loss percentage and tensile strength loss percentage.

The hidden layer is used for optimization of network and the number of hidden layers and neurons in each hidden layer are changed in order to find the best neural network architecture for the predictions with less error. According to the literature, the number of neurons were chosen as 5, 10,

15 and 20 in the hidden layer(s) [27 - 30]. Furthermore, various neuron numbers, close to the number of neurons in the best fit model, were also investigated for even better prediction results.

3. RESULTS AND DISCUSSION

3.1 Losses in fabric properties

The results of weight and tensile strength loss percentages of fabrics after thermal aging at 220°C and 300°C are given in Table 1 and Table 2, respectively. Weight loss percentages altered between 3.12% and 9.16% and average tensile strength loss percentages varied between 0.37% and 94.99%.

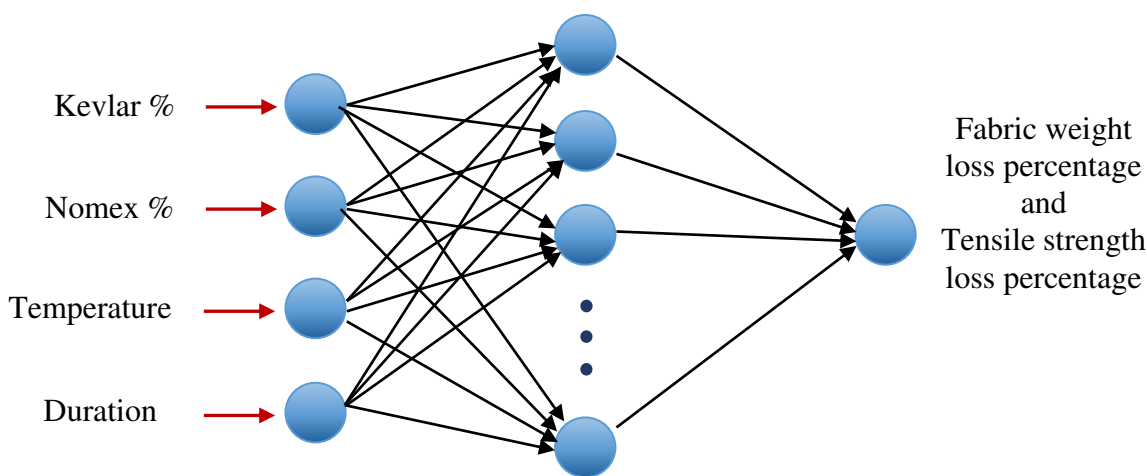


Figure 1. Structure of the proposed artificial neural network model

Table 1. Weight loss and tensile strength loss % of fabrics at 220°C

Experiment	Kevlar %	Nomex %	Duration (hours)	Weight Loss %	Tensile Strength Loss %
1	100	0	48	4.18	62.03
2	100	0	240	4.39	82.69
3	100	0	480	5.01	87.06
4	100	0	720	5.26	91.89
5	0	100	48	3.47	1.52
6	0	100	240	3.70	2.23
7	0	100	480	3.83	2.96
8	0	100	720	4.35	3.47
9	50	50	48	3.70	28.47
10	50	50	240	4.20	36.39
11	50	50	480	4.26	36.78
12	50	50	720	4.46	37.41
13	33.3	66.7	48	3.40	22.99
14	33.3	66.7	240	3.89	27.56
15	33.3	66.7	480	3.91	28.86
16	33.3	66.7	720	3.97	29.98
17	16.6	83.4	48	3.63	12.91
18	16.6	83.4	240	3.77	14.50
19	16.6	83.4	480	4.18	15.03
20	16.6	83.4	720	4.50	16.06

Table 2. Weight loss and tensile strength loss % of fabrics at 300°C

Experiment	Kevlar %	Nomex %	Duration (hours)	Weight Loss %	Tensile Strength Loss %
21	100	0	48	4.00	53.63
22	100	0	240	4.11	64.32
23	100	0	480	7.01	91.06
24	100	0	720	9.16	94.99
25	0	100	48	3.12	1.37
26	0	100	240	3.17	1.64
27	0	100	480	4.57	1.79
28	0	100	720	4.98	4.10
29	50	50	48	4.01	34.02
30	50	50	240	4.83	34.19
31	50	50	480	5.15	36.58
32	50	50	720	6.59	39.15
33	33.3	66.7	48	4.71	26.73
34	33.3	66.7	240	4.86	27.19
35	33.3	66.7	480	5.27	29.16
36	33.3	66.7	720	6.59	30.24
37	16.6	83.4	48	4.06	11.99
38	16.6	83.4	240	4.49	12.90
39	16.6	83.4	480	5.11	13.88
40	16.6	83.4	720	5.89	18.21

Fabric produced with %100 Kevlar yarns reached the maximum thermal decomposition rate with a 94.99% tensile strength loss percentage and 9.19% weight loss percentage at 300°C after 720 hours accelerated thermal aging process. The results showed that less tensile strength loss occurred when the Nomex yarn percentage was increased in the fabric composition. This was attributed to a disorder of the crystalline lattice in the perpendicular direction to the coplanar sheets that occurs simultaneously with an increase in the crystallite size in the direction parallel in the case of Kevlar [7]. Nomex shows a gradual decrease in crystallinity with increasing exposure time and this led to a reduction in tensile strength. Jain et.al. [31] investigated the weight loss after thermal aging and similarly it was observed that thermal aging was accompanied by the weight loss. This loss can be attributed to degradation and chemical reactions leading to flowing of gaseous components and small molecular weight compounds from the fabrics.

3.2 ANN model performance for weight loss percentages

In this study, the ANN models were implemented with Neural Network Toolbox of MATLAB R2021b software. The Levenberg-Marquardt [32] algorithm was used to train the proposed feed forward back propagation neural network model since previous studies showed that it is one of the most operative neural network training algorithms [33]. The training subset was first loaded to neural network in the Levenberg-Marquardt algorithm and the network parameters were updated and network was trained by utilizing the differences between the output and target values. After this process, another subset of parameters was used to verify the network. Required accuracy of training was achieved by repeating these processes for several times

until the mean squared error (MSE) reaches to the minimum error value. The MSE was calculated as

$$MSE = \frac{1}{n} \sum_{i=1}^n (y'_i - y_i)^2 \quad (2)$$

where y is an observed value and y' is a predicted value [27, 34]. The Gradient Descent with Momentum (GDM) learning algorithm was applied for the learning algorithm in MATLAB software. A TANSIGMOID transfer function for the hidden layer nodes was used to produce faster output rates in this study.

Various combinations for the number of hidden layers and number of neurons were tested to find the best fit model with maximum correlation on a hit and trial basis. The condition at which the maximum regression value was obtained in terms of training, testing and validation was considered as the final model infrastructure. The ANN model with one hidden layer and 20 neurons was found as the best model to predict the weight loss values. Table 3 shows observed and predicted values of weight loss percentages for ANN models with different number of neurons in the hidden layer. The selected number of neurons are represented with S .

The observed and proposed results were found very similar in most of the experiments in Table 3. Moreover, various Multilayer Perceptron (MLP) ANNs were also investigated for better estimations. However, the regression values of these networks weren't substantial as the ANN with one hidden layer/20 neurons. The results of the proposed networks for weight loss percentages in terms of MSE and regression (R) are exhibited in Table 4. R value measures the correlation between experiments and predictions.

Table 3. Observed and predicted weight loss percentage values for various ANN models

Experiment	Observed values for weight loss percentage	ANN (predicted) results				Difference (%) between observed and ANN results			
		S=5	S=10	S=15	S=20	S=5	S=10	S=15	S=20
1	4.18	4.68	3.12	4.34	4.24	11.96	25.36	3.76	1.37
2	4.39	4.43	3.12	4.54	4.45	0.98	28.92	3.32	1.39
3	5.01	4.45	4.96	5.01	5.30	11.12	1.02	0.03	5.82
4	5.26	5.35	5.26	5.17	5.27	1.66	0.02	1.71	0.25
5	3.47	3.66	3.62	3.43	3.39	5.39	4.20	1.11	2.23
6	3.7	3.60	3.65	3.52	3.72	2.77	1.34	4.86	0.51
7	3.83	3.64	3.84	3.76	3.87	4.91	0.39	1.75	1.13
8	4.35	4.03	4.46	4.32	4.35	7.26	2.57	0.66	0.05
9	3.7	3.92	3.64	3.71	3.64	5.86	1.62	0.29	1.56
10	4.2	3.87	4.23	4.17	4.18	7.92	0.74	0.75	0.56
11	4.26	4.02	4.56	4.38	4.25	5.65	6.96	2.88	0.35
12	4.46	4.78	4.42	4.19	4.47	7.24	0.90	6.05	0.23
13	3.4	3.75	3.51	3.53	3.49	10.19	3.10	3.94	2.61
14	3.89	3.68	3.79	3.88	3.91	5.36	2.44	0.23	0.52
15	3.91	3.78	4.00	4.09	4.05	3.26	2.24	4.62	3.63
16	3.97	4.40	3.93	4.27	4.51	10.75	1.04	7.47	13.59
17	3.63	3.68	3.59	3.47	3.39	1.45	1.12	4.53	6.62
18	3.77	3.62	3.75	3.60	3.75	4.10	0.60	4.40	0.47
19	4.18	3.67	4.18	3.69	3.93	12.22	0.02	11.65	5.89
20	4.5	4.11	4.35	4.32	4.44	8.63	3.37	4.11	1.34
21	4	5.21	4.04	4.85	4.03	30.34	1.06	21.28	0.70
22	4.11	5.38	4.56	5.20	4.52	30.82	10.99	26.49	9.97
23	7.01	5.93	7.11	6.51	7.03	15.40	1.44	7.20	0.33
24	9.16	6.88	9.01	8.22	9.03	24.94	1.63	10.27	1.39
25	3.12	3.95	3.61	3.63	3.44	26.73	15.58	16.49	10.31
26	3.17	4.02	3.73	3.69	3.56	26.96	17.66	16.47	12.41
27	4.57	4.32	4.53	3.99	4.09	5.54	0.92	12.63	10.43
28	4.98	5.16	8.32	5.08	5.04	3.61	67.09	1.99	1.21
29	4.01	4.84	4.32	4.43	4.11	20.74	7.75	10.38	2.48
30	4.83	4.97	4.50	4.67	4.33	2.87	6.83	3.38	10.35
31	5.15	5.43	5.16	5.61	5.14	5.50	0.18	8.88	0.13
32	6.59	6.39	6.66	7.15	6.55	2.96	1.13	8.44	0.56
33	4.71	4.60	4.80	4.52	4.59	2.24	1.96	4.11	2.62
34	4.86	4.72	4.94	4.68	4.84	2.84	1.67	3.76	0.36
35	5.27	5.16	5.43	5.27	5.56	2.06	3.08	0.02	5.55
36	6.59	6.14	6.54	6.37	6.39	6.86	0.77	3.30	3.02
37	4.06	4.24	4.30	4.07	4.05	4.45	5.83	0.22	0.35
38	4.49	4.34	4.41	4.14	4.30	3.35	1.69	7.82	4.27
39	5.11	4.73	4.84	4.49	5.13	7.49	5.21	12.18	0.30
40	5.89	5.70	6.03	5.61	5.97	3.24	2.41	4.82	1.31

Table 4. Results of some MLP-ANNs for weight loss percentages of fabrics after thermal aging

Number of hidden layers	Number of neurons in hidden layers	R values of weight loss %	MSE
1	5	0.86494	0.35425
1	10	0.87897	0.38205
1	15	0.94170	0.15010
1	20	0.98405	0.04164
2	5-5	0.96325	0.09655
2	10-5	0.92834	0.18360
2	10-10	0.97668	0.19425
3	5-5-5	0.96534	0.11076
3	10-10-10	0.96564	0.09286

As it is shown in Table 4, the R values are close to 1 for most of the proposed networks and vary between 0.86494 to 0.98405. The best R value, 0.98405, and minimum MSE, 0.04164, was obtained for ANN with 20 neurons in one hidden layer. The detailed results of training, validation and

testing subsets of the ANN which gave the highest R value are shown in Figure 2. According to the results, the ANN model with 20 neurons in one hidden layer can be used as an effective model for prediction of weight loss percentage of aramid fabrics.



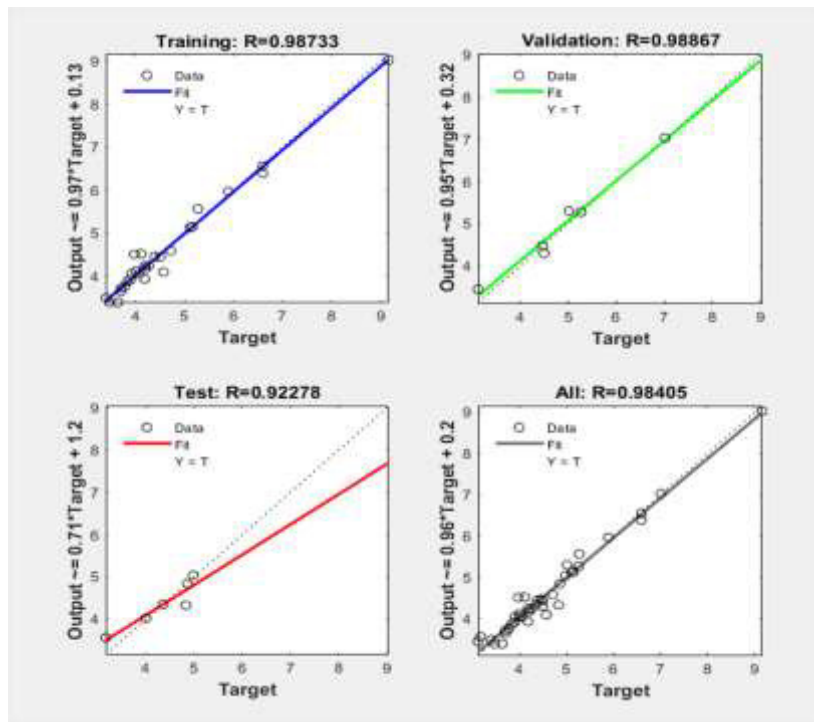


Figure 2. Results of the ANN for weight loss % (one hidden layer-20 neurons)

The performance of the ANN model is illustrated in Figure 3 for the estimated and observed values of weight loss percentages against the input variables.

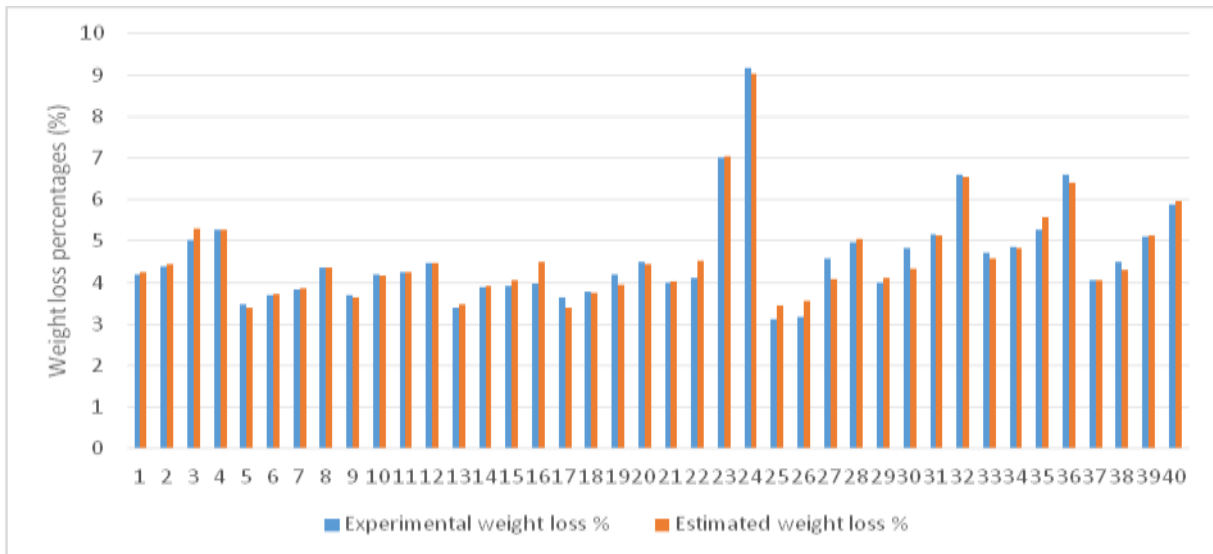


Figure 3. Comparative results for estimated and experimentally observed tensile strength loss percentages of aramid fabrics

3.3 ANN model performance for tensile strength loss percentages

Determining the amount of hidden layers and the number of neurons in each hidden layer is the challenge of using ANNs. Too many or too few number of neurons or layers will result in inaccurate output. Thus, different combinations for the number of hidden layers and neurons were tested for maximum correlation. The models with only one hidden layer didn't give good correlation between real

experimental data and estimated values. Thus, the best fit models with two and three hidden layers were selected to be given on Table 5.

Table 5 shows the observed and predicted values of tensile strength loss percentages for ANN models with two and three hidden layers.

Table 5. Observed and predicted tensile strength loss percentage values for various ANN models

Experiment	Observed value for tensile strength loss %	ANN (predicted) results				Difference (%) between observed and ANN results			
		S=10,10	S=10,15	S=15,15	S=5,5,5	S=10,10	S=10,15	S=15,15	S=5,5,5
1	62.03	62.02	62.03	65.49	61.30	0.02	0.00	5.58	1.17
2	82.69	86.38	82.69	82.69	79.05	4.47	0.00	0.00	4.40
3	87.06	85.56	87.06	87.06	86.53	1.72	0.00	0.00	0.61
4	91.89	84.93	91.89	91.89	91.64	7.57	0.00	0.00	0.28
5	1.52	1.71	1.53	1.52	1.64	12.24	0.42	0.00	8.22
6	2.23	1.97	2.23	3.60	2.14	11.61	0.16	61.65	4.04
7	2.96	3.05	2.96	4.64	2.76	2.92	0.04	56.91	6.90
8	3.47	2.20	3.47	3.47	3.30	36.52	0.00	0.00	4.91
9	28.47	28.47	28.47	28.47	30.95	0.00	0.00	0.00	8.72
10	36.39	31.48	32.12	36.39	35.80	13.49	11.74	0.00	1.63
11	36.78	36.79	36.78	36.78	36.09	0.03	0.00	0.00	1.87
12	37.41	37.40	40.38	37.41	38.29	0.01	7.94	0.00	2.35
13	22.99	25.42	23.34	22.99	22.69	10.55	1.50	0.00	1.31
14	27.56	27.57	27.56	27.56	27.69	0.03	0.00	0.00	0.48
15	28.86	28.87	28.86	34.36	31.52	0.04	0.00	19.05	9.21
16	29.98	29.98	29.98	29.98	29.35	0.00	0.00	0.00	2.09
17	12.91	12.90	12.91	8.36	13.30	0.07	0.00	35.24	3.03
18	14.5	16.71	21.50	14.50	14.04	15.28	48.31	0.00	3.17
19	15.03	16.33	15.03	15.03	14.76	8.66	0.01	0.00	1.77
20	16.06	16.06	16.39	16.06	16.35	0.01	2.05	0.00	1.80
21	53.63	53.56	52.88	51.58	53.80	0.14	1.41	3.82	0.33
22	64.32	64.69	65.71	64.32	64.10	0.57	2.17	0.00	0.34
23	91.06	90.72	91.06	85.97	91.10	0.37	0.00	5.59	0.04
24	94.99	94.88	94.95	92.57	94.22	0.12	0.05	2.55	0.81
25	1.37	1.60	0.86	1.69	1.38	16.58	37.45	23.32	1.08
26	1.64	1.57	1.13	1.64	1.52	4.13	31.21	0.00	7.13
27	1.79	1.78	1.89	1.79	2.17	0.36	5.67	0.00	21.40
28	4.1	3.91	3.02	4.10	3.49	4.75	26.29	0.00	14.92
29	34.02	33.10	34.02	34.02	34.59	2.71	0.00	0.00	1.68
30	34.19	34.22	34.29	34.19	34.94	0.10	0.28	0.00	2.20
31	36.58	36.53	35.79	36.58	36.04	0.13	2.17	0.00	1.47
32	39.15	39.15	39.15	39.15	37.93	0.00	0.00	0.00	3.12
33	26.73	26.64	26.73	26.73	27.25	0.33	0.01	0.00	1.96
34	27.19	27.35	27.19	27.19	27.70	0.60	0.01	0.00	1.89
35	29.16	29.18	29.16	29.16	29.14	0.08	0.01	0.00	0.07
36	30.24	37.69	30.24	30.24	31.68	24.65	0.00	0.00	4.77
37	11.99	12.87	11.99	12.72	12.72	7.34	0.01	6.06	6.06
38	12.9	12.60	12.78	12.90	13.55	2.31	0.91	0.00	5.04
39	13.88	11.98	14.71	13.74	15.70	13.70	6.00	0.98	13.09
40	18.21	18.24	18.21	17.09	19.25	0.19	0.01	6.15	5.73

The MSE and regression (R) results of the proposed networks for tensile strength loss percentages are shown in Table 6.

Table 6. Results of some MLP-ANNs for tensile strength loss percentages of fabrics after thermal aging

Number of hidden layers	Number of neurons in hidden layers	R	MSE
2	10-10	0.99718	4.09710
2	10-15	0.99923	2.04817
2	10-20	0.97861	7.30801
2	15-15	0.99822	2.63852
3	5-5-5	0.99935	1.04743
3	10-10-10	0.99381	9.45802

The most suitable network model, which produced the minimum value of MSE and maximum regression value, was found as ANN with 3 hidden layers that included 15 neurons in hidden layers totally. The R value of this model was calculated as 0.99935 which indicated that the model

had a very high potential for the prediction of tensile strength loss percentages of aramid woven fabrics close to the real experimental results. Thus, these results confirm that the neural network model reproduces tensile strength loss values for this system, within the experimental ranges

adopted in the fitting model. The detailed training, validation and testing results of the proposed ANN with the highest R value are shown in Figure 4.

The results of the best fit ANN model were also observed by plotting the estimated and observed values of weight loss percentages against the varying parameters (Figure 5).

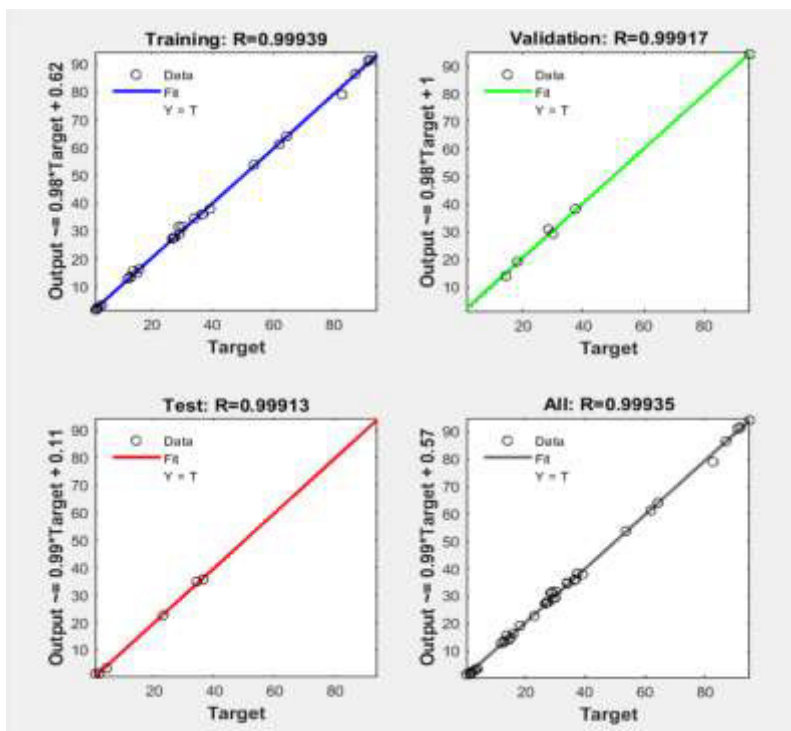


Figure 4. Results of the proposed MLP-ANN for tensile strength loss % (three hidden layers-5,5,5 neurons)

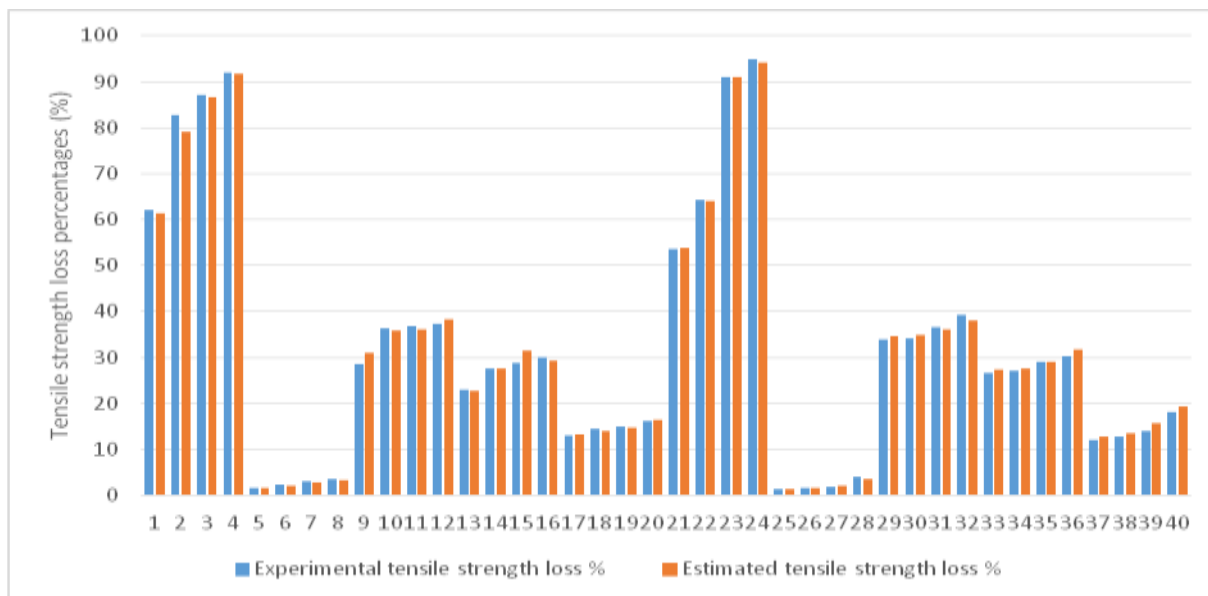


Figure 5. Comparison of results for estimated and experimentally observed tensile strength loss percentages of aramid fabrics

4. CONCLUSION

In this study, loss percentages of some physical properties of aramid woven fabrics after accelerated thermal aging

processes were investigated and predicted by using artificial neural network. Repeated heat and flame exposures can cause continuous decreases in mechanical properties of

materials and thermal protection given by flame-resistance protective clothing and increase injuries caused by body burn. Thus, it is important to determine the lifetime of the clothing for certain conditions before permanent damage occurs on the fabric structure. The losses in the properties of aramid fabrics after accelerated thermal aging process were successfully predicted by applying multi-layered neural networks and using a backpropagation algorithm in this study. On the basis of the proposed ANN models, it was possible to obtain quantitative information on changes in fabric properties for any temperature and exposure time. An analysis was also conducted to investigate the relationship between the estimated results of the proposed ANN models and the experimental data. As a result of using the ANN model, the values of the determination coefficient (R) for weight loss percentage and tensile strength loss percentage were found to be 0.98405 and

0.99923, respectively. The time required for the fibers to loss 50% of their original tensile strength is defined as the material thermal life. Thus, the ANN models generated in this study help to predict the lifetime of protective flame-retardant clothing according to the durations that the clothes expose to a certain degree of heat. Further studies could be investigated for other performance properties and thermal resistance of different fiber blended aramid fabrics after accelerated thermal aging.

Acknowledgement

Funding: The author(s) received no financial support for the research, authorship, and/or publication of this article.

Conflicts of interest: No potential conflict of interest was reported by the authors.

REFERENCES

1. Khaliq Z, Zulifqar A. 2020. Textile Mechanics: Fibers and Yarns. In J. Hu, B. Kumar and J. Lu (Eds), *Handbook of Fibrous Materials*, Wiley, 435-455.
2. Vassiliadis S, Rangoussi M, Cay A, Provatidis C. 2010. Artificial Neural Networks and Their Applications in the Engineering of Fabrics. In Dobnik Dubrovski P (Ed), *Woven Fabric Engineering*. IntechOpen, 111-134.
3. Bhattacharjee D, Kothari V.K. 2007. A Neural Network System for Prediction of Thermal Resistance of Textile Fabrics. *Textile Research Journal*, 77:4-12.
4. Chattopadhyay R, Guha A. 2004. Artificial Neural Networks: Applications to Textiles. *Textile Progress*, 35:1-46.
5. Arıkan Kargı VS. 2014. A Comparison of Artificial Neural Networks and Multiple Linear Regression Models as Predictors of Fabric Weft Defects. *Tekstil ve Konfeksiyon*, 24 (3), 309-316.
6. Tarafdar A, Shahi NC, Singh A, Sroh R. 2018. Artificial Neural Network Modeling of Water Activity: A Low Energy Approach to Freeze Drying. *Food and Bioprocess Technology*, 11:164-171.
7. Dolez PI, Tomer NS, Malajati Y. 2019. A quantitative method to compare the effect of thermal aging on the mechanical performance of fire protective fabrics. *Journal of Applied Polymer Science*, 136(1):47045.
8. Deng M, Tian M, Wang Y, Wang M. 2020. Quantitatively evaluating the effects of flash fire exposure on the mechanical performance of thermal protective clothing. *International Journal of Clothing Science and Technology*, 32 (3), 412-429.
9. Hoque MS, Saha A, Chung HJ, Dolez PI. 2022. Hydrothermal aging of fire - protective fabrics. *Journal of Applied Polymer Science*, 139 (30), e52666.
10. Wang M, Li J. 2016. Thermal protection retention of fire protective clothing after repeated flash fire exposure. *Journal of Industrial Textiles*, 46(3), 737-755.
11. Aidani R, Dolez PI, Vu-khanh T. 2011. Effect of Thermal Aging on the Mechanical and Barrier Properties of an e-PTFE/NomexVR Moisture Membrane Used in Firefighters' Protective Suits. *Journal of Applied Polymer Science*, 121:3101-3110.
12. Cho C, Nam SL, de la Mata AP, Harynyuk JJ, Elias AL, Chung HJ, Dolez PI. 2022. Investigation of the accelerated thermal aging behavior of polyetherimide and lifetime prediction at elevated temperature. *Journal of Applied Polymer Science*, 139(15), 51955.
13. Liu X, Tian M, Wang Y, Su Y, Li J. 2021. Modeling to predict thermal aging for flame-retardant fabrics considering thermal stability under fire exposure. *Textile Research Journal*, 91:2656-2668.
14. Lemmi TS, Barburski M, Kabziński A, Frukacz K. 2021. Effect of Thermal Aging on the Mechanical Properties of High Tenacity Polyester Yarn. *Materials*, 14(7):1666-1676.
15. Arrieta C, David E, Dolez P, Toan V-KJ. 2010. Thermal Aging of a Blend of High-Performance Fibers. *Journal of Applied Polymer Science*, 115(5), 3031-3039.
16. Rezaazadeh M, Torvi DA. 2011. Assessment of factors affecting the continuing performance of firefighters' protective clothing: a literature review. *Fire Technology*, 47(3):565-599.
17. Lu Y, Wang L, Gao Q. 2018. Predicting tensile strength of fabrics used in firefighters' protective clothing after multiple radiation exposures. *Journal of The Textile Institute*, 109:338-344.
18. Mandal S, Song G. 2014. An empirical analysis of thermal protective performance of fabrics used in protective clothing. *Annals of Occupational Hygiene*, 58(8):1065-1077.
19. Mandal S, Annaheim S, Greve J, Camenzind M, Rossi RM. 2019. Modeling for predicting the thermal protective and thermophysiological comfort performance of fabrics used in firefighters' clothing. *Textile Research Journal*, 89(14), 2836-2849.
20. Iyer RV, Sudhakar A, Vijayan K. 2006. Decomposition behavior of Kevlar 49 fibres: Part II. At T values < Td. *High Perform. Polymers*, 18:495-517.
21. Tian M, Wang Q, Xiao Y, Su Y, Zhang X, Li J. 2020. Investigating the thermal-protective performance of fire-retardant fabrics considering garment aperture structures exposed to flames. *Materials*, 13(16), 3579.
22. Brown, J R, and Browne, N M. *Environmental effects on the mechanical properties of high-performance fibres. [PBI, Nomex, and Kevlar 49]*. United States: N. p., 1976. Web.
23. Talukdar P, Das A, Alagirusamy R. 2016. Heat and mass transfer through thermal protective clothing—A review. *International Journal of Thermal Sciences*, 106, 32-56.
24. Serban A. 2019. The Impact of Heat Stress in Firefighter Fatalities. Honeywell Safety and Productivity Solutions. <https://sps.honeywell.com/us/en/support/blog/safety/the-impact-of-heat-stress-in-firefighter-fatalities>, Accessed 06 Jan 2023
25. Ozgen B, Pamuk G. 2014. Effects of thermal aging on Kevlar and Nomex fabrics. *Industria Textila*, 65(5):254-262.



-
-
26. International Standards Office. (2013). ISO 13934-1-Textiles-tensile properties of fabrics-part 1: Determination of maximum force and elongation at maximum force using the strip method: Bibliographical references: Electronic documents.
 27. Eyupoglu C, Eyupoglu S, Merdan N. 2019. Improvement of thermal insulation properties of polyester nonwoven and estimation of thermal conductivity coefficients using artificial neural network. *Journal of Testing and Evaluation*, 47(2):20180129.
 28. Veit, D. (Ed.). 2012. Simulation in textile technology: Theory and applications. Woodhead Publishing.
 29. Omerogullari Basyigit, Z., Eyupoglu, C., Eyupoglu, S., & Merdan, N. 2023. Investigation and Feed - Forward Neural Network - Based Estimation of Dyeing Properties of Air Plasma Treated Wool Fabric Dyed with Natural Dye Obtained from Hibiscus Sabdariffa. Coloration Technology.
 30. Eyupoglu, C., Eyupoglu, S., & Merdan, N. 2022. Investigation of dyeing properties of mohair fiber dyed with natural dyes obtained from candelariella reflexa. *Journal of Natural Fibers*, 19(16), 12829-12848.
 31. Jain, A., & Vijayan, K. 2002. Thermally induced structural changes in Nomex fibres. *Bulletin of Materials Science*, 25, 341-346.
 32. More JJ. 1978. The Levenberg-Marquardt algorithm: Implementation and Theory. In Watson GA (Ed.) *Numerical Analysis*. Berlin, Heidelberg: Springer; 105-116.
 33. Eyupoglu C, Eyupoglu S, Merdan N. 2021. A multilayer perceptron artificial neural network model for estimation of ultraviolet protection properties of polyester microfiber fabric. *Journal of The Textile Institute*, 112:1403-1416.
 34. Wackerly D, Mendenhall W, Scheaffer RL. 2008. *Mathematical Statistics with Applications*. Thomson Brooks/Cole, Belmont.